MICROMECHANICAL MODELLING FOR DEFORMATIONAL BEHAVIOR OF STRAIN HARDENING CEMENT-BASED COMPOSITES

UMBREEN-US-SAHAR

September, 2015

MICROMECHANICAL MODELLING FOR DEFORMATIONAL BEHAVIOR OF STRAIN HARDENING CEMENT-BASED COMPOSITES

ひずみ硬化型セメント系材料の変形挙動の微視的構造モデル

by

UMBREEN-US-SAHAR

A Dissertation
Submitted to
The Department of Civil Engineering
Yokohama National University

In Partial Fulfillment of the Requirements
for the Degree of
Doctor of Philosophy

Graduate School of Urban Innovation
Yokohama National University
Yokohama, Japan
September, 2015

MICROMECHANICAL MODELLING FOR DEFORMATIONAL BEHAVIOR OF STRAIN HARDENING CEMENT-BASED COMPOSITES

ABSTRACT

The strain hardening cement-based composites (SHCC) has become an important material to use as structural material and as patch repair material. The durability of this material under short term loading and time dependent loading has been investigated and it became a significantly accepted material under shear, fatigue and seismic loadings. The SHCC is designed for large tensile strain capacity at moderate tensile strength. This tensile ductility is obtained through balanced fiber and matrix properties, to allow effective crack bridging by fibers, whereby cracks are controlled to widths in the micro-range. Evidence is emerging that the crack control is maintained also in more general loading conditions, including flexure and shear both in pure SHCC and with steel bar reinforcement (R/SHCC).

The diffusivity process governs the longer term migration of water and chlorides into the material through the micro-pores. Under service conditions, which inevitably include cracks in structures built from cement composites, long term durability is controlled by reduced diffusivity. The experiments show that crack widths may be limited to within a threshold value of 100μm by inherent crack control in SHCC that confirms the potential of SHCC to be used as durable structures. If structure built of SHCC or R/SHCC are designed to operate in the multiple cracking region then it must be ensured that crack width control is retained under various loadings histories, including cyclic loading, loading at various rates and sustained loading. For that purpose, there is need to build a constitutive model to simulate the multiple cracking, crack widths control under static and time-dependent loading. The focus of the present research is to model the time-dependent behavior for tensile creep and drying shrinkage of SHCC so that this material can effectively be simulated for various loading conditions.

In the past much focus has been given to investigate the mechanism of mechanical behavior of SHCC under static and sustained loading including fatigue and cyclic loading as the main application field of SHCC have been observed as patching repair material for

bridge decks. But for sustained loading behavior, it has been observed that there is lesser work has been done by the researchers. The most recently the experiments have been done to investigate mechanism of tensile creep and time-dependent crack widths along with formation of new cracks. In the field of modelling of these mechanisms again very less development has been observed. Thus the present study deals with the modelling of SHCC under time-dependent loading to confirm the mechanism of tensile creep for durability design of SHCC under sustained loading. For this purpose as first step, the constitutive multi-layered microplane model has been proposed in the present study for static uniaxial tensile loading to simulate stress-strain relationship, multiple cracking and crack widths. In the second part of this research work, the multi-layered microplane model has been extended to simulate time-dependent behavior of SHCC. A brief outline of the dissertation and findings is summarized below

Chapter 1 comprises of the general introduction, background of the problem being investigated, research significance and practical applications of the research findings. Some of the information and knowledge which play an important role in this research and might be unfamiliar to some engineers are briefed in Chapter 2 as literature review.

Chapter 3 consists of model methodology for uniaxial tensile loading. This portion of the research is partitioned into three parts. The first part consists of analytical model to simulate the uniaxial stress-strain relationship by using tri-linear function. The microplane model has been considered as base of the presented analytical model. The original microplane model has been implemented for concrete and brittle plastics with exponential function for uniaxial tensile loading. The behavior of SHCC as pseudo-ductile material is tri-linear under uniaxial tensile loading conditions. To simulate this behavior, the use of tri-linear function is the most appropriate methodology that resulted in satisfactory agreement with the experimental data. The important and significant material parameters are identified and explained in detail. In the second part of this chapter, the crack widths under uniaxial tensile loading have been simulated by using equivalent tangential fiber bridging stiffness approach. The crack widths are simulated in the strain hardening zone of SHCC. In the third part of the chapter, the crack spacing and distribution has been simulated for multiple cracking phenomenon of SHCC. All of these models have been compared with experimental data and resulted in good agreement.

Chapter 4 comprises of four parts. In the first part, the analytical model is presented to simulate the uniaxial tensile behavior by using multi-layered microplane model. This model methodology has been presented based on statistical variation of fiber volume due to spatial distribution of short random synthetic fibers. The focus of this analytical approach is to model the strain-hardening region that is accompanied by multiple cracking. This methodology is implemented for multi-layered microplane model. The concept of multilayers attributes the multiple cracking phenomenon of SHCC. The stress-strain relationship for multiple cracking is simulated for three types of fibers, i.e., PVA, carbon and aramid fibers. The material parameters are expressed as function of fiber type.

In the second part of this chapter, the crack width is simulated based on cracking strain approach. The mechanism under uniaxial tensile loading reveals that the crack widths are attributed to fiber pull-out displacements for SHCC. Based on this mechanism, the analytical model is proposed to simulate total crack widths. In the third part of the chapter, the crack spacing and distribution is modelled based on varying strength along the length of specimen. In the fourth part, the uniaxial compression behavior is simulated based on microplane model using arctan function. All of the proposed models are compared with experimental data for SHCC that show a satisfactory agreement.

Chapter 5 represents the time-dependent modelling of SHCC by using multi-layered microplane model. The proposed model is basically an extension of the model proposed in chapter 4. This proposed model in chapter 5 includes drying shrinkage and tensile creep parameters. The tensile creep is further based on matrix creep and time-dependent fiber pull-out displacements. The fiber creep itself is proved to be almost negligible as by the experiments done on single fiber creep by the researchers in the recent past. Thus the above mentioned mechanisms are incorporated in the proposed model to simulate time-dependent behavior of SHCC. The time-dependent crack widths are also simulated along with number of cracks. The results of simulation of the model presented are compared with the experimental data to ensure the applicability and validity of the model for time-dependent behavior of SHCC.

Finally Chapter 6 consists of a summary of conclusions and recommendations that can be drawn from the above mentioned work. Subsequent discussion is also explained with the recommendations for future research.

ACKNOWLEDGEMENTS

My deepest gratitude and sincere thanks goes to my research advisor for his professional, genuine guidance and valuable advice to accomplish the dissertation on time. It is a privilege to work with him. Great appreciation is expressed for the members of examination committee for their contribution in reviewing this research work. I am grateful to thank all the laboratory staffs and the former laboratory students for their guidance and support in reviewing this research work. I would like to thank the faculty members of the Department of Civil Engineering, Yokohama National University for giving me this opportunity to pursue my doctoral study in well and proper guided and cooperated manner.

Special thank also goes to all my colleagues in the Concrete Laboratory for their moral support and disinterested assistance they have provided through constant encouragement, and pleasant atmosphere of friendship, which made it possible for me to finish my work. I also extend my acknowledgement to the Ministry of Education, Culture, Sports, Science and Technology of Japan (Monbukagakusho) for the financial grant to conduct this research. The research would not have been possible without their generous support.

I am deeply indebted to my Mother, my Late Father (May God Rest His Soul in Peace and Forgive All our Sins, Ameen), my Younger Sister and my Husband for their constant support, dedicated encouragement, and extensive sacrifices bought upon through my stay in Japan.

This dissertation is dedicated to:

My Parents,

My Husband and daughter

With gratitude and love

CONTENTS

LISTS OF FIGURES

LIST OF TABLES

NOMENCLATURE

ε_n	normal strain
σ_n	normal stress
σ_{cr}	first cracking strength
ε_{cr}	first cracking strain
ε_t	strain at maximum tensile strength
σ_t	maximum tensile strength
ε_u	ultimate tensile strain
E_0	initial modulus
ν	Poisson's ratio
V_f	Volume fraction of fibers
k_{mf}	equivalent tangential fiber bridging stiffness
$d\varepsilon_{cri}$	strain increment for *i*-th cracked part
$d\varepsilon_{ui}$	strain increment for *i*-th uncracked part
u_{fi}	pull out displacement of fiber at *i*-th crack
k_{fi}	bridging stiffness of fibers at *i*-th crack
$(w_i)^I$	crack width of *i*-th crack
$(w)^T$	total crack width
C_N°	initial secant modulus
C_N	normal secant modulus
ε_{ij}^a	additional elastic strain
E_f	fiber elastic modulus
$\dot{\varepsilon}_{rs}^{sh}$	rate of shrinkage strain
$\dot{w}_{c(t)}$	rate of time-dependent crack width
$\dot{\varepsilon}_{rs}^{creep'}$	rate of tensile matrix creep
$\dot{\varepsilon}_{rs}^{creep^{cr}}$	rate of creep cracking strain

Chapter 1
INTRODUCTION

1.1 Background

Concrete has been used over many centuries as a reliable, fairly durable building material. Two of the main advantages of concrete are that it has a high compressive strength and can be cast on the construction site into almost any shape and size. The short comings of concrete is becoming more and more prominent in this day and age due to the emphases of design moving towards economical design rather than a durable design. The most prominent disadvantages of concrete are the brittleness during failure and the low tensile strength, which is about one tenth of the compression strength. The low tensile strength is compensated with steel reinforcing, but micro cracking still occurs during the normal use of concrete. These micro cracks lead to durability problems as water penetrates the concrete through the cracks and aggravates the corrosion of the steel reinforcing which in turn results in structural degradation.

SHCC (Strain Hardening Cement-based Composites) is a type of HPC (High Performance Concrete) that was engineered to overcome these weaknesses of ordinary concrete by adding flexible short randomly distributed polymer fibers. It shows high ductility as it can resist the full tensile load at a strain of more than 3 % compared to concrete which fails on average at a strain of 0.01 % in tension. When using SHCC instead of ordinary concrete the strain capacity increases more than 300 times. This leads to a high energy absorption capacity of SHCC, along with multiple cracking as shown in Fig. 1.1 and Fig. 1.2. The stress-strain relationship of SHCC as compared to ordinary concrete and FRC (Fiber Reinforced Concrete) is schematically shown in the Fig. 1.2. SHCC shows highly ductile behavior and large elastic strains.

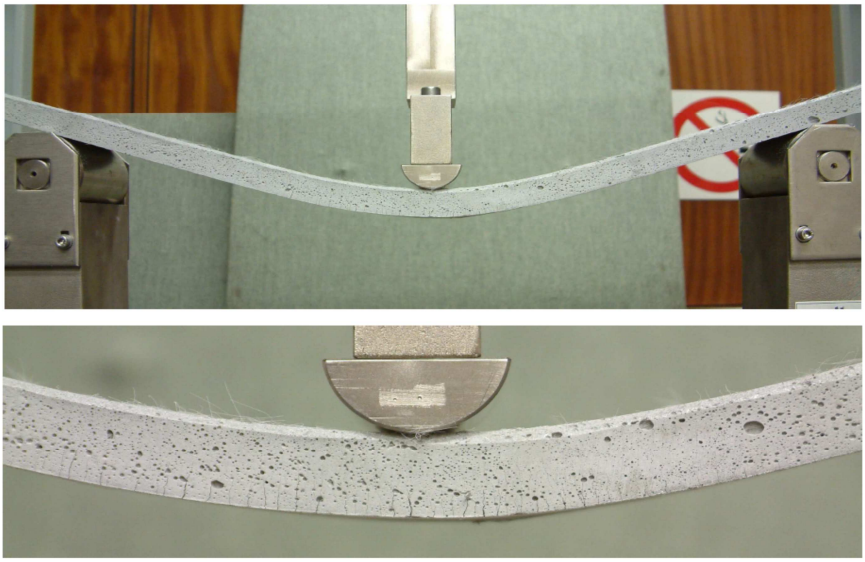

Figure 1.1 Example of the ductility of ECC and the multiple cracking[1)]

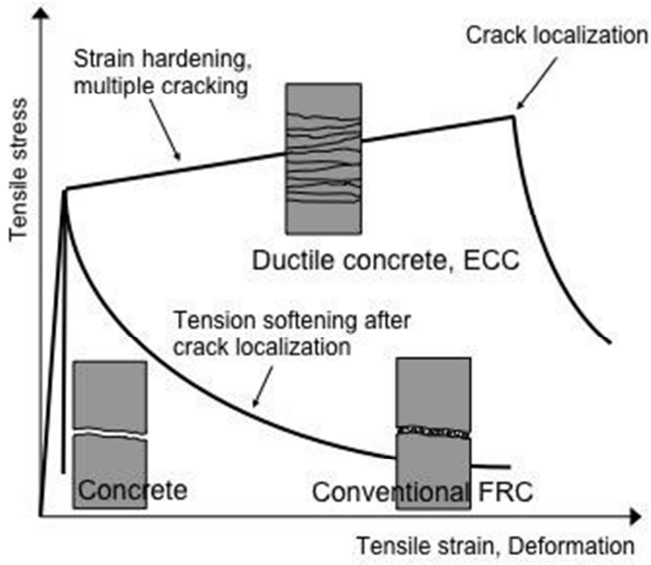

Fig. 1.2 Material performance of conventional concrete, fiber-reinforced concrete, and SHCC under tension load[2)]

During the increase of strain under tensile loading of ECC, a constant strain hardening effect is found and many, closely spaced, micro cracks are formed in the material. These multiple cracks are bridged by the short synthetic fibers resulting in controlled crack width of SHCC material, i.e., less than 100 μm. This property of strain hardening cement-based composites reduces the problem of water penetration and thus improves the durability of structures. ECC (Engineered Cementitious Composite) or SHCC however cost more than ordinary concrete, but if the material is used to exploit its advantages, it becomes a competitive material in the building industry. In several applications the advantages of ECC may be exploited:

- Due to the high ductility and flexibility of SHCC it can be used in designated areas in a multi-storey structure to withstand earthquake loadings. SHCC can be used as the material for the hinge areas as well as shear walls and panels.
- Due to the high ductility, thin membrane members, i.e. less than 15 mm thick, can be made e.g. pipes and tiles.
- Repair material: Due to the high strain capacity and energy absorption, SHCC is ideal to be used as repair material, especially for bonded overlays.
- Due to the fine and multiple cracking phenomenon of SHCC, it can be used as a permanent formwork for concrete members. This will also add to the shear resistance of the member as SHCC has a higher shear resistance than ordinary concrete.

The mechanical behavior of SHCC has been well researched over the past 10 years for short-term macroscopic behavior, but little work has been done on the time-dependent behavior and fewer researches have been published on the tensile creep characteristics of SHCC. There is no indication whether this high ductility and energy absorption capability is sustainable if the material is exposed to a long term load. Premature and unexpected failure could occur over a period of time at a load lower that the ultimate load determined with short-term tests in laboratories. The durability of the structure may become susceptible due to formation of time-dependent cracks and widening of cracks due to sustained loading. Also, a robust finite element material model is not available to simulate the static behavior of SHCC, not to mention the long term creep behavior. The finite element models available

(Han et al[3], Simone et al[4], Kabele 2000[5]) either have shortcomings, especially simulating the localization, or are too complex, intended for fundamental academic research. Without an accurate and robust finite element model, it is also difficult to predict the long term tensile creep deflection of any structure incorporating SHCC. These shortcomings in the research and development of SHCC form the basis of the research project reported in this dissertation. The main focus of the present study is to investigate and numerically model the micromechanical deformational behavior of SHCC with multiple cracking, number of cracks, crack spacing under uniaxial tensile loading. The time-dependent behavior of SHCC is modelled by using multi-layered microplane model. This model has an advantage that the phenomenon of multiple cracking can be well explained for small sized specimen equal to about the size of one element used in FEM for simulation of larger structures.

1.2 Objective and Significance of Research

The main objectives of this research can be summarized as follows

Table 1.1 Main objectives of present research

Analytical model for uniaxial tensile loading of SHCC	Develop an analytical model able to predict the uniaxial tensile stress-strain relationship of SHCC based on microplane model using tri-linear tension property and multi-layered microplane model.
Analytical model for time-dependent behavior of SHCC	Develop an analytical model able to predict time-dependent behavior of SHCC based on multi-layered microplane model as well as the time-dependent change of crack spacing and number of cracks.
Analytical model for crack widths	Develop an analytical model able to predict the crack widths of SHCC material under short-term behavior.
Identification of material parameters for static and sustained loading	Identify the material properties for stress-strain relationship of SHCC for uniaxial tensile and uniaxial compression, crack width, time-dependent (tensile creep and shrinkage) model for SHCC.
Simulation of multiple cracking	Develop a model to simulate the multiple cracking of SHCC along with crack distribution and spacing under short-term loading.
Verification of analytical model	Verify the present model by using identified material parameters by comparing the results with experimental data.

The stress-strain relationship for uniaxial tensile loading involves various mechanisms to be defined and analyzed. These mechanisms are mainly focused in strain hardening region. The strain hardening of SHCC material is accompanied by multiple cracking and resulted in ductile behavior. The mechanism of strain hardening is analyzed with two different approaches. The strain hardening is caused due to stiffness recovery either due to interlocking of the material particles with fiber interfacial surface during pull out of fibers or due to interaction of a single fiber with other fibers dispersed randomly in the matrix. This mechanism is simulated by using statistical variation of fiber volume/tensile strengths from first crack to maximum number of cracks with equal statistical increased interval following uniform distribution. The use of statistical variation is found to be the most appropriate tool to model the strain hardening behavior of SHCC. The phenomenon of multiple cracking needs more attention to be predicted accurately for durability design of SHCC structure especially when SHCC is used as repair material. The control of crack widths is another property of SHCC that needs equivalent attention to be analytically modelled.

These mechanisms are directly associated with the fiber properties as the fiber bridging strength is considered the main source of cracking strength of SHCC. Hence the material is modelled by dividing the material into many layers of cracked and uncracked parts. The cracks are bridged by the fibers. The PVA (Polyvinyl Alcoholic Fibers) are mainly used for SHCC. The common mix proportion and fiber properties details will be explained in the later chapter. These short fibers are randomly distributed within the matrix mix. This random distribution is simulated by considering statistical variation of fiber volume within matrix. The tensile strength of SHCC is dependent on fiber volume. Therefore, if fiber volume/area of fibers bridging the cracks is considered varied from crack to crack in increasing order then the each new crack will be initiated at higher tensile strength as compared to previous one. This simulation approach will satisfy the increase of load/stress during strain hardening of SHCC.

Based on this approach, the crack width and stress-strain relationship for uniaxial tensile loading can be simulated. The microplane model is taken as basic tool for the

implementation of analytical models for the mechanisms of strain hardening cement-based composites. Microplane model is based on the kinematic constraints on each crack, i.e., the strain components on each microplane (crack) are considered as resolved component of macroscopic strain vector. Then these microplanes are considered distributed uniformly on the surface of sphere as some function (The detail of these functions will be discussed in later chapter). These functions then will be integrated over the surface of sphere to result in macroscopic behavior.

Firstly the multi-layered model is implemented in microplane model to simulate uniaxial tensile stress-strain relationship. Further this multilayered-model is modified to model the time-dependent behavior of SHCC for tensile creep and shrinkage. The time dependent crack widths are considered as main source of time-dependent deformations. These deformations are modelled and compared with experimental data.

1.3 Research Application

A number of investigations have been conducted on the applications of ECC in structural applications at the University of Michigan in the US, the University of Stellenbosch, the University of Tokyo, Kajima Corporation, and the Building Research Institute, Tsukuba City in Japan. These studies include the use of ECC/SHCC in shear elements subjected to cyclic loading, in mechanical fuse elements in beam-column connections, in shear wall retrofitting of R/C buildings; in R/C beams as durable cover for re-bar corrosion control, and in general concrete structural repair.

Other investigations on ECC and its applications are being planned in Denmark and Australia. To investigate the structural strength and ductility of reinforced beams under cyclic loads, PVA-ECC (with V_f = 2%) beams with conventional steel reinforcements (R/ECC) have been tested with four point off-set loading, with the mid-span subjected to fully reversed uniform shear load by Kanda et al.[6] .Varied parameters in the tests include the span/depth ratio and amount of shear reinforcement. Control specimens with ordinary concrete (R/C) of similar compressive strength (30 MPa) as the ECC were also tested. The

results of test show the double set of diagonal crack patterns in the shear span of the failed specimens. The R/ECC specimens reveal a much higher crack density, about four times that of the R/C specimens. Almost all cracks have opening less than 0.1 mm in the R/ECC compared with mm-size cracks in the R/C specimens.

The load-deformation envelope curves for the test specimens are summarized in Fig 1.3. It is concluded that by replacing plain concrete with ECC in the shear beam, load capacity increased by 50% and ultimate deformation by 200% under shear tension failure mode (comparing ECC-1-0 to RC-1-0), an load capacity increased by 50% and ultimate deformation remains the same under shear compression failure mode (comparing ECC-1-1 to RC-1-1). These observations and Fig. 1.3 suggest that R/ECC out-performs R/C in shear performance (load capacity, ductility and crack control). R/ECC beams behave in a ductile manner even without transverse reinforcement (but is further enhanced by combining ECC with transverse reinforcement), and remain ductile even for short span shear elements which

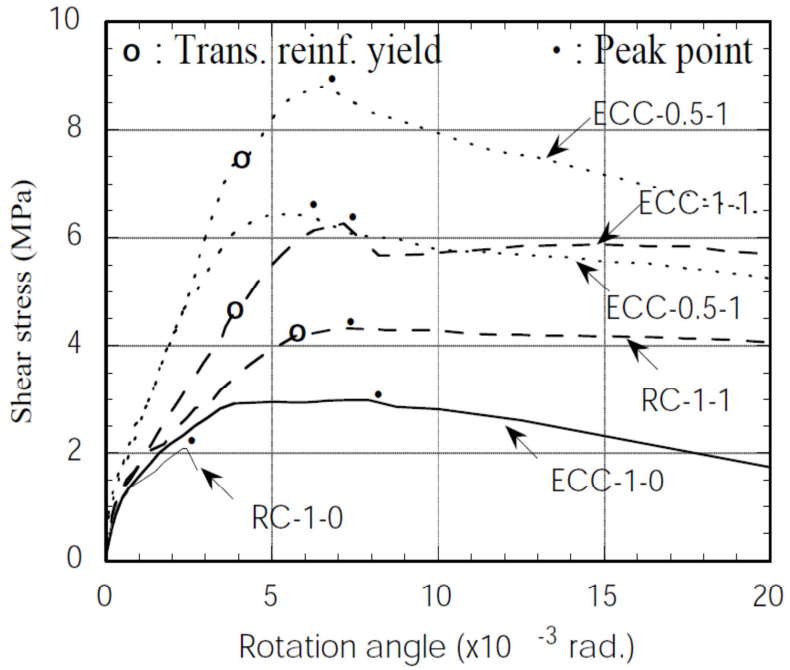

Fig. 1.3 Shear stress-relationship envelope curves for the various specimens each curve is labeled (Material-span/depth ratio-shear reinforcement%)[6)]

are known to fail in a brittle manner with normal concrete. This investigation establishes confidence in the application of ECCs in structural shear elements. The use of ECC in the hinging zone of a beam-column connection was investigated by Mishra[7]. Using normal detailing, it was found that the hysteretic loops were more full in the PE-ECC connection with many more load cycles sustained, resulting in a total energy absorption 2.8 times that of the R/C specimen. The cracking behavior was similar to those described above for the shear beam specimens. Because of the lower first crack strength of this ECC, the damage initiates inside the hinge zone as designed. This investigation suggests the potential of ECC to serve as a mechanical fuse in critical structural systems which may be subjected to severe earthquake loads.

The use of a PVA-ECC in precast shear panels for building wall retrofits is being investigated numerically by Kabele at el.[8] and experimentally by Kanda et al.[6]. Using a FEM simulation of rigidly jointed shear panels and a material constitutive model which captures the strain-hardening behavior of ECC, it is found that the PVA-ECC panel sustained much higher seismic load and deformation capacity in comparison with similar panels made with plain concrete. The ability of the ECC to relax the stress and redistribute the damage at the joints to the interior of the shear panel is responsible for the improved structural strength and ductility observed in the ECC panels. The prevention of localized fracture at the joint was also demonstrated in a shear test of a dry joint using steel bolt as shown in Fig. 1.4.

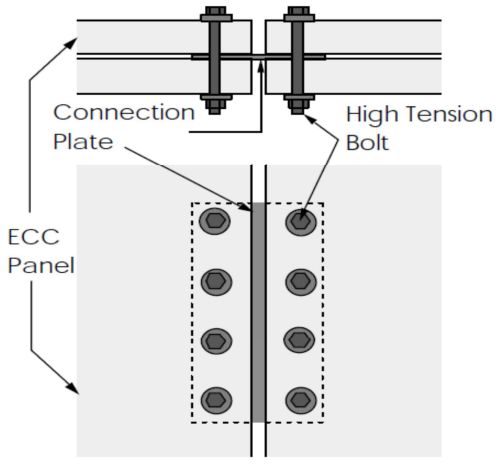

Fig. 1.4 Dry joint configuration[6]

The damage tolerant property of ECC prompted its application in the above mentioned dry joint. A critical test of this concept was conducted with indentation tests of steel plates on PVA-ECC slabs. The test was conducted for the assessment of maximum allowable bolt force used in the joint between panels for rapid on-site retrofit installations. Fig. 1.5 shows the test results. The maximum bolt force for the ECC slab was about double that of the control mortar slab, while the deformation capacity was almost one order of magnitude higher. The mortar failed by a brittle fracture mode given in Fig. 1.5 while a 'plastic' indent was observed for the ECC specimen. The superior damage tolerance of ECC further increases allowable bolt force due to high material reliability compared with mortar, thus enabling one to achieve high performance panel joint with simple details. Other potential applications apart from structural application studies briefly described above, ECC has also been investigated as a protective layer for enhancing the corrosion durability of R/C structures[9].

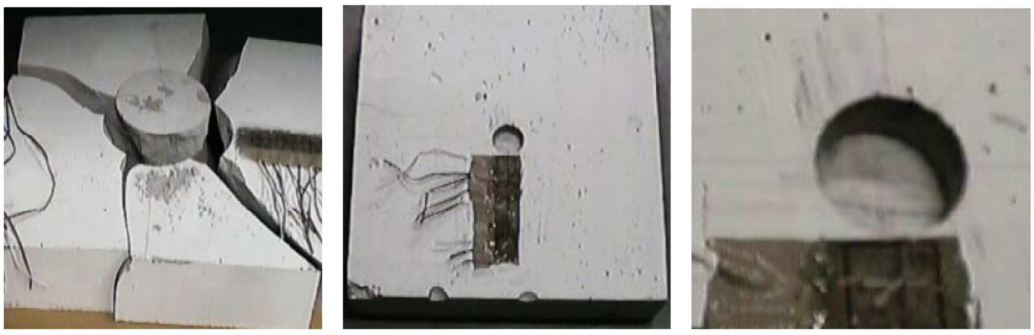

Fig. 1.5 Failure modes of a) Mortar slab b) PVA-ECC slab and c) Close up view near indent[6]

Infilled frames have been investigated by many researches during the last few decades. The frame structures incorporating infill walls have shown definite economic and performance advantages over conventional rigid-frame structure when structure are required to resist large lateral loads due to earthquake ground motion. Recently Kim et al.[10] has done research in this field. The objective of this study was to investigate the effect of ductility of SHCC and multiple cracking on seismic performance of infill walls subjected to displacement reversals.

In this respect, the research work has been reported under the state-of-the-art of the durability of fiber-reinforced strain-hardening cement-based composites (SHCC). This report has been compiled by the subcommittee on durability of RILEM Technical Committee 208-HFC[11]. This report covers research work on durability of SHCC from 2005-2009. During the recent past, the most remarkable research has been done by Wang et al.[12] in which the increase in durability of SHCC is investigated by using an integral water repellent cement-based matrix.

The fine cracks and anti-spall properties of the PE-ECC demonstrate the potential of this material in achieving the durability function. In addition, PE-ECC reveals a novel kink-crack trapping behavior when used as a repair material in concrete structures[13]. For this purpose, the bonded overlays are used in concrete and reinforced concrete repair and rehabilitate applications. Case studies have been performed by laboratory experiments and comparative FE analysis to verify and validate these models and the characterized parameters[14]. This behavior eliminates the deterioration mechanisms of delamination and spalling in the repair material commonly observed in repaired concrete structures. Some additional potential applications of ECC are in high energy absorption structures/devices, including short columns, dampers, joints for steel elements, and 8 connections for hybrid steel/RC structures. Structures subjected to impact or 3-D loading may also take advantage of the isotropic energy absorption behavior of SHCC, such as highway pavements, bridge decks, and blast-resistant building core elements. In addition, structures subjected to large deformations such as underground structures which need to conform to soil deformation and requires leak prevention, are also potential targets for SHCC applications.

Other applications of ECC being considered are in permanent formwork, extruded elements with structural properties, FRP reinforced concrete structures, and as a binder for radio-active waste treatment[15] for leaching control. These applications require a strong background of information of multiple cracking to understand the mechanism of mechanical behavior of SHCC under static and sustained loadings. For durability design of SHCC, a comprehensive numerical modelling tool is required so that the micromechanics of SHCC can be efficiently modelled to design structures with more efficient properties in future. The

present research is a contribution in the field of numerical modelling of micromechanical deformational behavior of SHCC especially for number of cracks, cracking strains and multiple cracking behavior under short-term and time-dependent loading.

1.4. Outline of Dissertation

A brief outline of the thesis is summarized below.

Chapter 1:
Introduction, problem statement, research significance and application.

Chapter 2:
Literature reviews

Chapter 3:
Static modelling of SHCC for uniaxial tensile loading by implementing trilinear function property in microplane model, modelling of crack width and crack distribution, verification of model with experimental data

Chapter 4:
Static modelling of SHCC for uniaxial tensile loading by using multi-layered microplane model, modelling of crack width and crack distribution, simulation of uniaxial compression behavior of SHCC by using microplane model and finally verification of model

Chapter 5:
Time-dependent modelling of SHCC for tensile creep and drying shrinkage by using multi-layered microplane model, modelling of time-dependent crack widths along with number of cracks, verification of model by experimental data

Chapter 6:
Conclusions and recommendations

Chapter 2
MECHANICAL BEHAVIOR OF SHCC

This chapter is a compilation of the knowledge that was useful during the course of present research and has been here with the view that some of the engineers and other researchers might not be familiar with this knowledge. This literature review proved very helpful for the present research.

2.1 Strain Hardening Cement-Based Composites

High-performance fiber-reinforced cementitious composites (HPFRCCs) are a group of fiber-reinforced cement-based composites which possesses the unique ability to flex and self-strengthen before fracturing. This particular class of concrete was developed with the goal of solving the structural problems inherent with today's typical concrete, such as its tendency to fail in a brittle manner under excessive loading and its lack of long-term durability. Because of their design and composition, HPFRCCs possess the remarkable ability to strain harden under excessive loading. In layman's terms, this means they have the ability to flex or deform before fracturing, a behavior similar to that exhibited by most metals under tensile or bending stresses. Because of this capability, HPFRCCs are more resistant to cracking and last considerably longer than normal concrete. Another extremely desirable property of HPFRCCs is their low density. A less dense and hence lighter material means that HPFRCCs could eventually require much less energy to produce and handle, deeming them a more economic building material. Because of HPFRCCs lightweight composition and ability to strain harden, it has been proposed that they could eventually become a more durable and efficient alternative to typical concrete.

HPFRCCs are simply a subcategory of ductile fiber-reinforced cementitious composites (DFRCCs) that possess the ability to strain harden under both bending and tensile loads, not to be confused with other DFRCCs that only strain harden under bending loads. Now a day this especial category is dealt with the name of ECC (Engineered Cementitious

Composites) or SHCC (Strain Hardening Cement-based Composites). ECC/SHCC is an easily molded mortar-based composite reinforced with specially selected short random fibers, usually polymer fibers. Unlike regular concrete, SHCC has a strain capacity in the range of 3–7% compared to 0.1% for ordinary portland cement (OPC). SHCC therefore acts more like a ductile metal than a brittle glass (as does OPC concrete), leading to a wide variety of applications[16].

Strain hardening, the most coveted capability of SHCC, occurs when a material is loaded past its elastic limit and begins to deform plastically as shown in Fig. 2.1. This stretching or 'straining' action actually strengthens the material. This phenomenon is made possible through the development of multiple microscopic cracks, opposed to the single crack/strain softening behavior exhibited by typical fiber-reinforced concretes. It occurs in SHCC as several fibers slip past one another. SHCC is cured under normal temperature. Therefore time-dependent deformation will occur.

One aspect of HPFRCC design involves preventing crack propagation, or the tendency of a crack to increase in length, ultimately leading to material fracture. This occurrence is hindered by the presence of fiber bridging, a property that most SHCC are specifically designed to possess. Fiber bridging is the act of several fibers exerting a force across the width of a crack in an attempt to prevent the crack from developing further. This capability is what gives bendable concrete its ductile properties[17].

Table 2.1 Example of mix proportion of SHCC

Water	**Cement**	**Fly Ash**	**Slag**	**Fine sand**	**Super-plasticizer**	**Viscous agent**	**PVA Fibers (Ductile type: 13 REC series)**
20.65%	20.65%	26%	5.17%	26%	0.51%	0.15%	1.25%

*Water/Binder Ratio= 0.4 and Aggregates/Binder Ratio = 0.5

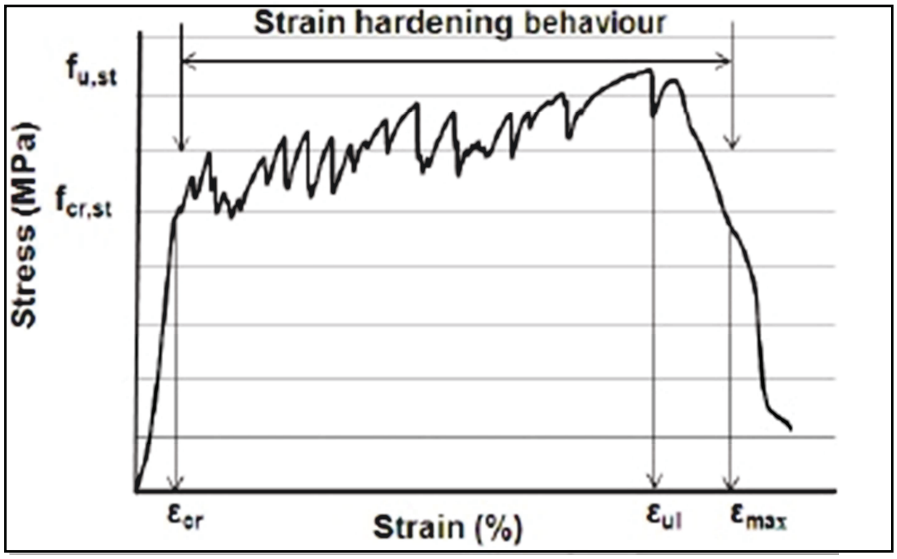

Fig. 2.1 Strain hardening behavior of PVA-SHCC, Zijl[17)]

The role of aggregate in the tensile mechanical behavior of certain types of SHCC has been studied intensely by Li et al.[18)]. It has been clearly demonstrated that the matrix strength, expressed by the first cracking strength σ_{fc}, and toughness, expressed by the crack tip toughness J_{tip}, are increased with increased sand contents. Thereby tensile ductility is reduced. It has been demonstrated theoretically that the ratio between the complementary energy J_b' of the fiber bridging stress-crack opening, to the matrix crack tip toughness must be larger than one for strain hardening, i.e., $J_b' / J_{tip} > 1$. However, the requirement for this ratio has been measured to be $J_b' / J_{tip} \geq 3$ for multiple cracking saturation, reflecting material variability not accounted for in theoretical models[19)]. However, the crack spacing is nearly doubled with this increase in aggregate contents.

The role of fly ash (FA) in the mechanical behavior of certain classes of SHCC has been studied by several researchers, i.e., Peled, Shah[20)] and Gao, van Zijl[21)]. The cement replacement with FA has been shown to reduce the matrix strength. It has been postulated that the fiber-matrix interfacial zone is modified, leading to improved fiber slip from the matrix instead of fiber breakage. In contrast, cement replacement with large quantities (up to 50% by mass) of groung granulate Corex slagment (GGCS), led to strong matrix, which in

turn led to higher SHCC tensile strength, but slightly larger crack spacing and crack widths[21].The typical mix proportion for SHCC is shown in Table 2.1.

2.2 Types of Fibers for SHCC

2.2.1 PVA (Polyvinyl Alcohol) fibers

High strength PVA fibers have been developed mainly for asbestos replacement. The fibers are produced by wet or dry spinning, and boron is added to achieve high strength and stiffness by forming intermolecular bonds. The fibers are surface treated to enhance their compatibility with matrix and to enable efficient dispersion. The surface treatment combined with the inherent affinity of this polymer for water, due to the presence of OH^- groups, leads not only to efficient dispersion, but also to a strong bond in the hardened composite.

PVA fibers are used in typical type of SHCC. PVA fibers tend to rupture instead of pull-out of a cementitious matrix, due to the strong chemical bonding and the resulting slip-hardening response during pull-out. Li et al.[22] were able to produce composites with an ultimate tensile strain exceeding 4% and a tensile strength of 4.5 MPa, with a fiber volume of only 2.0%. The specimens exhibited multiple cracking with crack widths at ultimate strain limited to below 100 μm. PVA FRC can be produced in number of ways, including premixing and shotcreting. Thin sheets, pipes and other shapes have also been produced using an extrusion process.

The alkali resistance of PVA fibers can be quite high (PVA fibers (Type-A), see appendix C) after immersion in a cement slurry at 80 ^0C for 14 days. This behavior is superior to fibers such as polyester and glass. The fiber is thermally stable, with no strength loss after exposure to temperature of 150 ^0C, and is insensitive to biological attack. This is reflected in the ageing performance of the composite, which shows no sign of reduction in strength as shown in Fig 2.2. However at the same time, the toughness of the composite was reduced, particularly within the first year of ageing. It has also been found that the PVA-cement composite has a better freeze-thaw durability[23]. The typical PVA fiber mechanical properties are given in Table 2.2.

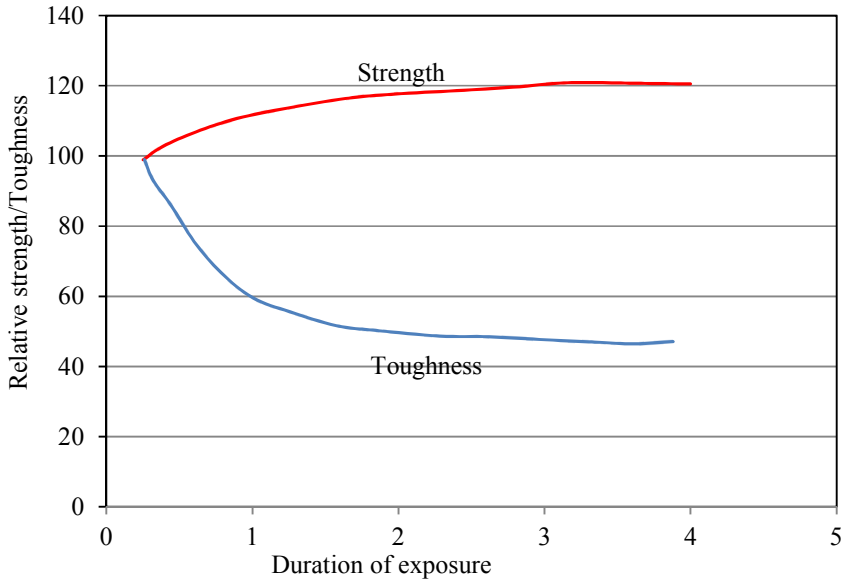

Fig 2.2 Effect of natural ageing on the retention of properties of PVA fiber-reinforced cementitious composite (Hikasa and Genba[24])

Table 2.2 Properties of high tenacity PVA fibers

Property	**Type of PVA fibers**	
	PVA (Type-A)[24]	**PVA (Avg)[25]**
Density (kg/m^3)	1300	1300
Diameter (μm)	10-40	10.4
Tensile strength (MPa)	1470	1200-1500
Modulus of Elasticity (GPa)	36.3	20-25

The different types of commercially available PVA fibers are shown in Fig. 2.3.

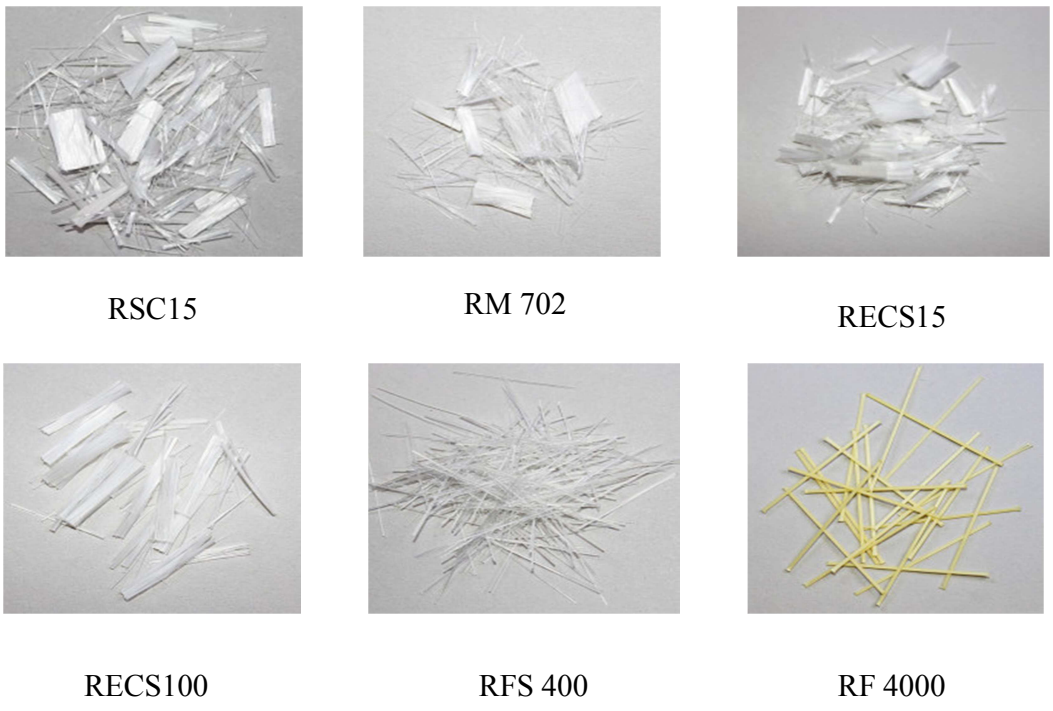

Fig 2.3 Types of different PVA fibers (Type-B)[26)]

2.2.2 Carbon fibers

Carbon fibers consist of tows, each made up of numerous (~10,000) filaments. The filaments are 7-15 μm in diameter, and consist of small crystallites of 'turbostratic' graphite, which is one of the allotropic forms of carbon. In the graphite crystal, carbon atoms are arranged in a hexagonal array in a plane. The planes are stacked together, with covalent bonds together. To obtain a high modulus and strength, the layered planes of graphite must be aligned parallel to the fiber axis as shown in Fig. 2.4. The two main processes for making carbon fibers are based on different starting materials, either polyacrylonitrile (PAN carbon fibers) or petroleum and coal tar pitch (pitch carbon fibers). Both processes involve heat treatments, and various grades of carbon fibers can be obtained with each, depending on the combination of heat treatment, stretching and oxidation[23)]. Typical properties are presented in Table 2.3.

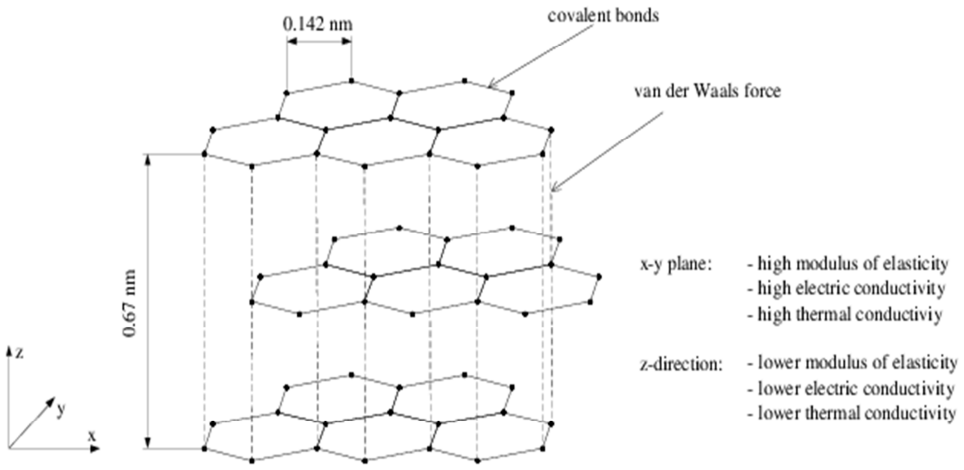

Fig. 2.4 Arrangement of carbon atoms in graphite layer[27)]

Table 2.3 Properties of carbon fibers.

Property	**PAN**		**Pitch**
	Type I	**Type II**	
Diameter (μm)	7.0-9.7	7.6-8.6	18
Density (kg/m^3)	1950	1750	1600
Modulus of Elasticity (GPa)	390	250	30-32
Tensile strength (MPa)	2200	2700	600-750
Elongation at break (%)	0.5	1.0	2.0-2.4

The PAN carbon fibers are of higher quality (and higher cost), and are sometimes classified into two types, I and II, with type I having a higher modulus of elasticity and strength. The pitch carbon fibers have a much lower modulus of elasticity and strength, but they are much less expensive than the PAN fibers. Nonetheless, the pitch fibers still have superior properties to most other synthetic fibers, and their modulus of elasticity is equal to or greater than that of the cement matrix. This, combined with their lower price, has made them more attractive for cement reinforcement. Mesophase (high modulus) pitch-based

carbon fibers are also new available, with properties generally intermediate between those of the other two types. The pitch fibers were developed in Japan and much of the work on using these fibers in FRC has been carried out[28].

The effect of mixing short carbon fibers, mainly of the pitch type, has been studied extensively, mostly using fibers less than 10mm in length. It appears that the tow disperses into individual filaments and so the aspect ratio of such fibers is quite high, more than 100, since the diameter of the individual filaments is about 10 μm. Thus, the reinforcing effect of these short fibers is quite high, even with volume contents less than 4%. Both pitch and PAN based fibers can greatly increases the tensile strength of the composites, as shown in Fig. 2.5. Carbon fibers lead to a slight increase in compressive strength up to fiber volume 3% as shown in Fig 2.6, after which the strength begins to decline, probably because of the difficulty in fully compacting high fiber volume materials. The load-deflection curves clearly indicate the marked improvement in flexural strength and post-cracking behavior achieved with carbon fibers[31].

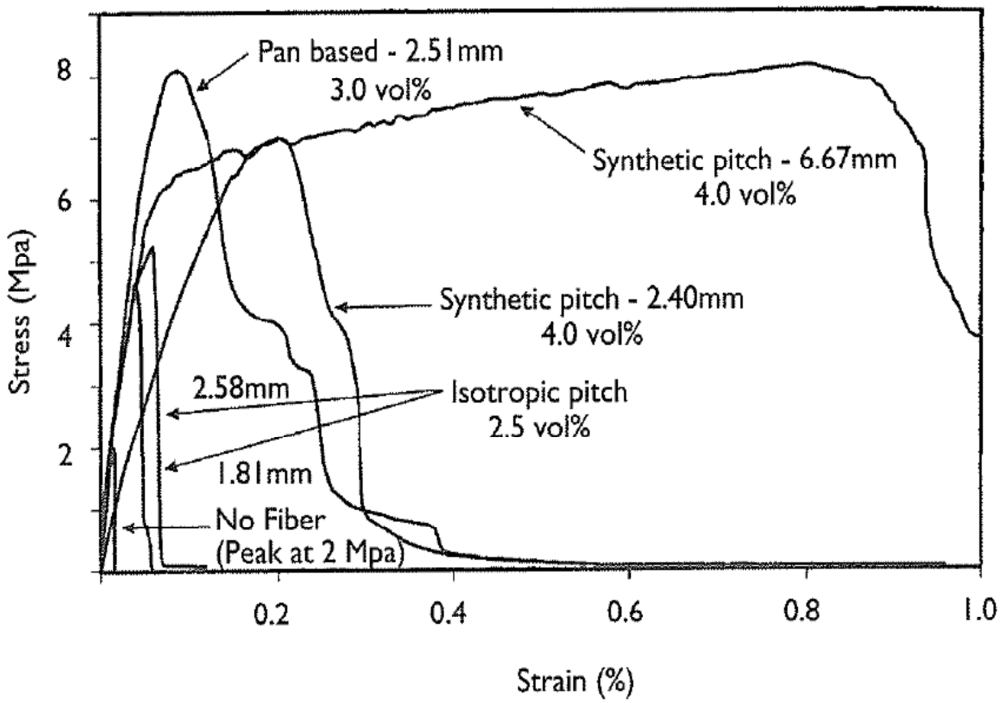

Fig. 2.5 Uniaxial tensile testing of carbon fiber reinforced cement.(Li and Obla[29])

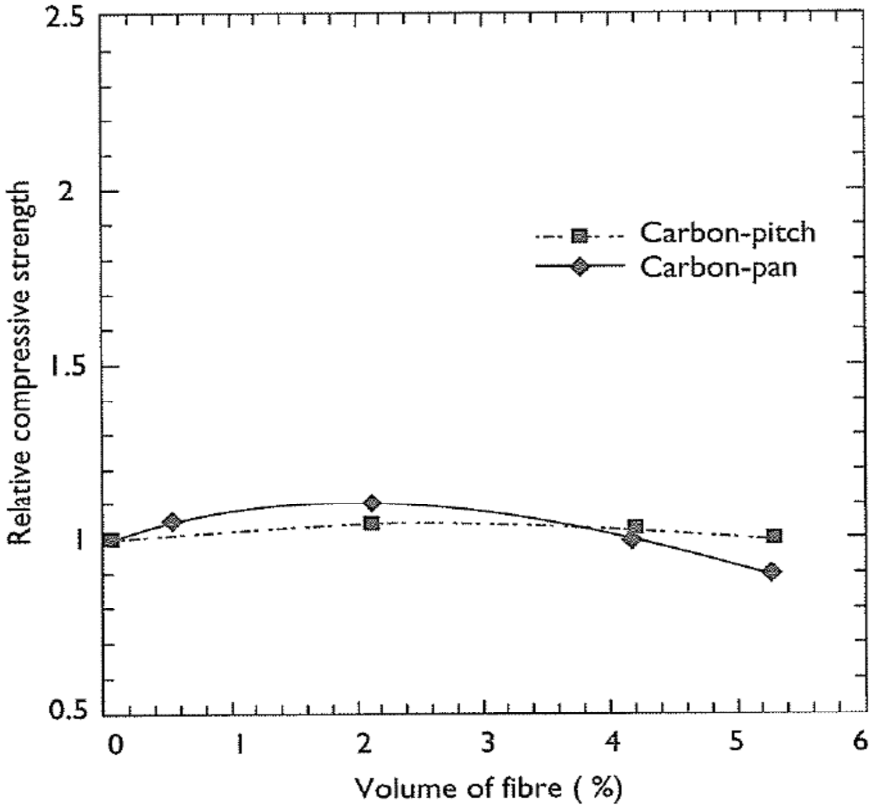

Fig. 2.6 Effect of carbon fiber content on compressive strength (Li and Mishra[30])

2.2.3 Aramid (Kevlar) fibers

Aramid is one of the first commercial polymeric fibers in which high strength and elastic modulus is achieved by chain alignment. It is an aromatic polyamide called poly (para-phenylene teraphtalamide). It is also known by the trade name Kevlar, given by the DuPont Company to its aramid fiber. The aromatic rings provide the molecule with rigidity, and in the production process these stiff molecules are aligned parallel to the fiber axis, thus leading to a modulus of elasticity which can be as high as 130 GPa. A fiber consists of planner sheets of molecules linked together by hydrogen bonding as shown in Fig 2.7 (a). The sheets are stacked together radially to form the fiber as in Fig. 2.7 (b). The bonds between the sheets are weak, and therefore the fiber has a low longitudinal shear modulus and poor transverse properties[23]. The properties of the fibers, and in particular the modulus of elasticity, depend on the degree of alignment as given in Table 2.4.

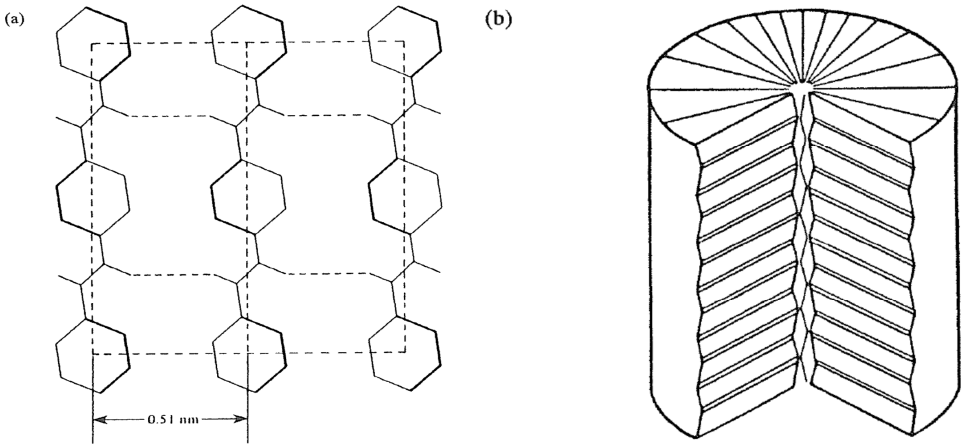

Fig 2.7 Structure of aramid fiber: a) planner array of the chain molecules, b) radial stacking of the planes in the fiber (Dobb at al.[32])

Table 2.4 Properties of aramid fibers.

Property	**Kevlar 49**	**Kevlar 29**	**HM-50**
Diameter (µm)	11.9	12	12.4
Density (kg/m^3)	1450	1440	1390
Modulus of Elasticity (GPa)	125	69	77
Tensile strength (MPa)	2800-3600	2900	3100
Elongation at break (%)	2.2-2.8	4.4	4.2

The properties of cement reinforced with aramid fibers have been studied in composites with short and randomly dispersed fibers, produced either by the spray technique or by premixing, with fiber contents in the range of 1-5% by volume. The general stress-strain curves show that these composites exhibit the usual characteristics expected on the basis of the ACK model, with the fiber reinforcement enhancing the ultimate strength and strain over the first crack strength and strain, leading to a tough composites[33]. The effect of fiber content and length shows the expected increase in flexural strength and toughness with these two parameters as shown in Fig. 2.8. The increase in fiber contents is, of course,

associated with a reduction in the flow properties of the fresh mix[34]. The increase in strength and toughness with aramid fibers are not always the same, with some studies showing greater effects than others. A much greater strengthening effect was reported, as expected, for continuous and aligned fiber reinforcement[35].

Treatment of the aramid fibers with polymers has been found to be an efficient way of increasing the flexural properties of the composites. It has been found that the tensile strength of the aramid composite is only 70% of the expected value, and suggested that this was the result of poor bonding[34]. The tensile creep of Kevlar fibers has also been studied and the bending creep of cementitious composites made with these fibers (2.4% by volume of short random 2-dimensioanlly dispersed fibers). The creep coefficient of the aramid fibers themselves has been found to be smaller than those of other synthetic fibers. The creep of the composite is of the same order of magnitude as that expected in a plain matrix[36].

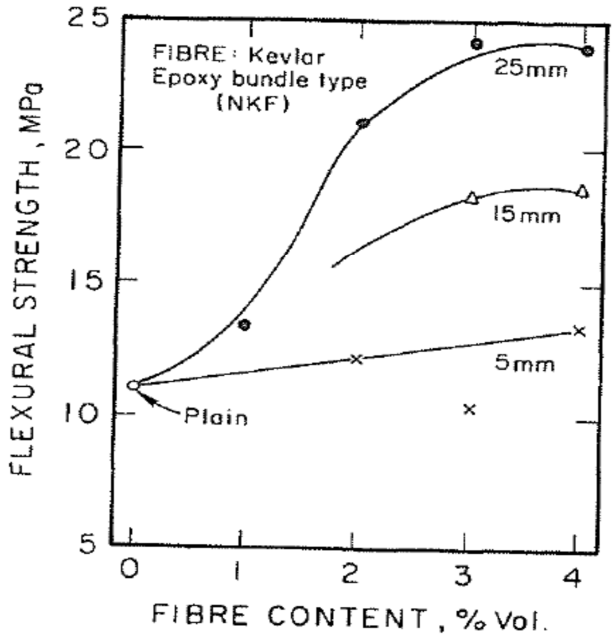

Fig. 2.8 Effect of fiber length and content on the flexural strength of mortars reinforced with aramid (Kevlar) fibers (Ohgishi et al.[34])

2.3 Behavior of Strain Hardening Cementitious Composites

The mechanical behavior of SHCC can be investigated under two major categories, i.e., short-term behavior and time-dependent behavior. These behaviors are described briefly in the following sections.

2.3.1 Short-term behavior of SHCC

The characteristic behavior of SHCC under monotonic tensile loading can be explained as microscopic defects trigger the formation of matrix cracks at first cracking strength. As the first crack forms, the fiber bridges the crack, transmitting tensile stresses across the crack surfaces. The applied load must be increased in order to force further crack formation. This leads to subsequent development of another crack at the second weakest cross-section. The scenario then repeats itself, resulting in a set of almost uniformly distributed cracks. The strain capacity is reached at the maximum load when the localization of the failure occurs. Due to moderate opening of a large number of fine cracks, a strain capacity of several percent can be observed.

This mechanism of SHCC under uniaxial tensile loading is observed by doing experiments using standard specimen dimensions and test set up. The geometry dimensions and test set up is shown in Fig. 2.9. A Zwick Z250 Universal Testing Machine has been used for the static tensile tests. The deformations are measured using 10mm HBM LVDT's fixed to an aluminium frame. The load is measured using 500kg HBM load cell. Typical dog bone shaped specimens are used for uniaxial tensile test. The specimens are cured for 14 days at $23\,^{0}C$ before testing. A thin layer of ground lime stone mixed with water is painted on the surface in order to aid with the crack observation. The relative humidity is maintained during test equal to 65%.

The phenomenon of multiple cracking and controlled crack width is also associated with uniaxial tensile stress-strain behavior. From the results of experiments on SHCC for

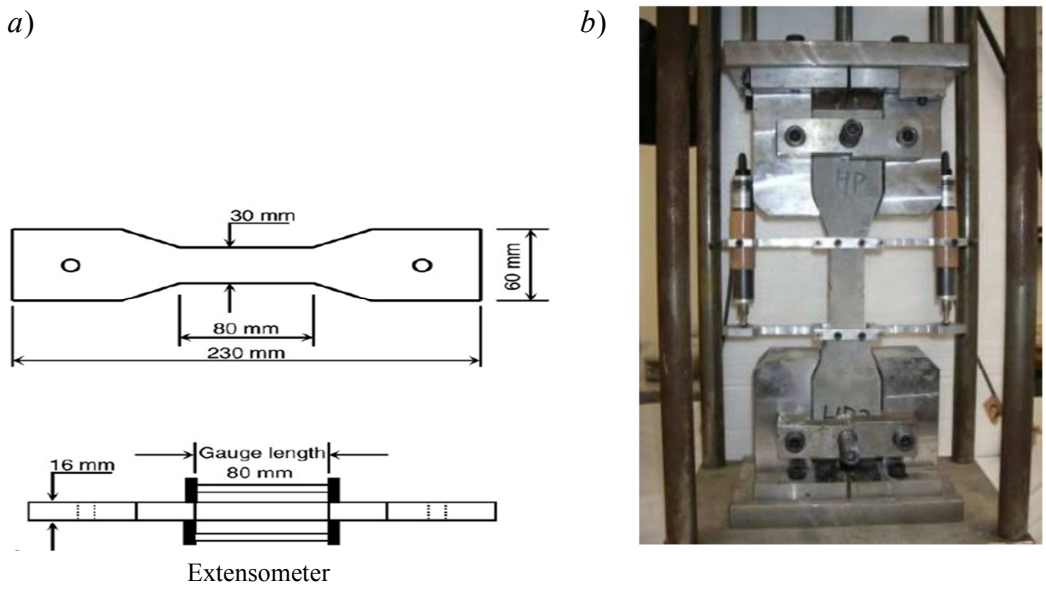

Fig. 2.9 a) Specimen geometry for uniaxial tensile loading b) Test set up for uniaxial tensile Loading[37)]

uniaxial tension, the numerical model has been presented by many researchers in the past decade for SHCC subjected to tensile loading. Han et al.[3)] and Vorel and Boshoff[38)] introduced the constitutive relations for SHCC based on the reproduction of experimental results obtained from test on bulk SHCC specimens. The derived formulas are adequate for use in structural analysis. However, the approach does not enable the analysis of the mechanism of material deformation behavior and failure depending on the specific micro-structural properties. The micro-structural properties such as multiple cracking and controlled crack widths are very important to predict the durability design of SHCC material especially when used as repair material.

For the representative volume elements of the material, Kabele[39)] defined the stress vs. strain relationship, which considered micromechanical phenomenon and further employed spatial averaging in order to link the scales of observation. He used the fiber-pullout description according to Lin et al.[40)]. One of the model has been presented by Jun and Mechtcherine[41)] in which the multi-scale modelling approach has been introduced. The pull out behavior of individual fiber is modelled by multi-linear approximation of the

experimental results while using statistics in order to describe the variance observed in the experiments. Fiber embedment length and inclination serve as the main parameters. The stress-crack-opening relationship for the individual cracks is derived from the concerted action of fibers involved in crack bridging. Subsequently, the joint response of individual cracks interconnected in series and the contribution of the uncracked matrix resulted in the overall stress–strain response of SHCC exposed to tensile loading.

In the field of numerical modelling, another remarkable research has been done by Vorel and Boshoff[42]. To model the specific behavior of SHCC in tension, the application of classical constitutive material models used for quasi-brittle materials is not straightforward. The proposed numerical model is based on a rotating crack assumption to capture the strain hardening and softening, the multiple cracking, the crack localization and multiple orthogonal crack patterns. A schematic representation of orthogonal cracking using the rotating crack model is shown using global and local axis in Fig. 2.10. In heterogeneous materials where micro-cracking occurs prior to the formation of a macro-crack, the rotating crack model may be more realistic than the fixed crack model.

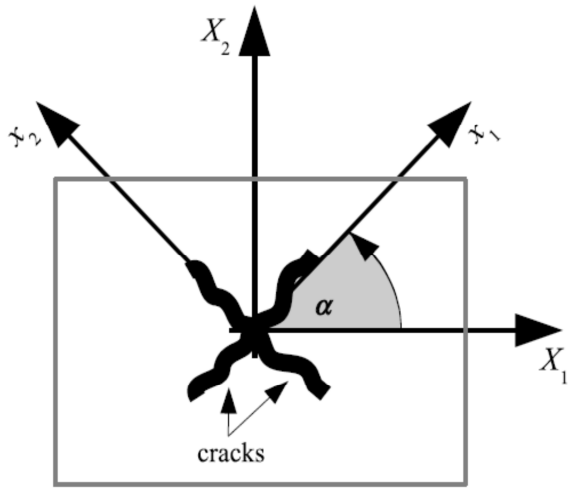

Fig. 2.10 Coordinates and transformation angle[42]

Micro-cracks are formed orthogonal to the major principal stress when the tensile strength is first violated. However, upon rotation of the principal stress axes new micro-cracks arise in the ‘‘rotated’’ direction and it is most likely that upon termination of the stress rotation, the latter micro-cracks will grow into macro-cracks. This justifies the choice of a rotating crack model from a physical perspective. A complete description of the rotating crack model can be found. The presented model is implemented in the open source finite element code OOFEM for plane stress elements using a coaxial rotating crack method (RCM) with two orthogonal cracks. This numerical approach is classified as the smeared crack model with the softening defined by means of the cohesive crack and overlapping crack model.

A stochastic approach is presented by Kabele[43] for the finite element modelling of multiple cracking in fiber reinforced cementitious composites. In this study, the multiple cracking behavior and failure of SHCC material in uniaxial tensile tests has been analyzed by means of stochastic finite elements, where material properties are assigned as random fields over the analyzed domain. Individual cracks are presented using the crack band approach. The effect of crack bridging provided by fibers is implemented by hardening-softening cohesive law. In this study a hypothesis has been proposed that the cited phenomenon can be attributed to material inhomogeneity which occurs on a large scale, for example due to uneven fiber dispersion or presence of spots with higher matrix porosity. This study lacks the information about number of cracks and crack spacing/distribution. It represents the macroscopic behavior (constitutive relationship).

2.3.2 Time-dependent behavior of SHCC

The mechanical behavior of cement-based material is highly time-dependent and rate-dependent not only for dynamic cases, but also in the quasi-static loading range, where inertia and wave effects are negligible. Creep is a well-known phenomenon in terms of continued deformation under sustained load. The most prominent micromechanical mechanisms of the time dependence are moisture migration at a low to medium load and micro-cracking at a high load. Heterogeneities in the microstructure cause stress peaks,

which may exceed inter-particular bond and has this micro-cracking as a result. In tension, the effect of the micro-cracking is worsened and will cause a sudden and brittle failure if the material is not reinforced [44].

Mihashi andWittmann[45] created method is commonly used whereby the time-dependent strain of a cement-based material under a sustained load is divided into three components, namely drying shrinkage, basic creep and drying creep. Drying shrinkage is the length change of an unsealed and unrestrained specimen in a climate controlled environment and basic creep is the length change of a sealed specimen under a constant load. Drying creep is the increased creep found when a specimen is loaded and allowed to dry as the combination of the drying shrinkage and the basic creep measurements are less than the total measured length changed.

In Fiber Reinforced Cement-based Composites (FRCC) the same time-dependent mechanisms act, while more are introduced in terms of fibers and the fiber-matrix interaction. Experimental studies on FRCC report conflicting findings on the effect of the fibers on creep and shrinkage. In order to appropriately apply SHCC in the construction industry, it is essential to understand and characterize its long-term behavior. The experimental results of rate-dependent tensile and flexural tests are reported as well as the uni-axial tensile creep of uncracked SHCC specimens. The results of shrinkage tests of SHCC are also reported[46].

The experimental work has been done for pre-cracked SHCC specimen to investigate tensile creep mechanism by Boshoff et al.[47] In this research, an important phenomenon related to time-dependent characteristics of SHCC has been identified, i.e., more cracks can initiate during the sustained tensile load. It has also observed that the tensile creep rate and magnitude increase after SHCC has cracked. An increase of creep strain rate was found. The source of widening of cracks has also been investigated by performing single fiber pull-out tests. The experimental program to investigate the source of the tensile creep behavior of cracked SHCC consisted out of three parts. Firstly, tensile creep tests were performed on cracked specimens at different load levels to investigate the influence of cracks on the

Table 2.5 Comparison of test set up for tensile creep and shrinkage of SHCC

	William P. Boshoff, Gideon P.A.G. van Zijl[46)]	W.P. Boshoff, C.J. Andendorff & G.A.P.G van Zijl[47)]
Size and shape of specimens	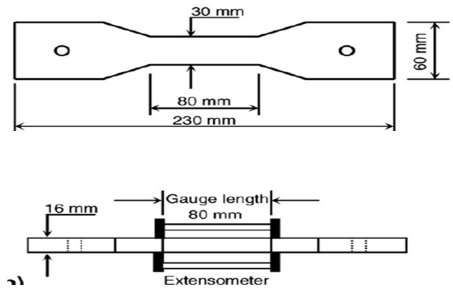 Fig. 2.11 The tensile creep test specimen	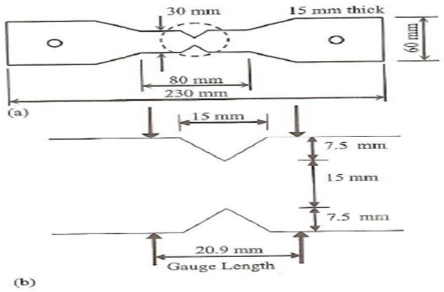 Fig. 2.12 The tensile creep test specimen notched at the mid of specimen
Number of specimens	Two specimens were tested for each creep and drying shrinkage test.	Six notched specimens were tested for creep test.
Environmental conditions	During curing and testing, the environmental temperature is kept 23°C and humidity 65 ± 5%.	During curing and testing, the environmental temperature is kept 23 ± 1°C and humidity 65 ± 5%.
Mix proportion	Water/binder ratio = 0.4 Aggregate/binder ratio = 0.5 PVA fiber (Ductile type:13 REC series)	Water/binder ratio = 0.4 Aggregate/binder ratio = 0.5 PVA fiber (Ductile type: PVA-RECS 15)
Sealing conditions for drying shrinkage test.	Specimens are protected using steel plate covers and stripped three days after casting.	Specimens are protected using steel plate covers and stripped three days after casting.
Strain measurement.	Strain of each specimen is measured with two LVDTs fixed to an aluminium frame.	Strain of each specimen is measured with two LVDTs fixed to an aluminium frame.
Loading conditions	The force acting on the specimens are calibrated by placing a HBM U2a 500 kg load cell in the position of specimen. Load is kept as high as 50% of the ultimate tensile load.	The force acting on the specimens are calibrated by placing a HBM U2a 500 kg load cell in the position of specimen. Load is kept as high as 60% of the ultimate tensile load.

	William P. Boshoff, Gideon P.A.G. van Zijl[46)]	W.P. Boshoff, C.J. Andendorff & G.A.P.G van Zijl[48)]
Test setup for drying shrinkage.	To measure drying shrinkage strain, specimens were allowed to dry with no axial constraint and length change was measured overtime. 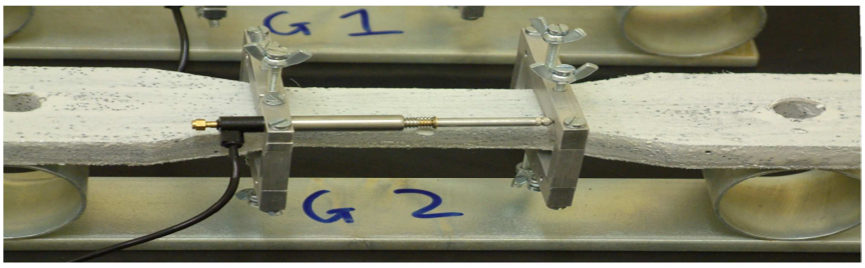 Fig. 2.13 Shrinkage test setup	
Test setup for creep.	The tensile creep tests were performed using a method of applying the load with free hanging weights acting with a level arm on specimens in series. 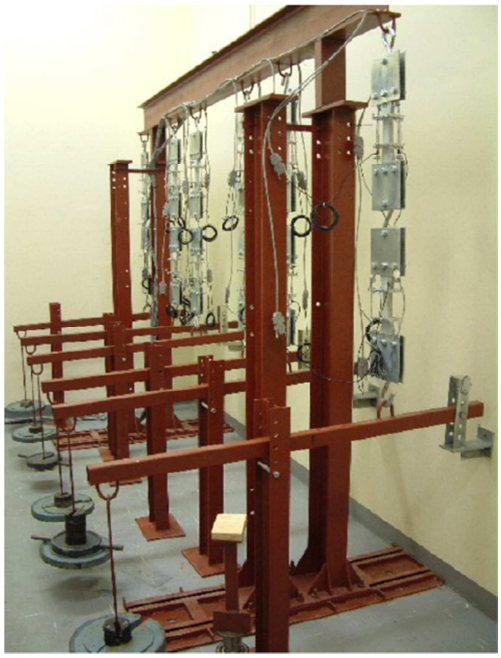 Fig. 2.14 Tensile creep setup	
Test duration	Total duration of test for creep and shrinkage is 8 months.	Total duration of test for creep and shrinkage is 16 days.

development of creep deformations. Secondly, pull-out creep tests were done on single fibers embedded in the SHCC matrix. Lastly, creep tests were carried out on single fibers to find the influence of fiber creep on the time-dependent behavior of SHCC. The same experimentation has been done for notched pre-cracked SHCC specimen[48].

2.4 Cracking Strain by Single Fiber Pull out

The main feature of HPFRCC in general and SHCC in particular is the formation of multiple cracking at increasing composite tensile stress. This behavior hinges on two complementary requirements; specifically the peak bridging stress $\sigma_{B,peak}$ exerted by the fibers at the cracked section must exceed the first cracking strength of the matrix σ_{fc}, i.e.

$$\sigma_{B,peak} > \sigma_{fc} \tag{2.1}$$

such that the applied stress prior to matrix cracking can be carried by the fibers after matrix cracking. Furthermore, at formation of a matrix crack, propagation must occur at constant ambient stress σ_{ss} and constant crack opening δ_{ss} (Fig. 2.15) in order to achieve a uniform cross-sectional stress distribution[49]. The latter condition can be expressed as an energy balance between the external work, the energy necessary to propagate the matrix crack, and the energy dissipated by the bridging fibers, i.e.

$$\sigma_{ss}\delta_{ss} = G_{tip} + \int_0^{\delta_{ss}} \sigma_B(\delta)d\delta \tag{2.2}$$

where G_{tip} is the matrix toughness and δ is the crack opening.

The combination of both conditions yields an upper limit for the matrix toughness G_{tip}

$$G_{tip} < \sigma_{B,peak}\delta_{peak} - \int_0^{\delta_{ss}} \sigma_B(\delta)d\delta \tag{2.3}$$

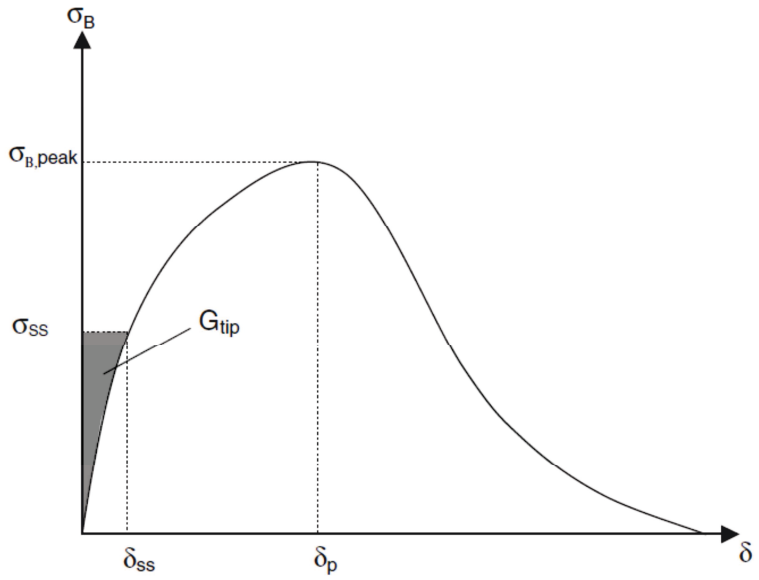

Fig. 2.15 $\sigma_B - \delta$ curve and parameters for composite strain hardening[49)]

The energy supplied at maximum fiber bridging stress $\sigma_{B,peak}$ and corresponding crack opening δ_{peak} reduced by the energy consumed in elastic fiber stretching and irreversible fiber pullout must be sufficient to accommodate steady state crack propagation, i.e. must exceed the matrix toughness at the crack tip G_{tip} .

The properties of the fiber and the fiber/matrix interface, characterized by the bridging stress/crack opening relationship ($\sigma_B - \delta$ curve), determine the opening of an individual crack at a given deformation state of the composite and subsequent temporary reduction in composite stress (Fig. 2.16). Prior to matrix cracking, the composite tensile stiffness E is essentially equal to the stiffness of the cementitious matrix and first cracking occurs when the ambient stress is sufficient to initiate propagation of cracking at the location of the largest matrix flaw (Fig. 2.17).

The instantaneous stress drop at formation of a crack corresponds to a reduction in elastically stored energy δU in the composite, as indicated by the area OAA0 (Fig. 2.16) equal to the energy consumed by crack formation W_m in the cementitious matrix as well as

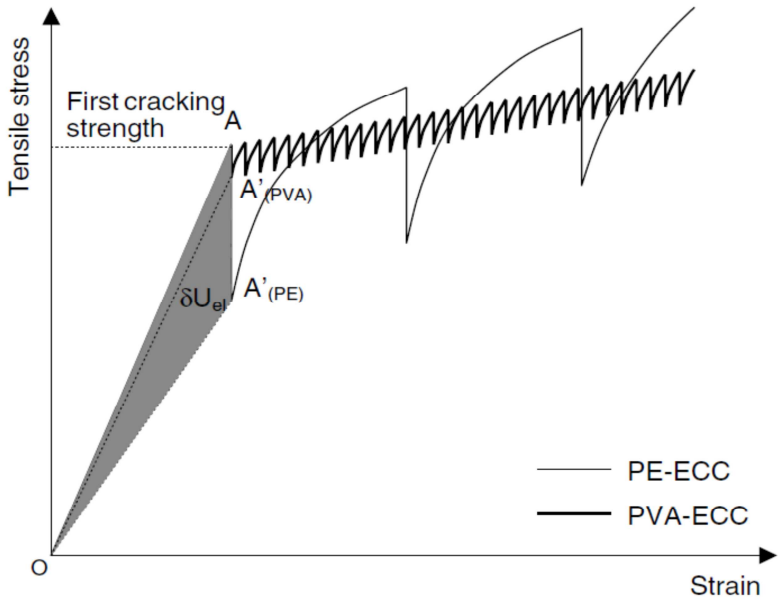

Fig. 2.16 Composite response at crack formation[50)]

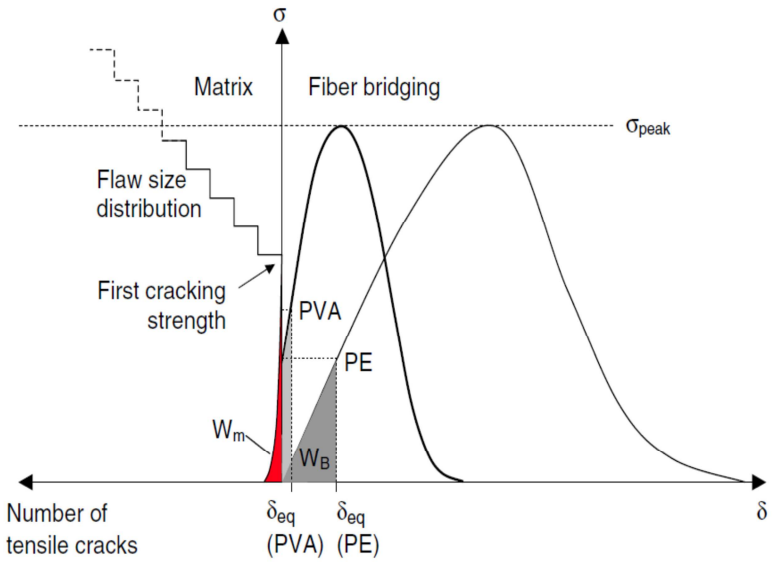

Fig. 2.17 Influence of constituents on composite crack formation[50)]

the sum of energy W_B stored in elastic fiber stretching and consumed by fiber pullout (Fig. 2.17). Assuming similar matrix toughness G_{tip} in PE-ECC and PVAECC, the shape of the

$\sigma_B - \delta$ curve largely influences the elastic energy reduction and magnitude of stress drop in the composite[50].

To investigate the cracking strain mechanism, the experiments on single fiber pull out were needed for SHCC. In this field many researchers have done the remarkable studies, i.e., Kabele et al.[51] and Jun[52]. The single fiber pull out tests have been performed[52]. In these tests, 12 mm long PVA fibers (Kuraray Co., Ltd., Kuralon KII REC15) with a specified diameter of 40 μm were used as dispersed reinforcement for the SHCC investigated. Single fibers were tested in order to provide their basic mechanical characteristics which are essential for the material modelling. Moreover, additional information was expected from this tension testing with respect to the behavior of fiber under cyclic loading. Still further, due to the specific test setup the results should help in interpreting the results obtained in the subsequent fiber pullout tests. Fiber was glued between two mounting plates of the testing machine using a commercially available adhesive for metals and plastic materials. Fig. 2.18 gives further details of the setup in use.

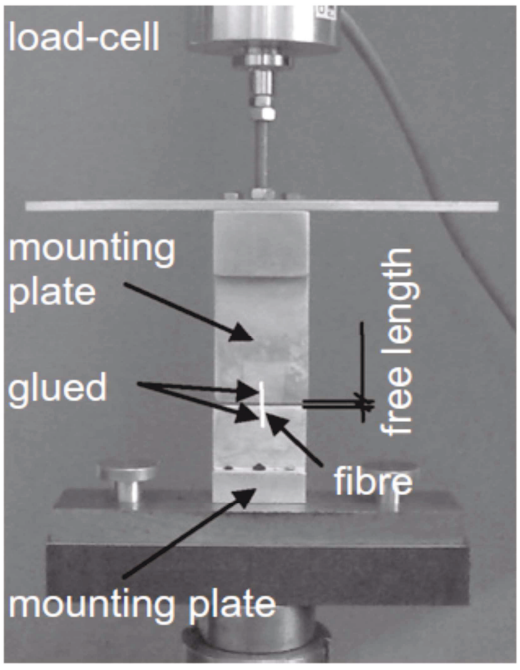

Fig. 2.18 Setup used for fiber testing, load cell and mounting plates of testing device[52]

Deformations were monitored both by measuring the machine cross head displacement and by evaluating the images obtained with a high-resolution camera with a macro-object lens. The photographs taken during the tests and evaluated using special software were used to find out if there is possibly an influence of imperfect gluing or the deformation of the load cell itself on the results observed. Fiber free length (between the glued ends) to be tested was set to 5 mm. Fig. 2.19 shows the details of specimen preparation for single fiber pull out.

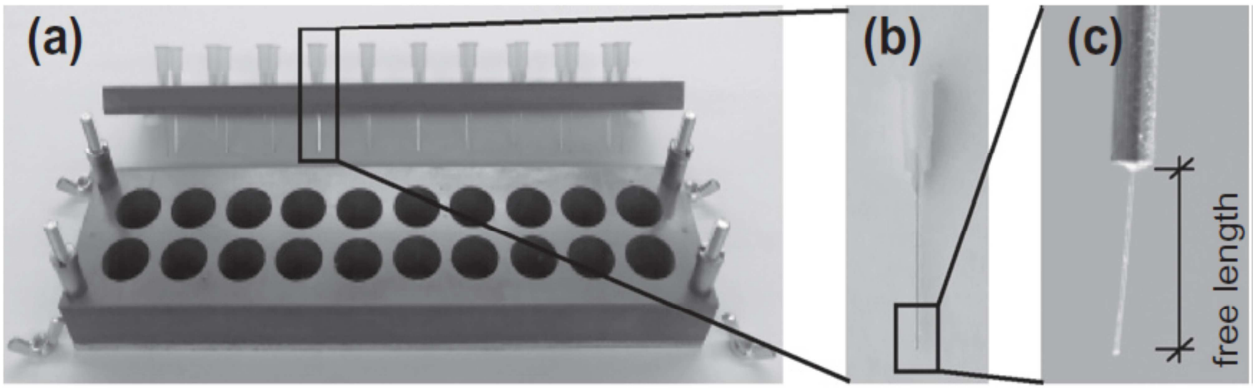

Fig. 2.19 Production of specimens for the fiber pullout tests: (a) mould and cannula frame, (b) single cannula, (c) detail of a fixed fiber[52)]

2.5 Equivalent Continuum Model of Multiple Cracking

The mechanical behavior of SHCC is mainly dependent on multiple cracking phenomenon under uniaxial tensile loading. In the past many researchers gave much focus to investigate the mechanism of multiple cracking for short random fibers and to model this behavior. The steady-state and multiple cracking of short random fiber composites were studied by Li and Leung[49)], based on a cohesive crack-mechanics approach. The first crack strength and strain are derived in terms of fiber, matrix and interface micromechanical properties. The conditions for steady-state cracking and multiple cracking are found to depend on two nondimensionalized parameters that embody all relevant material micromechanical parameters. The influence of a snubbing effect due to local fiber/matrix interaction for randomly oriented crack-bridging fibers on the composite properties is also studied.

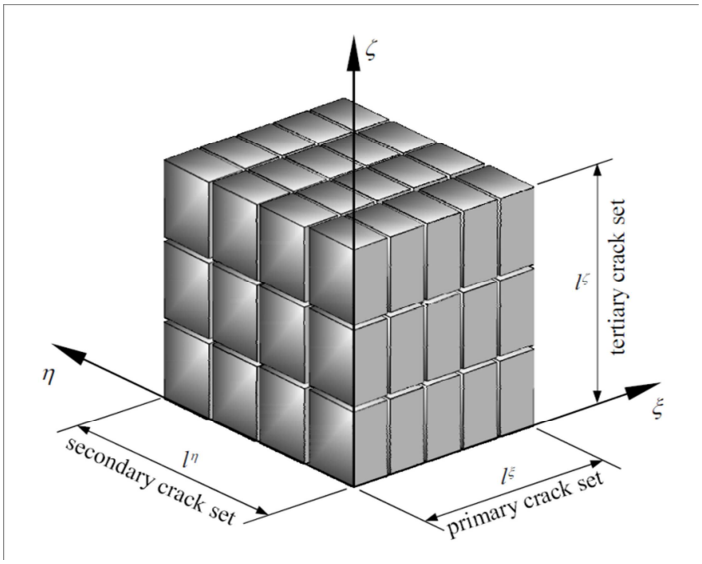

Fig. 2.20 Prismatic RVE with three orthogonal sets of multiple cracks[53)]

A constitutive model for a material (fiber reinforced cementitious composite) that exhibits multiple cracking is developed by Kabele[53).] The model represents a cracked solid as a continuum with identical macro-mechanical properties (equivalent continuum). The constitutive law of the equivalent continuum is obtained as the relationship between overall stress and overall strain of a representative volume element (RVE). The RVE is modeled as a solid element intersected by up to three sets of matrix cracks bridged by fibers as shown in Fig. 2.20 in which three RVE is presented in the form of three orthogonal sets of multiple cracks.

Micromechanics is employed to relate the opening and sliding displacements of these cracks to the tractions transmitted across the cracks by bridging fibers as shown in Fig. 2.21. It has been observed that the RVE can be modelled as a solid body intersected by the surface of discontinuity. These surface cracks shown in Fig. 2.21. The constitutive law is implemented into an FEM program, which is used to reproduce an experiment conducted on a shear beam. It is possible to identify a volume element, which contains numerous cracks, such an element is called a representative volume element (RVE).

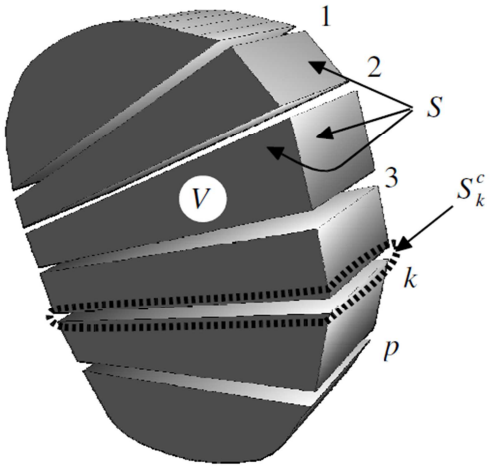

Fig. 2.21 Representative volume element of a material in multiple cracking state[53)]

Then it is acceptable and computationally convenient to idealize the structural member as one consisting of a homogeneous and continuous material (so-called equivalent continuum), whose macroscopic mechanical behavior is the same as that of real cracked material. To ensure this equivalence, the constitutive law of the equivalent continuum may be determined as a relationship between the overall stress and overall strain of RVE. These macroscopic quantities are defined as volume averages of corresponding local quantities taken over the RVE. The local stresses and strains are estimated through a mathematical model of the RVE, which captures the RVE's dominant micro-structures and micro-mechanisms of its deformation.

In this equivalent continuum model, the macroscopic strain corresponds to the average strain in the continuous material between cracks, while cracking strain represents the contribution to the total macroscopic strain due to cracks. The cracking strain vector depends on relative displacement vector of crack surfaces. The component of this vector, which is normal to the crack surface, is called crack opening displacement (COD) while tangential components are called crack sliding displacements (CSD) or crack slip.

2.6 CC3DNONLINEARCEMENTITIOUS 2 SHCC Material Model by ATENA V.5

The CC3DNONLINCEMENTITIOUS2SHCC is suitable for fiber reinforced concrete, such as SHCC (Strain Hardening Cementitious Composites) and HPFRCC or UHPFRC (high and ultrahigh performance fiber reinforced concrete) materials. The tensile softening regime and the shear retention factor are modified based on the model, proposed in KABELE[53] as shown in Fig. 2.22. This model is based on a notion of a representative volume element (RVE), which contains distributed multiple cracks (hardening) as well as localized cracks (softening)[54] as in Fig. 2.23.

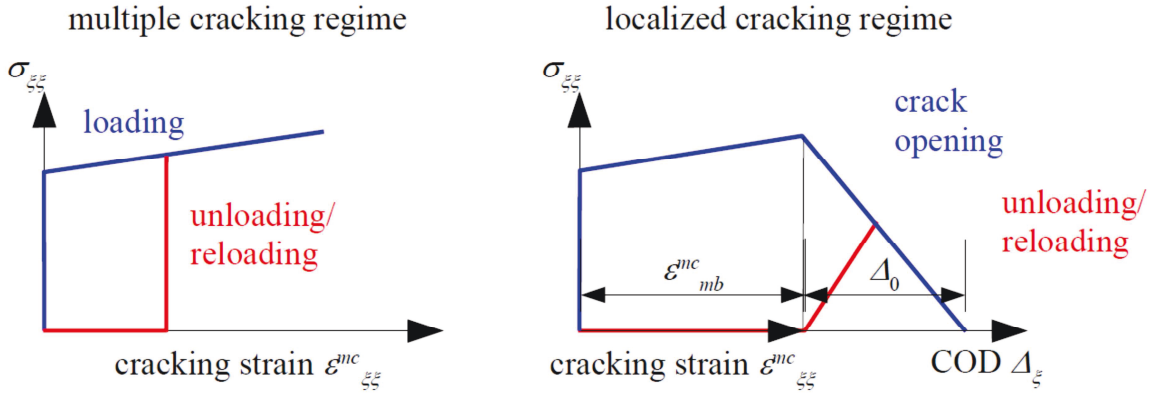

Fig. 2.22 Stress vs. cracking strain relations in crack-normal direction[54]

The basic assumptions for model for multiple cracking regime (hardening) are as follows

- A set of parallel planar multiple cracks forms when maximum principal stress $\sigma_{max}=\sigma_{fc}$ (first crack strength).
- Crack planes are perpendicular to the direction of σ_{max} (ξ-axis).
- The direction of a crack set is fixed.
- Secondary crack set may form in direction perpendicular to primary set if the maximum normal stress in the corresponding direction (η-axis) exceeds σ_{fc} .
- Cracks may slide if the direction of principal stress changes.
- Crack opening and sliding are resisted by fiber bridging.

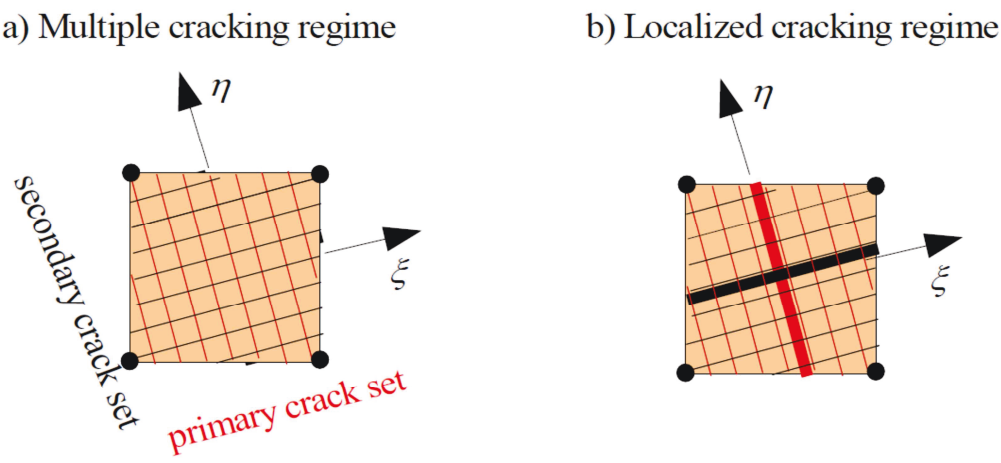

Fig. 2.23 Representative volume element with cracks[54)]

- Crack opening and sliding displacements are averaged over the RVE as cracking strains $\varepsilon_{ij}^{mc,\xi}, \varepsilon_{ij}^{mc,\eta}$ (notation: lower indices – components of tensor or vector, upper indices – multiple or localized crack mc, lc and association with primary or secondary crack dirction ξ, η)

The assumptions for model of localized cracking regime (softening) are as follows

- A localized crack forms within a set of multiple cracks if the corresponding normal cracking strain exceeds the level of $\varepsilon^{mc}{}_{mb}$ (cracking strain capacity, a material constant).
- Opening and sliding displacements of the $\Delta_i^{\xi}, \Delta_i^{\eta}$ localized cracks are treated by the crack band model (i.e. they are transformed into cracking strains $\varepsilon_{ij}^{lc,\xi}, \varepsilon_{ij}^{lc,\eta}$ by dividing them with corresponding band width $w^{\xi}{}_c$ or $w^{\eta}{}_c$).

The overall strain of the RVE is then obtained as a sum of strain of material between cracks (which may possibly contain nonlinear plastic strain due to compressive yielding), cracking strains due to multiple cracks, and cracking strains due to localized cracks:

$$\varepsilon_{ij} = \varepsilon_{ij}^{s} + \varepsilon_{ij}^{mc,\xi} + \varepsilon_{ij}^{mc,\eta} + \varepsilon_{ij}^{lc,\xi} + \varepsilon_{ij}^{lc,\eta} \tag{2.4}$$

where ε_{ij}^{s} represents the strain of the continuous material between cracks.

For crack opening model, the crack-normal stress components are related to cracking strains corresponding to opening of multiple and localized cracks by piecewise linear relations depicted in Fig. 2.22 (although linear hardening and softening are shown, a user should be allowed to input piecewise linear curves). Note that for multiple cracks, it is assumed that they do not close unless exposed to crack-normal compression (plasticity-like unloading) while a localized crack is assumed to close so that normal stress decreases linearly to reach zero at zero COD (these assumptions may need to be revised in the future to some combination of plasticity and damage-like closure). The model for crack sliding phenomenon is implemented by means of a variable shear retention factor[54).]

2.7 Microplane Model

A generalized microplane model for brittle-plastic heterogeneous materials such as concrete is presented by Bazant et al.[55).] This model describes not only tensile cracking but also nonlinear triaxial response in compression and shear. The constitutive properties are characterized separately on planes of various orientations within the material, called the microplanes, on which only few stress and strain components and no tensorial requirements need to be observed. These requirements are satisfied automatically by integration over all spatial directions. For integration over the surface of imaginary hemisphere, the Bazant and Oh[56)] 21-point integration formula is used which gives practically sufficient accuracy from calculations. The smaller number of points gives unacceptable results, especially in the strain-softening range. The position of these 21 integration points on spherical hemisphere is shown in Fig 2.24.

The state of each microplane is characterized by normal deviatoric and volumetric strains and shear strain, which makes it possible to match any Poisson ratio. The microplane strains are assumed to be the resolved components of the macroscopic strain tensor. This model presented involves many fewer free material parameters than the existing comprehensive macroscopic phenomenological constitutive models for concrete. The advancement in the microplane model resulted a series of microplane model from M1 to M7f.

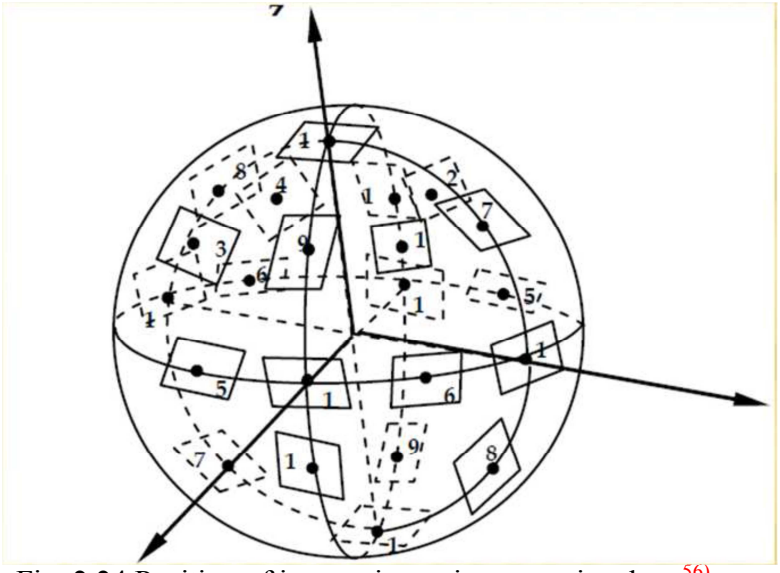

Fig. 2.24 Position of integration points on unit sphere[56)]

A number of further improvements are made in Model M4[57)] including a work-conjugate definition of the volumetric-deviatoric split, improved formulations of boundary surfaces, frictional yield limits and damage, sequential identification of material parameters by data fitting, and a capability to control various response features by material parameters. Formulation of a numerical algorithm, experimental calibration, and application examples are explained in this improved study. Two follow-up papers further extend model M4 to strain-rate sensitivity or creep and to arbitrarily large finite strain. The concrete creep behavior is incorporated in to Microplane model M4 for nonlinear triaxial behavior of concrete, including tensile fracturing and behavior under compression[58)]. In that context, the Maxwell chain is considered more effective than the Kelvin chain, because of the kinematic constraints of the microplanes used in M4. This study shows how to determine the continuous relaxation spectrum for the Maxwell chain, based on the solidification theory for aging creep of concrete.

The microplane modeling approach, which had already been successful for concrete, was shown capable of describing the nonlinear hardening–softening behavior and fracturing of FRC under not only uniaxial but also general multiaxial loading. The model M5f generalizes the previous model for concrete without fibers, the distinguishing feature of which is a series coupling of kinematically and statically constrained microplane systems.

This feature allows simulating the evolution of dense narrow cracks of many orientations into wide cracks of one distinct orientation. The crack opening on a statically constrained microplane is used to determine the resistance of fibers normal to the microplane as shown in Fig. 2.25. An effective iterative algorithm suitable for each loading step of finite element analysis is developed, and a simple sequential procedure for identifying the model parameters from test data is formulated[59]. The model allows a close match of published test data on uniaxial and multiaxial stress–strain curves, and on multiaxial failure envelopes.

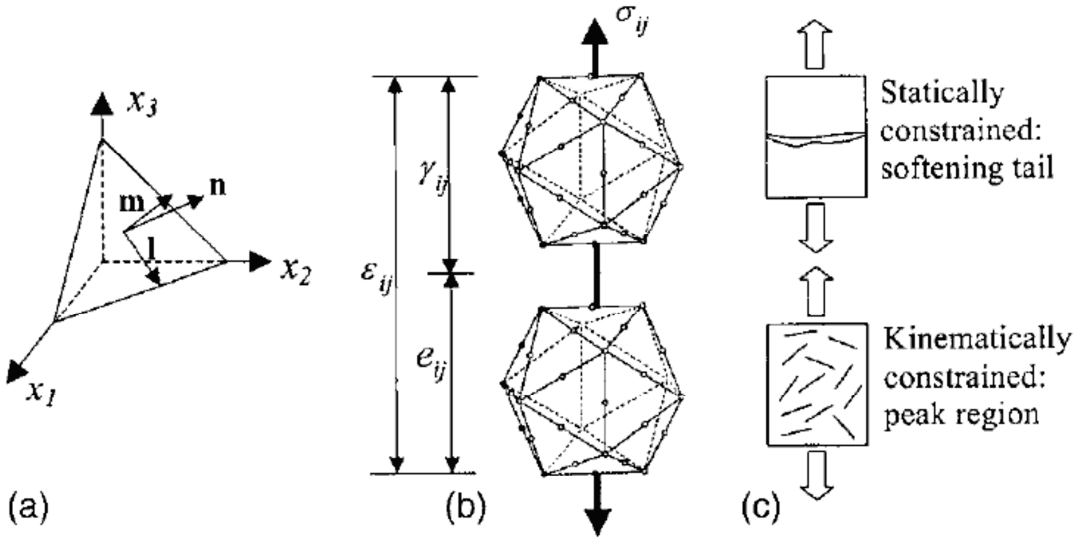

Fig. 2.25 a) Local coordinate system on a microplane; b) coupling of a kinematically and a statically constrained system in microplane Model M5; and c) main purpose of each microplane system in Model M5[59]

The microplane model M6f[60] for fiber reinforced concrete features several improvements over the earlier versions:

- An explicit volumetric-deviatoric split to no split transition formulation in tension which eliminates spurious contraction under tension that the earlier models suffered.
- Tension-compression load cycles are now correctly simulated using the loading/unloading rules prescribed in the transition function.
- A new micro- macro stress equilibrium equation in which the work of volumetric stresses on deviatoric strains and the work of deviatoric stresses on volumetric strains

are explicitly accounted for is introduced to correctly model the pressure sensitive dilatant behavior of low to normal strength concretes.

- The volumetric boundary is made a function of the maximum principal strain difference in addition to the volumetric strains, so as to extend the data fitting capability to lower strength concretes.
- The cohesion in the friction boundary now approaches zero linearly, instead of asymptotically with growing tensile volumetric strains, so as to generate an earlier decaying tail in the uniaxial tension and compression.

Model M7f[61)] is a new model for fiber reinforced concretes under static and dynamic loads. It includes a more realistic description of the fiber pullout and breakage along with an improved continuous dependence of the effect of fibers on the fiber volume fraction.
This improvement includes following three stages:

- The first stage is hardening one, where the stress is transferred to fibers gradually as crack forms in the matrix perpendicular to crack.
- In the second stage, as crack opens, the fibers nearest to the crack start pulling out, whereas the fiber away from the crack mouth are still hardening.
- The last stage of the fiber constitutive law describes the pullout of all fibers bridging the crack, which results in overall strain-softening.

The parallel coupling of fiber bridging and crack opening in the matrix explains the fluctuations observed in experimental data as well as the variations of the computed ultimate (failure) strain as a function of the fiber volume fraction in fiber reinforced concretes of various kinds.

A micromechanical constitutive relationship that can describe the mechanical behavior of fiber reinforced concrete is presented by Sumitro and Tsubaki[62)]. The constitutive properties are characterized separately on a microplane. The composite mechanical behavior which is affected by fiber ad concrete matrix properties of each microplane is modelled.

Several empirical parameters are summarized as function of fiber volume fraction and aspect ratio. This study can be used in a finite element analysis of SFRC.

The concept of multi-layers in terms of multi-laminate structure has been proposed by Pande and Xiong[63] for rocks in which a new framework for the development of constitutive models based on certain aspects of physical theories of plasticity is proposed. The resulting Multi-laminate model of clays has the same response as the critical state model provided no rotation of principal stress axes takes place during plastic flow. The influence of rotation of the principal stress axes on the volumetric and deviatoric plastic strains has been numerically evaluated. In undrained saturated, normally consolidated clays considerable excess pore pressure may build up due to rotation of the principal axes only.

Numerical studies of the collapse of footings indicate that significant rotations do not take place in this class of problems and consequently the collapse load is marginally reduced. In the continuation of the same research study the time-dependent behavior has also been studied for clays considering multi-laminate structure. In this study[64], a new model for rocks and rock-like material with multiple planes of weakness is proposed. The behavior of the assembly applies tensile and Mohr-Coulomb shear limits on each such plane with possible strain dependence of frictional properties. The visco-plastic algorithm which allows the incorporation of time effects is used to obtain static solutions. A generalization of the model to include arbitrary three-dimensional distribution of laminae in 'quasi-plane strain' is included. The effect of various flow rules adopted for plastic straining is indicated.

2.8 Applications of SHCC

ECC have found use in a number of large-scale applications in Japan, Korea, Switzerland, Australia and the U.S. These applications include:

- The Mitaka Dam near Hiroshima was repaired using ECC in 2003. The surface of the then 60-year old dam was severely damaged, showing evidence of cracks, spalling, and some water leakage. A 20 mm-thick layer of ECC was applied by spraying over the 600 m^2 surface[65].

- Also in 2003, an earth retaining wall in Gifu, Japan, was repaired using ECC. Ordinary portland cement could not be used due to the severity of the cracking in the original structure, which would have caused reflective cracking. ECC was intended to minimize this danger; after one year only microcracks of tolerable width were observed[66].
- The 95 m (312 ft.) Glorio Roppongi high-rise apartment building in Tokyo contains a total of 54 ECC coupling beams (two per story) intended to mitigate earthquake damage. The properties of ECC (high damage tolerance, high energy absorption, and ability to deform under shear) give it superior properties in seismic resistance applications when compared to ordinary portland cement. Similar structures include the 41-story Nabeaure Yokohama Tower (four coupling beams per floor)[67].
- The 1 km (0.62 mi) long Mihara Bridge in Hokkaido, Japan was opened to traffic in 2005 see Fig. 2.26. The steel-reinforced road bed contains nearly 800 m^3 of ECC material. The tensile ductility and tight crack control behavior of ECC led to a 40% reduction in material used during construction[68].
- Similarly, a 225-mm thick ECC bridge deck on interstate 94 in Michigan was completed in 2005. 30 m^3 of material was used, delivered on-site in standard mixing trucks. Due to the unique mechanical properties of ECC, this deck also used less material than a proposed deck made of ordinary portland cement. The University of Michigan and the Michigan Department of Transportation are monitoring the bridge in an attempt to verify the theoretical superior durability of ECC; after four years of monitoring, performance remained undiminished. The researches in this field have been done by Li et al.[69] and Lepech and Li[70].
- The first self-consolidating and high-early-strength ECC patch repair was placed on Ellsworth Road Bridge over US-23 in November 2006 as shown in Fig. 2.27. The high-early-strength ECC can achieve a compressive strength of 23.59 ± 1.40 MPa

(3422.16 ± 203.33 psi) in four hours and 55.59 ± 2.17 MPa (8062.90 ± 315.03 psi) in 28 days, allowing for fast repair and re-opening the session to traffic. The high-early-strength ECC repair has shown superior long-term durability in field conditions compared to typical concrete repair materials. The researches for this application have been carried out by Li et al.[71] and Li[72].

Fig. 2.26 Mihara Bridge, Hokkaido[73]

Fig. 2.27 Ellsworth Road Bridge[74]

Chapter 3

MODELLING OF SHCC BY MICROPLANE MODEL WITH TRI-LINEAR TENSION PROPERTY

3.1 Introduction

The strain hardening cementitious composites is the material which exhibits strain-hardening, quasi-ductile behavior due to bridging of fine multiple cracks by short, randomly distributed polymer fibers. The strain hardening is followed by the phenomenon of multiple cracking which can be simulated along with crack spacing/distribution and number of cracks by uniaxial tensile stress-strain relationship of material. The fiber pull out displacement are attributed to crack width development of SHCC. To model the crack widths the bridging fiber stiffness is an important parameter considered in the present model.

The constitutive relationship for SHCC under monotonic and cyclic tensile loading has been derived by Jun and Mechtcherine[75]. In this study, the constitutive relationships are developed on the basis of a multi-scale modelling approach which considers the determining physical phenomena observed in experimental investigations. The multi-scale model is based on reproducing the fiber-pull out behavior under monotonic loading by multi-linear approximations while statistics are used to describe the variation of the results as observed in the experiments. Hence for simulating the stress-strain relationship for uniaxial tensile loading, the multi-linear concept is implemented.

A similar kind of research has been done by Vorel and Boshoff[76] in which a constitutive model for SHCC has been developed that can be used to simulate structural components with SHCC under different types of loading conditions. The material response

for virgin loading in tension is defined by means of total effective strains for the ascending branches and as a cohesive crack for the softening part to ensure the proper energy dissipation. The elastic part is assumed to be linear, the hardening branch is Hermite polynomial function and the softening is described by the power function.

In the present study, the constitutive stress-strain relationship under uniaxial tensile loading for SHCC is derived by tri-linear function using microplane model. The microplane model is a generalized model for brittle-plastic heterogeneous material such as concrete which describes not only tensile cracking but also nonlinear triaxial response in compression and shear. In microplane model, the constitutive properties are characterized separately on planes of various orientations within the material, called the microplanes. Kinematic constraint is used on these microplanes, i.e., the total strain vector on each microplane (crack) is assumed to be resolved component of the macroscopic strain tensor while the fibers are assumed to be directed to normal to each microplane. The state of each microplane is described by normal deviatoric and volumetric strain and by shear strain (further split into two orthogonal components)[81]. The microplane model is selected for the present research due to some significant advantages as compared to the previous classical tensorial models. These advantages can be summarized as follows:

- The constitutive law is written in terms of vectors rather than tensors. The modeler need not to worry about tensorial invariances because it is automatically satisfied by combining the responses from microplanes of all possible orientations.
- The microplane model can be applied for general multiaxial loading conditions of the material such as concrete and rock with microcracks in various directions.
- The inelastic physical phenomenon associated with surfaces, such as the slip, friction, tensile cracking, lateral confinement on a given plane or its spreading can be characterized directly in terms of the stress and strain on the surface on which they take place. This contrasts with the previous tensorial models in which a relation between the invariants and is regarded as friction although it is only a poor overall measure of friction that is unable to capture frictional slip on any particular plane.

- The microplane model is equivalent to infinitely many simultaneous (active or inactive) loading surfaces of all possible orientations, at least one for each microplane. This enables the model to automatically capture the apparent deviations from normality.
- A vast number of combinations of loading or unloading on various microplanes are possible and some microplanes even unload for monotonic loading on the macroscale. This is an important source of path dependence in the microplane model, and allows a simple yet physically realistic representation of the Bauschinger effect at reverse loading and of hysteresis under cyclic loading.
- With the microplane approach, anisotropic materials can also be modelled. It suffices to use either orientation dependent model parameters or an orientation dependent weight function in the integral expression for the virtual work on the micro-level.
- The inherent conceptual simplicity of the model, gained by dealing with stress and strain components rather than tensors and their invariants, facilitates understanding. This is important since modelling of complex materials is as much an art as a science.
- Due to conceptual simplicity, one advantage of using microplane model is that the material can be described by fewer material parameters and the constitutive relationship can be modified based on behavior of material.

The given stress-strain relationship is quantified for the crack spacing and number of cracks by following strength criterion which shows a good agreement with experimental data. The results will be presented later in the chapter. The crack spacing/distribution needs careful attention in the field of modelling. SHCC shows a unique fine and multiple cracking behaviors. In the present study, the more focus has been given to model multiple cracking of SHCC.

3.2 Model Description

3.2.1 Tri-linear function of SHCC to model uniaxial tensile loading

The present model is based on work of Bazant and Gambarova[77]. In the present microplane model for SHCC, the constitutive properties are characterized separately on

planes of various orientations within the material, called microplanes. Kinematic constraints are used on these microplanes, i.e., the total strain vector on each microplane is assumed to be resolved component of the macroscopic strain tensor. In the present study, only the normal component of strain considered for simplicity which can be defined as equal to resolved macroscopic strain tensor for the same plane as shown in Fig. 3.1.

For this analysis, there is need to define the constitutive law for the microplanes relating normal stress σ_n and normal strain ε_n. Normal stress as function of normal strain

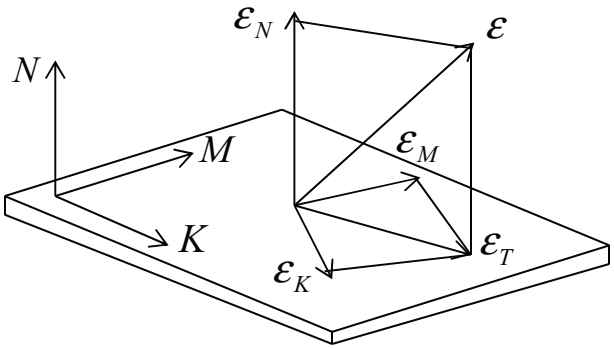

Fig. 3.1 Strain components on microplane

must rise first elastically and then reach to first cracking strength σ_{cr}. For SHCC, the statistical variation is assumed for fiber volume as tensile strength of SHCC is considered directly proportional to fiber volume. Hence the subsequent multiple cracks are produced at the least tensile strength of material causing increase in tensile load up to maximum tensile strength σ_t corresponding to strain ε_t. After maximum tensile strength, the softening starts due to rupture/debonding of fibers and strain reaches up to ultimate strain ε_u as shown in Fig. 3.2. The overall stress-strain relationship can be divided in to three parts: elastic behavior, strain hardening behavior and softening behavior. Each behavior is simulated by using linear relationship. The strain hardening behavior is accompanied by multiple cracking is a function of equivalent tangential fiber bridging stiffness which follows statistical variation with uniform distribution.

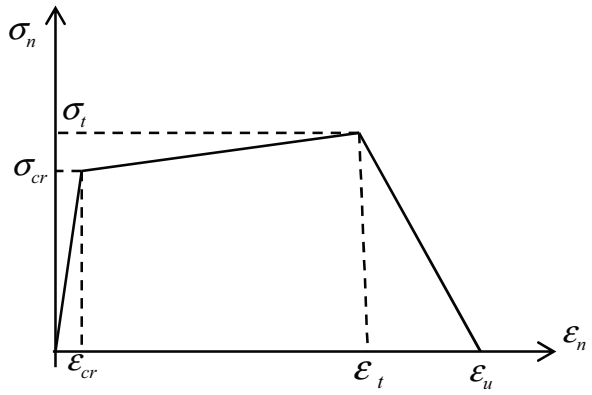

Fig. 3.2 Schematic diagram of uniaxial tri-linear behavior of SHCC

The stress-strain relationship to use in constitutive relationship based on tri-linear function of SHCC is explained in Eq. 3.1

$$\sigma_n = \begin{cases} E_o \varepsilon_n & \varepsilon_n \le \varepsilon_{cr} \\ \left(\dfrac{\sigma_t - \sigma_{cr}}{\varepsilon_t - \varepsilon_{cr}} \right) \varepsilon_n & \varepsilon_{cr} < \varepsilon_n \le \varepsilon_t \\ \left(\dfrac{\sigma_t}{\varepsilon_u - \varepsilon_t} \right) \varepsilon_n & \varepsilon_n > \varepsilon_u \end{cases} \tag{3.1}$$

where E_0 is the initial elastic modulus of the material. σ_{cr} is the first cracking strength of material, σ_t is the maximum strength, ε_{cr} is the first cracking strain, ε_t is the strain at maximum tensile strength, ε_u is the ultimate tensile strain. The detailed derivation for the microplane equations used in the presented model for incremental stiffness and stress-strain relationship for each microplane are explained by work by Bazant and Gambarova[77]. The basic microplane equations for incremental stiffness and stress-strain relationship is given as follows

$$\Delta \sigma_{ij} = D_{ijkm} \Delta \varepsilon_{km} \tag{3.2}$$

where $\Delta \sigma_{ij}$ is the incremental normal stress, $\Delta \varepsilon_{km}$ is the incremental normal strain and D_{ijkm} is the stiffness tensor that can be evaluated as

$$D_{ijkm} = \frac{3}{2\pi} \int n_i n_j n_k n_m C_N f(\vec{n}) ds \tag{3.3}$$

In Eq. 3.3, $n_i n_j n_k n_m$ are the direction cosines, C_N is the normal secant modulus of SHCC and $f(\vec{n}) = 1$ is a weight function of the normal direction that can introduce anisotropy in its initial state.

3.2.2 Crack width model

To model crack width, the equivalent tangential fiber bridging stiffness is calculated that is equal to slope of strain hardening part of tri-linear stress-strain curve of SHCC. This is done by using a certain multiplying coefficient as whole of the fiber stiffness is not transferred to the cracked part practically. Therefore, the total stiffness of the material in terms of equivalent fiber bridging stiffness can be calculated as

$$k = \frac{k_{mf}}{N} \tag{3.4}$$

where k_{mf} is the equivalent tangential fiber bridging stiffness and N is the number of cracks obtained from experimental data. Hence the crack width can be calculated in strain hardening zone as

$$w_i = c_i l (f_{ti} / k_i) \tag{3.5}$$

where f_{ti} is the tensile strength of *i*-th crack, k_i is the stiffness of *i*-th crack and c_i is the coefficient to balance the stiffness transfer from cracked to uncracked part and l is the length of specimen.

3.2.3 Crack spacing/distribution model

The multiple cracking of SHCC can be modelled by introducing multilayers in microplane model. For this purpose, simplified assumptions closer to real scenario are considered for simplifications, i.e.,

a) All of the multiple cracks occur at the same time at the beginning of cracking. This resulted in formation of potential cracks when stress is equal to first cracking strength.
b) All of the cracks open in the same way.
c) The number of cracks is obtained from experimental data.
d) The visible cracks appear at the equal interval of global strain as shown in Fig. 3.3.

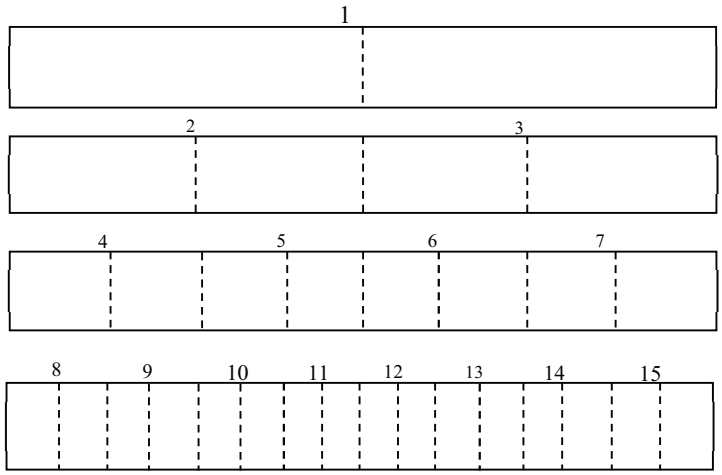

Fig. 3.3 Multiple cracking (visible) under uniaxial tensile loading.

The number of multiple cracks are taken from experimental data or can be estimated by the crack spacing calculated by Lee et al.[100]. The crack spacing can be estimated knowing the length of fibers used for SHCC as follows:

$$x'_{\theta} = \frac{1}{2}(L_f - \sqrt{L_f - 2\pi L_f x'}) \tag{3.6}$$

$$x' = \frac{V_m}{V_f} \cdot \frac{\sigma_{mu} d_f}{4\tau_0} \tag{3.7}$$

where L_f is the length of fiber V_m and V_f are the volume of matrix and fiber respectively. σ_{mu} is the matrix ultimate strength, d_f is the diameter of fiber and τ_0 is the interfacial bond strength. Fig. 3.3 shows the crack distribution/spacing model for multiple cracking under uniaxial tensile loading of SHCC. The dash lines represent the visible (potential) cracks along the length of specimen. The number on the crack lines shows the sequential position of multiple cracking along the length. This sequence continued till the critical crack spacing for SHCC reaches. At this stage, localization starts and softening occurs.

3.3 Comparison of Analytical Results with Experimental Data for Uniaxial Tension

For the verification purpose, the work by Zijl[78)] is used for uniaxial tensile loading test data. The properties of SHCC mix are given in Table 3.1. The simulation based on first cracking strength and maximum tensile strength of the material and corresponding strains. The more emphasis has been given to the strain-hardening region of material as compared to softening part. The initial elastic modulus is attributed to initial elastic behavior of SHCC up to first cracking strength. By using the tri-linear tensile property of SHCC in microplane model, the stress-strain relationship is modelled. The microplane parameters are selected as initial stiffness equal to 11640 MPa and Poisson's ratio equal to 0.20. The value of coordinates of tri-linear function for normal stress and strain are first taken from experimental data and then adjusted to fit the curve by trial and error. This can be done by using a multiplier for stresses that is equal to 2.8 for modelling of presented data values. The verifications results are shown in Fig.3.4. The adjusted values of parameters used in this model are listed in Table 3.2. which represents a satisfactory data fits for the experimental data. The initial stiffness is used to simulate the elastic behavior of material. After the first cracking stress, the first cracking strain, first cracking stress, maximum tensile strain and maximum tensile stress are the parameters that control the strain hardening and multiple cracking behavior of SHCC.

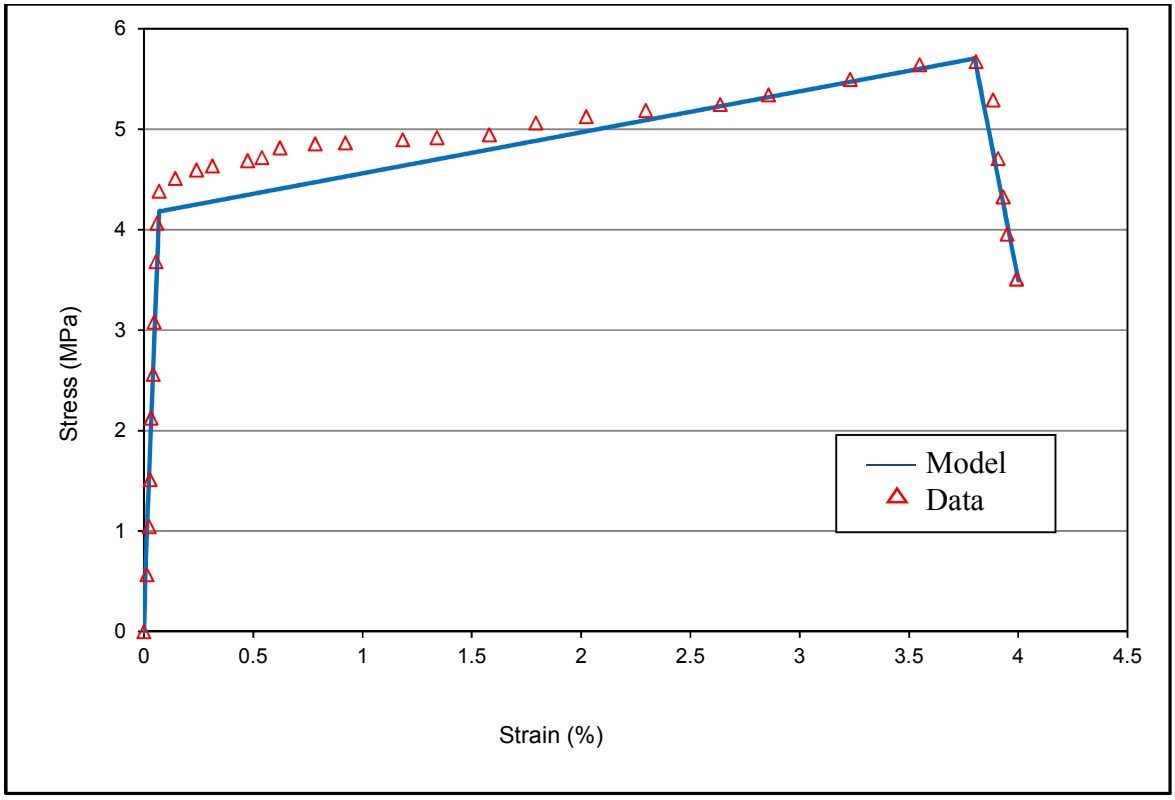

Fig. 3.4 Comparison results of stress-strain relationship for uniaxial tensile loading of SHCC.

Table 3.1 Properties of material for uniaxial tensile loading and crack width

Fiber type	**PVA**
Fiber volume	2.5%
Length of fiber	12mm
Diameter of fiber	39μm
Specimen size	304X76.2X12.7 mm
Gauge Length	80 mm
Curing	24h in mould, 28d in water, 1 day air dry

Table 3.2 Material model parameters for stress-strain behavior of SHCC under uniaxial tensile loading

Parameters	Uniaxial Tension
Initial Stiffness E_0	11640 MPa
Poisson's ratio ν	0.20
First cracking strain ε_{cr}	0.00069
First cracking stress σ_{cr}	4.2
Maximum tensile strain ε_t	0.038
Maximum tensile stress σ_t	5.8
Ultimate strain ε_u	0.043

3.4 Comparison of Analytical Results with Experimental Data for Crack Width

The crack widths are modelled by using Eq.3.5 and equivalent tangential fiber stiffness is calculated by the slope of strain-hardening part of tri-linear curve of SHCC given in Fig. 3.4. Finally c_i is adjusted for each increasing total crack width with increase in tensile strength of material. The model results are compared with experimental data which shows satisfactory verification as presented in Fig. 3.5. For the simulation of crack widths, the tensile strengths are taken from the experimental data assuming the uniform distribution of tensile strength in the strain hardening zone starting from minimum tensile strength (first cracking strength) to the maximum tensile strength. This assumption is appropriate to simulate the crack width during strain hardening of SHCC. The slope of the strain hardening linear function is calculated as equivalent tangential fiber bridging stiffness as strain hardening physically a function of fiber bridging across the cracks. The crack width for number of cracks is calculated and compared with the experimental data. The material properties for the experimental material for crack width are given in Table 3.1.

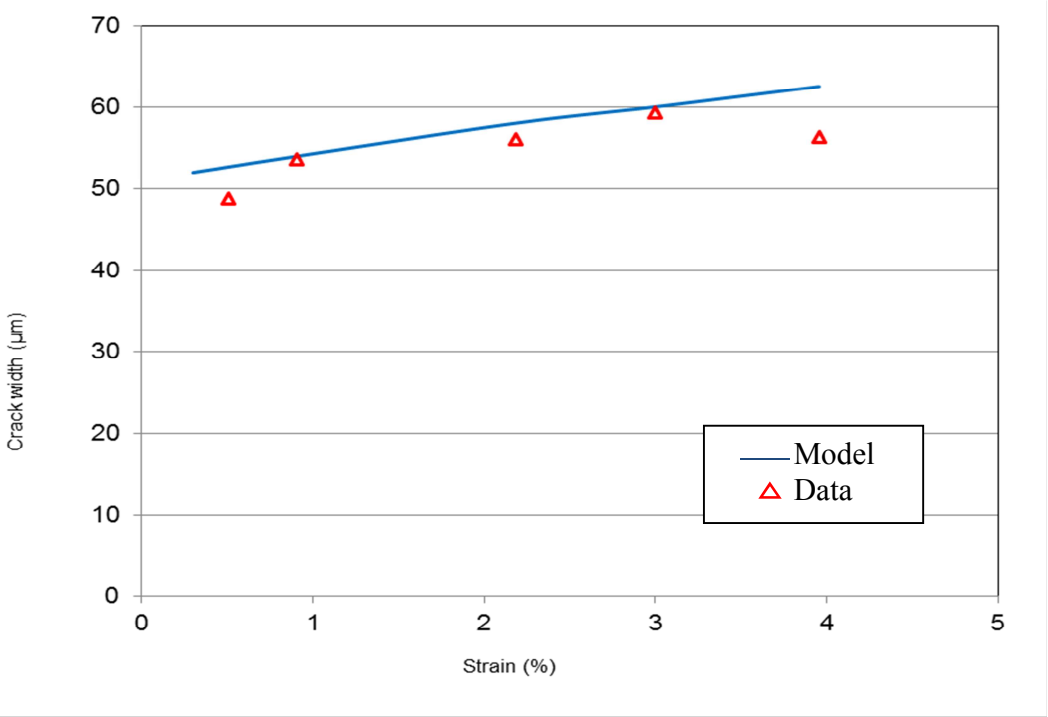

Fig. 3.5 Comparison result of crack width of SHCC for uniaxial tensile loading.

3.5 Comparison of Analytical Results with Experimental Data for Crack Spacing/Distribution

The multiple cracking with crack spacing and number of cracks are simulated by using experimental work by Rokugo et al.[79]. In this work the multiple cracking is observed for three different thickness of SHCC specimen. The mix proportion of SHCC specimens were given in detail in reference[79]. The present model is based on the multiple cracking behavior of 50 mm thick specimen. The rest of the material properties are shown in Table 3.3.

The multiple cracking with crack spacing and number of cracks are modelled by following the assumption described in section 3.2.3. The results of model are compared with experimental data for 0.63%, 1.88% and 5.00% of global strain values. The visible modelled cracks are shown by dotted lines in Fig. 3.6 which show a good agreement with data values.

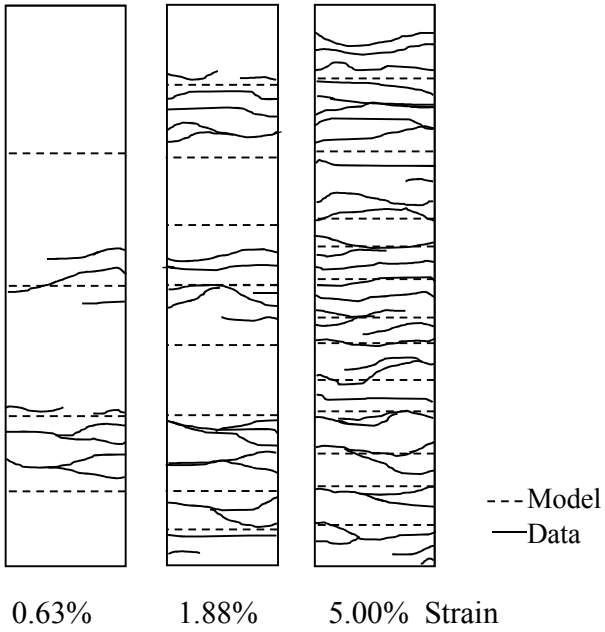

Fig. 3.6 Comparison results of crack spacing/distribution of SHCC for uniaxial tensile laoding.

Table 3.3 Properties of material for crack spacing/distribution

Fiber type	**PVA**
Fiber volume	2.0%
Length of fiber	12mm
Diameter of fiber	40μm
Specimen size	330X60X50 mm
Gauge Length	80 mm

3.6 Discussion on Results

The results of simulation for uniaxial tensile loading compared with experimental data represents that the tri-linear function may prove an efficient tool to model tension property of SHCC as shown in Fig. 3.4. This property is simulated in terms of secant

modulus in normal direction. The normal component of stresses and strains on each microplane is considered for simplicity. Also, the tangential component of the strain is considered almost negligible as synthetic fibers are much flexible producing almost insignificant shear resistance in tangential direction. In this way the proposed model can be more simplified with less parameters to be identified. This is the main advantage of the use of microplane model that microplane model involves less parameters.

There is potential in the present model to modify considering the volumetric and deviatoric components of stresses and strains along with tangential component to get well described macroscopic behavior of SHCC. The crack width data is modelled by considering equivalent tangential stiffness of bridging fibers. This simulation approach gives almost closer data fit results. Here the model parameter c_i needed to adjust at each increment of strain. This makes the calculation process a little tideous. In spite of this fact, the present model seems sufficient to simulate crack width as shown in Fig. 3.5.

The crack distribution is simulated along with crack spacing. This behavior of multiple cracking is very important to model for durability point of view. The Fig. 3.6 shows comparison of crack distribution with experimental data. This specimen is tested under uniaxial tensile loading giving first cracking strength as 3.9 MPa and maximum tensile strength as 4.5 MPa resulting in ductile behavior. From multiple cracking simulation results, it is clear that the assumptions those are considered for the present model are much closer to the practical scenario and give more factual results.

The following can be the conclusion of presented research study based on discussions on results

1) The microplane model is applied to model the tensile behavior of SHCC using a tri-linear tension property.
2) Crack width simulation results are justified by experimental data using equivalent tangential fiber stiffness approach.
3) The multiple cracking and the crack spacing are given by the present model in good agreement with test data.

3.7 Summary

This chapter covers the simulation of stress-strain relation for uniaxial tensile loading of SHCC, crack widths and crack spacing/distribution of multiple cracking for SHCC. The verification results are reported giving good agreement with experimental data. The approach of application of microplane model is resulted in more practical results. The microplane model is three dimensional models. This property makes it more flexible to implement this model to model uniaxial tension, biaxial compression as well as for multi axial loading. The aim of present research is to study time-dependent behavior of SHCC. The present model in this chapter may prove a gate way to model creep and shrinkage behavior of SHCC that will be described in later chapters.

Chapter 4

MULTI-LAYERED MICROPLANE MODEL FOR SHCC

4.1 Introduction

Strain hardening cementitious composites is the material which exhibits strain hardening, quasi-ductile behavior due to bridging of fine multiple cracks by short, randomly distributed polymer fibers as shown in Fig. 4.1. The strain hardening is followed by the phenomenon of increased tensile load with increased overall elongation. The favorable mechanical properties of this material offer many possible applications in new and old structures as well as in the strengthening and repair of structural elements made of reinforced concrete or other traditional materials[37).]

Several research projects have proposed different modelling approaches for SHCC subjected to tensile loading. Han et al.[3)] and Vorel and Boshoff[80)] introduced the constitutive relations for SHCC based on the reproduction of experimental results obtained from the test on bulk SHCC specimen. The derived formulas are adequate for the use in structural analysis. Much less focus has been given on the effect on mechanical properties of SHCC based on statistical variation in material properties and still it is needed to explain the modelling of material micromechanical behavior based on statistical variation that can be implemented for not only uniaxial tension and compression but also for biaxial and multiaxial behavior of SHCC. Besides this more study is very essential to model crack width and number of cracks in a multiple cracking system.

The present model reflects the fact that the fiber volume fraction V_f in reality varies between individual crack planes (mainly due to material processing in fresh state). This

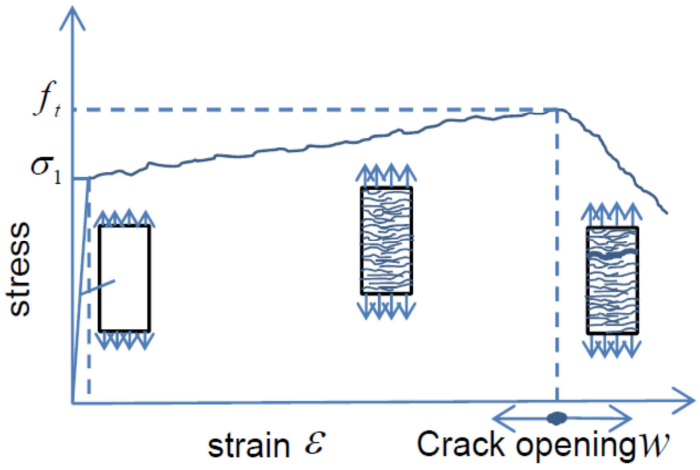

Fig. 4.1 Schematic diagram showing stress-strain relationship with multiple cracking in SHCC.

implies that V_f is a random variable. This study presents the multi-layered model for SHCC that can predict stress-strain relationship under uniaxial tensile loading(after combining with microplane model) as well as the uniaxial compression behavior. Namely, this study presents explicitly prediction for total crack width.

In microplane model, the constitutive properties are characterized separately on planes of various orientations within the material, called the microplanes. Kinematic constraint is used on these microplanes, i.e., the total strain vector on each microplane (crack) is assumed to be resolved component of the macroscopic strain tensor while the fibers are assumed to be directed to normal to each microplane. The state of each microplane is described by normal deviatoric and volumetric strain and by shear strain (further split into two orthogonal components)[81]. The microplane model is selected for the present research due to some significant advantages as compared to the previous classical tensorial models. These advantages are explained in Chapter 2 in detail. One of the reasons of selecting the microplane model for the present study is its contribution towards use of kinematic hardening rule in strain space[101].

The microplane model M1[77] is used for the present simulation that considers the normal microplane stresses, defines as nonlinear hardening-softening exponent function of the normal microplane strain. It resulted in sudden transition from elastic behavior to softening, causing the peaks of macroscopic response curve to be sharper as compared to smooth rounded peaks used in the modified version of microplane model M4[57] in which more material parameters are used to adjust the strain hardening behavior of material. The microplane model has flexibility to adjust the hardening behavior as per material response in the strain hardening zone.

The stress-strain relationship for uniaxial tensile loading involves various mechanisms to be defined and analyzed. These mechanisms are mainly focused in strain hardening region. The strain hardening of SHCC material is accompanied by multiple cracking and resulted in ductile behavior. The mechanism of strain hardening is analyzed with two different approaches. The strain hardening is caused due to stiffness recovery either due to interlocking of the material particles with fiber interfacial surface during pull out of fibers or due to interaction of a single fiber with other fibers dispersed randomly in the matrix. This mechanism is simulated by using statistical variation of fiber volume/tensile strengths from first crack to maximum number of cracks with equal statistical increased interval following uniform distribution. The use of statistical variation is found to be the most appropriate tool to model the strain hardening behavior of SHCC.

The stress strain relationship for uniaxial tensile loading is represented by exponential function in the present study. The first part of the exponential function represents the elastic behavior. The nonlinearity is introduced after first crack is appeared which is continued as kinematic hardening till strain softening starts. The kinematic hardening is a function of fiber pull out and strain softening is a function of fiber debonding/rupture. The material parameters used in the present simulation are representative of overall stress-strain relationship of SHCC under uniaxial tension. The appropriateness of each material parameter has been discussed later in this chapter. Each curve of the multi-layered microplane model represent the overall behavior of the material at each increase of number of crack which is a function of increasing tensile strength based on statistical variation (uniform distribution) of the tensile

strengths/fiber volume. The envelope of all these behaviors resulted in total hardening behavior of the material due to fiber pull out bridging across the multiple cracks.

4.2 Numerical Model for crack width

The Fig.4.2 shows the material condition when stress σ is applied to SHCC specimen (with original length L_0 and length after elongation is L). The applied stress is less than the tensile strength before cracking. Therefore, the elastic modulus of SHCC (by composite law) E and tensile strength (by empirical relationship) f_t can be expressed as

$$E = V_m E_m + V_f E_f = (1 - V_f) E_m + V_f E_f \tag{4.1}$$

$$f_t = V_m f_{tm} + V_f f_{tf} = (1 - V_f) f_{tm} + V_f f_{tf} \tag{4.2}$$

Where V_f is local fiber volume fraction, V_m is volume fraction of matrix, E_f is elastic modulus of fiber, E_m is elastic modulus of matrix, f_{tm} is tensile strength of matrix, f_{tf} is tensile strength of fiber. When

$$\sigma = E\varepsilon < f_t \tag{4.3}$$

then

$$\varepsilon = \Delta u / L_0 \tag{4.4}$$

where σ is applied tensile stress in uncracked part, Δu is change in length after applying stress and ε is strain in uncracked part.

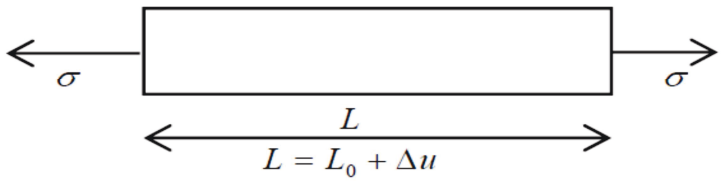

Fig. 4.2 Material conditions before cracking

4.2.1 Assumptions

The following assumptions are used for the multi-layered model based on multiple cracking system.

1) $P_i = P_{fi}$, where P_i and P_{fi} are the loads in i-th uncracked and cracked part respectively.
2) $\sigma_{fi} < \sigma_{f0}$, where σ_{fi} is the fiber pullout stress in bridging fibers at i-th crack and σ_{f0} is the maximum bridging stress of fibers acting on a microplane with normal vector **n** as shown in Fig 4.3(a),(b),(c).
3) Bilinear relationship for the bridging (pullout) stress-fiber pullout displacement is assumed Fig.4.3 (b). Fig. 4.3 (c) shows an example of a multi-linear relationship.

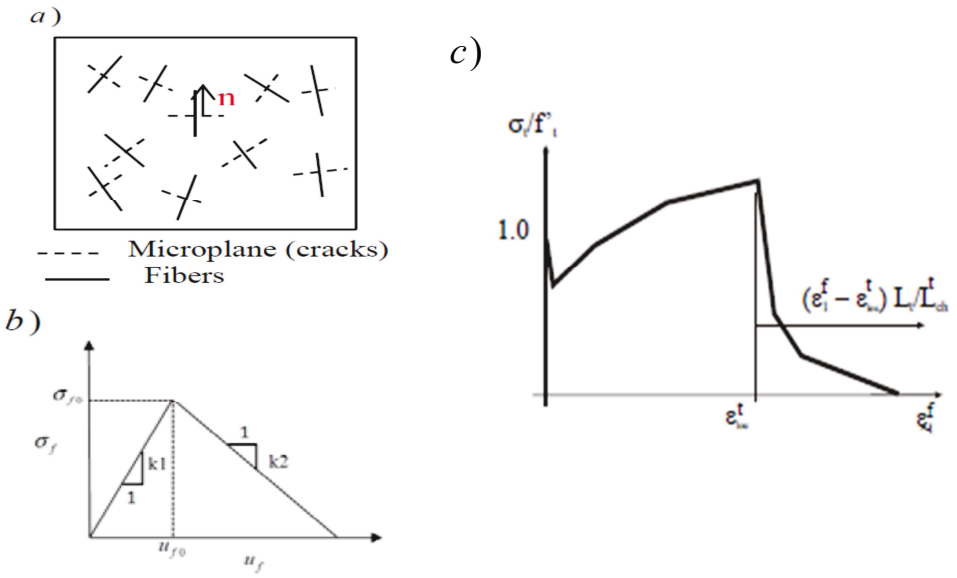

Fig. 4.3 a) Fibers and microplanes b), c) The fiber pullout force~displacement relationship

4.2.2 Statistical variation of material properties

Due to spatial distribution of short fibers, the material properties (strength, stiffness, bridging stress-fiber displacement relationship and number of bridging fibers) have a certain amount of statistical variation. The above properties are considered to be proportional to the

local fiber volume fraction V_f . Therefore, V_f is considered the principal independent parameter. The uniform distribution of the fiber volume is considered in the present study. Hence tensile strength is distributed uniformly with equal statistical intervals for each increasing number of crack. This assumption is appropriately produce satisfactory results for crack width simulations.

The cracking process of SHCC is given as follows:

- The first crack appears at the point where the tensile strength is minimum.
- The subsequent cracks are formed sequentially by the order of tensile strength from the small values to the large values.
- The crack width is calculated by the bridging stress-strain fiber displacement relationship.
- The total elongation of SHCC is calculated by summing the current length of uncracked part and crack width.
- When the fiber displacement is equal to the ultimate fiber displacement, the localization starts at that crack.

4.2.3 Model Description

Multiple cracking behavior can be modelled by expressing total strain by summation of strains in the uncracked part and those in the cracked part[82).]

$$d\varepsilon = \sum_{i=1}^{N_C} (\varepsilon_i) \tag{4.5}$$

$$d\varepsilon_i = d\varepsilon_{cri} + d\varepsilon_{ui} \tag{4.6}$$

where N_C is the number of cracks, $d\varepsilon_{cri}$ and $d\varepsilon_{ui}$ are the strain increments for cracked and uncracked part respectively. The multiple cracking system is shown in Fig.4.4 where L_{ui} and L_{ci} are the lengths of uncracked part and cracked part at *i*-th crack respectively. The total strain, then, can be obtained by the substitution of the equations for strain increments of uncracked and cracked parts in Eq. 4.6.

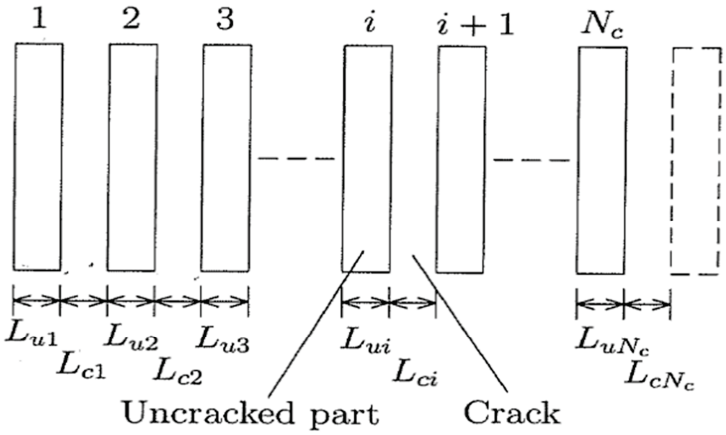

Fig. 4.4 Multiple cracking system in SHCC

Due to spatial distribution of short fibers, the material properties have a certain amount of statistical variation concluding that V_f is the only independent parameter. The statistical distribution of the fiber volume fraction V_f is assumed to follow the uniform distribution with mean m_{V_f}, the standard deviation σ_{V_f} and the coefficient of variation as follows

$$w_{V_f} = \frac{\sigma_{V_f}}{m_{V_f}} \tag{4.7}$$

It is assumed that cracking sequence is in the increasing order of tensile strength of SHCC. Now at first crack

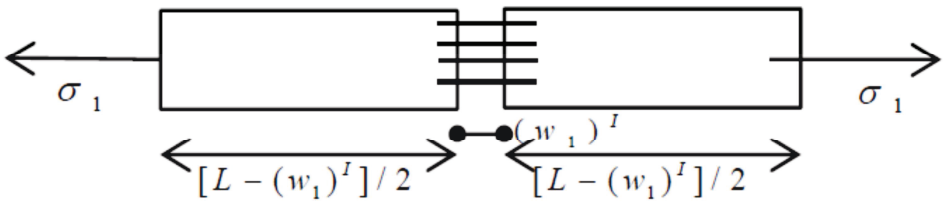

Fig. 4.5 Material condition after first crack

$$\sigma_1 = f_{t1} \tag{4.8}$$

where σ_1 and f_{t1} are the stress applied and the tensile strength of material at first crack respectively as in Fig. 4.5. To apply assumption (1), the following relations are considered.

$$P_{f1} = P, \qquad \sigma_f A_{f1} = f_{t1} A \tag{4.9}$$

Considering assumption (3),

$$\sigma_f = \frac{A}{A_{f1}} f_{t1} \tag{4.10}$$

$$u_{f1} = \frac{\sigma_f}{k_{f1}} = \frac{A.f_{t1}}{A_{f1}k_{f1}} = (w_1)^I \tag{4.11}$$

where u_{f1} is the fiber pullout displacement at first crack, k_{f1} is the stiffness of fiber at first crack and $(w_1)^I$ is the individual crack width of the first crack. For 2nd crack, the condition is $f_{t1} < f_{t2}$ (due to statistical variation of tensile strength) see Fig. 4.6. Hence when $\sigma_2 = f_{t2}$, 2nd crack will appear. The individual width at 2nd crack level is $(w_2)^I$ that can be evaluated as

$$(w_2)^I = \frac{Af_{t2}}{A_{f2}k_{f2}} \tag{4.12}$$

where f_{t2} is the increased tensile strength at 2nd crack corresponding to increased local fiber volume. Meanwhile, the first crack width increases due to difference of load/stress at 2nd crack stage and 1st crack stage.

$$(\Delta w_1)^1 = \frac{P_{f2} - P_{f1}}{A_{f1}k_{f1}} = \frac{\Delta P_{f(1-2)}}{A_{f1}k_{f1}} \tag{4.13}$$

where P_{f1} and P_{f2} are the load at first crack stage and 2nd crack stage respectively, $\Delta P_{f(1-2)}$ is the difference of load at 1st and 2nd crack stage. and $(\Delta w_1)^1$ is the increase in first crack width due to difference of loading. Hence total crack width at 2nd crack is $(w_2)^T$ i.e,

$$(w_2)^T = (w_2)^I + (w_1)^I + (\Delta w_1)^1 \tag{4.14}$$

Following the same sequence, the equation to calculate displacement at i-th crack stage for N_C number of cracks can be expressed as follows.

$$(w_i)_T = \sum_{j=1}^{i} (w_j) + g_i \tag{4.15}$$

where $(w_i)_T$ is the total crack width at i-th crack stage and w_j is the crack width of j-th crack that can be evaluated as

$$w_j = \frac{Af_{t(j)}}{A_{f(j)}k_{f(j)}} \tag{4.16}$$

where k_{fj} is the stiffness of bridging fibers at j-th crack and f_{tj} is the tensile strength at j-th crack. In Eq. 4.15, g_i is the sum of all crack openings due to increase of load beyond the initial cracking load at each crack stage, i.e.,

$$\begin{aligned} g = &\sum_{i=2}^{N_C}\left(\frac{P_{fi}-P_{f(i-1)}}{k_{f(i-1)}.A_{f(i-1)}}\right)+\sum_{i=3}^{N_C}\left(\frac{P_{fi}-P_{f(i-1)}}{k_{f(i-2)}.A_{f(i-2)}}\right)+\ldots \\ &+\sum_{i=N_C-1}^{N_C}\left(\frac{P_{fi}-P_{f(i-1)}}{k_{f(i-1)}.A_{f(i-1)\ )}}\right)+\left(\frac{P_{fN_C}-P_{f(N_C-1)}}{k_{f(N_C-1)}.A_{f(N_C-1)\ )}}\right) \end{aligned} \tag{4.17}$$

where P_{fj} is the load at j-th crack stage and $P_{f(j-1)}$ is the load at $j-1$ crack stage. In Eq. 4.17, the summation is taken place while the upper limit is larger than the lower limit and last term is for $j = i$.

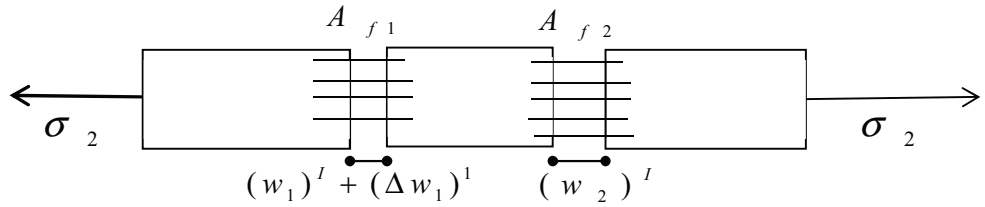

Fig 4.6 Material condition after 2nd crack

4.3 Multi-layered Microplane Model for Stress-strain Relationship

The incremental macroscopic stress-strain relation as per microplane model is given as

$$\Delta\sigma_{ij} = C_{ijrs}(\Delta\varepsilon_{rs} - \Delta\varepsilon_{rs}^{sh} - \Delta\varepsilon_{rs}^{T}) \tag{4.17}$$

where $\Delta\sigma_{ij}$ and $\Delta\varepsilon_{rs}$ are the macroscopic stress and strain increments, $\Delta\varepsilon_{rs}^{sh}$ and $\Delta\varepsilon_{rs}^{T}$ are the strain increments for shrinkage and thermal strains. C_{ijrs} is the stiffness tensor that can be evaluated as

$$C_{ijrs} = \frac{3\pi}{2}\int[n_i n_j n_r n_s C_D + \frac{1}{3}n_i n_j \delta_{rs}(C_V - C_D)]F(n)dS \tag{4.18}$$

where C_V and C_D are the incremental volumetric and deviatoric secant moduli for current loading for a microplane. (F(n) = 1 which is a weight function of the normal direction that can introduce anisotropy in its initial state). n with subscripts i, j, r, s are the direction cosines.

4.4 Comparison of Kabele's Model and Multi-layered Microplane Model

The model presented by Kabele[53)] is also a constitutive model for cracked solid as a continuum with identical macro-mechanical properties (equivalent continuum). The constitutive law of equivalent continuum in obtained as relationship between overall stress

and overall strain of RVE (Representative Volume Element) as shown in Fig. 2.20 and 2.21 in Chapter 2. In this model, the micromechanics is employed to relate the opening and sliding displacement of the cracks. The mechanical response of this model is dominated by multiple cracking. This model shows some similarities and also some differences from the multi-layered microplane model which are explained as follows:

- In Kabele's model, the RVE acts as a single point on which globally load is applied whereas in microplane model, load is also applied globally on a single point.
- In Kabele's model, the multiple cracking is assumed to be distributed in three dimensions as three set of cracks whereas in microplane model multiple cracks (multi-layers) are assumed to be distributed over the unit spherical surface equal to 21 integration points (microplanes).
- The summation of constitutive properties of RVE in three directions is equivalent to the properties of equivalent continuum (global behavior) whereas in microplane model, the summation of constitutive properties of all microplanes is equivalent to the properties of macroscopic behavior (global behavior) of structure.
- The effect of multiple cracking in one direction is not considered on multiple cracking in other directions, i.e., each set of multiple cracking is analyzed independently in each direction. This rule is similar in microplane model, i.e., the constitutive law is analyzed at each microplane independently.
- In Kabele's model, statistical variation of material properties is not considered while for present version of microplane model, the statistical variation of fiber volume/tensile strength is considered.
- In Kabele's model, the multiple cracking is treated by using tool of continuum mechanics while for multi-layered microplane model the multiple cracking is treated by using tool of micromechanics.

4.5 Crack Distribution Model

The crack distribution of SHCC can be modelled by assuming uniform discrete distribution of fibers. The cracking sequence can be explained based on various experimental

data. The first crack will appear at the middle of specimen with least fiber volume/tensile strength. The subsequent cracks will appear in the middle of each equally spaced section from left to right with statistically increasing fiber volume at each discrete interval (see Fig. 4.7). This process continues till crack spacing will equal to critical crack spacing. At this stage localization of cracks will start.

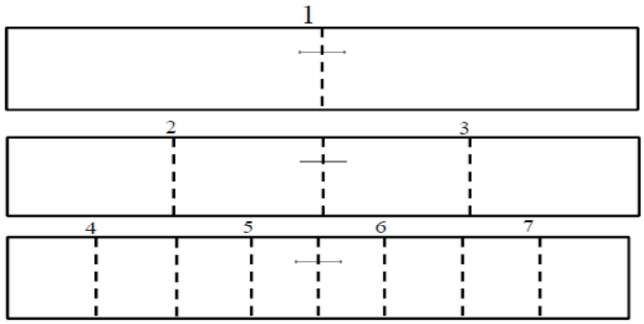

Fig. 4.7 Crack distribution/spacing model for SHCC

Table 4.1 Material properties for uniaxial tensile loading with PVA fiber

Properties	**Uniaxial tensile loading**[52)]
Fiber type	PVA fiber
Specimen size (mm)	100x40x24
Fiber volume (%)	2.25
Fiber length (mm)	12
Fiber diameter (μm)	40
Stress at first cracking (MPa)	3.6
Tensile strength (MPa)	4.7

4.6 Results

4.6.1 Comparison of analytical results with experimental data for uniaxial Tension

To demonstrate the capability of present multi-layered microplane model in predicting the uniaxial tensile stress-strain behavior, the analytical verification for SHCC is carried out and this is done by comparing results with experimental work[52] in which PVA fibers are used for SHCC. The matrix and fiber properties are given in Table 4.1.

For computation, the microplane model by Bazant and Gambarova[77] is followed. The strain hardening cementitious composites show almost negligible shear resistance as synthetic fibers are very flexible. Hence for present model, practically the resistance in tangential direction is neglected i.e. $C_T = 0$. Another simplification is made by considering normal stiffness equal to volumetric stiffness (deviatoric stiffness is assumed to be negligible), i.e., $C_N = C_V$ and $C_D = 0$. Further, the normal stiffness is used as tangent modulus in normal direction. Therefore, considering E_N equal to initial modulus, the expression for tangent modulus can be obtained as

$$C_N^T = E_N e^{-k\varepsilon_N{}^p}(1 - kp\varepsilon_N{}^p) \tag{4.19}$$

where k (softening parameter)and p are material constants and $\varepsilon_V = \varepsilon_N$.

For present simulation, four material parameters are used that is one of the reasons to use microplane model as micromechanical constitutive model. Microplane model needs minimum number of material parameters for simulation. These four parameters are Poisson's ratio ν, initial modulus E_N, softening parameter k and a positive constant p .The value of two parameters, i.e., Poisson's ratio and p are fixed prior to data fitting and then these values are kept constant for simulation of each curve for increasing number of cracks. The initial modulus and softening parameter is adjusted to adjust the peak values (tensile strengths) and initial slope of the curves of multi-layered model.

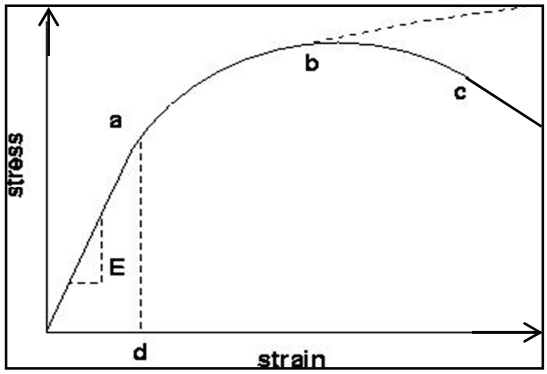

Fig. 4.8 A schematic diagram showing the physical meaning of exponential function used for simulation.

The above figure is showing schematically the physical meaning of exponential function used for the tensile stress-strain relationship for the present simulation. The first rising part of the exponential function represents the elastic behavior of composite under uniaxial tensile loading that is considered almost straight till point a. At point a, the first crack will appear. In case of strain hardening cementitious composites, point a is the peak point of the exponential function that represents the maximum tensile strength at which crack will appear, i.e., point a and point b is same. From point a to point c, the exponential function represents the strain hardening behavior of composite due to fiber pull out bridging across the crack that causes fall of stiffness due to slippage of fiber form the fiber-matrix interfacial surface. Strain hardening is incorporated by the concept of kinematic hardening rule in microplane model. Due to slippage, the material partials change their place at interfacial surface that causes interlocking. This interlocking cause stiffness recovery with enhanced strength capacity and stress again starts to be increased till next crack will appear at higher stress than the first one. The strain softening starts after point c when localization of cracks occurs.

The total macroscopic strain is considered as sum of strain due to microplane system e_{ij} and additional elastic strain ε_{ij}^{a}, i.e.,

$$\varepsilon_{ij} = e_{ij} + \varepsilon_{ij}^{a} \tag{4.20}$$

The related detail of derivation of ε_{ij}^{a} and definition and value of parameters are given in work by Bazant and Oh[56].

The comparison results of analytical and experimental data have been depicted in Fig. 4.9. The computation is done for ML (multi-layered) model for SHCC which represents the overall behavior as multi-layered microplane model that is obtained by the envelope (assembly) of the behavior of material at each statistically increased interval of tensile strength.

In ML (multi-layered) the initial stiffness, strain-hardening and multiple cracking of SHCC is verified. The assumption is made by considering statistical variation of tensile strength in strain hardening zone as uniformly distributed form minimum (first cracking strength) to maximum (maximum tensile strength) in equal statistical intervals. The number of statistical interval is function of number of multiple cracks. The information of about the number of cracks is taken from the experimental work for present simulation. The number of multiple cracks can also be estimated by using Eq. 3.6 and Eq. 3.7 if sufficient data is not available. The initial modulus is assumed same for each statistical interval while softening parameter is adjusted to fit the tensile strengths at each increasing number of cracks. The crack spacing is calculated as 8 mm. The adjusted material parameters for ML model are given in Table 4.2. The value of k is variable for each ML model, i.e., 110000, 90000, 85000, 80000, 78000, 76000, 75000, 74000, 71000, 69000, 67000, 64000, 62000 from 1st ML model to 12th ML model. The k parameter can be expressed as function of tensile strength so that one can obtain parameter for known values of tensile strengths. For PVA fibers k parameter can be expressed as $2 E 10^{6} f_t^{-2.096}$.

The stress strain relationship of SHCC with carbon fibers has also been a focus of research by many researchers. Li and Obla[29] worked on experiments on SHCC with carbon fibers under uniaxial tensile loading. They performed a series of experiments to investigate the effect of fiber length variation on tensile properties of carbon-fiber cement composites.

Table 4.2 Model parameters for analytical verification of uniaxial tesnile behavior with8PVA fibers

Model Parameters	**Uniaxial tension ML[52)]**
E_N (MPa)	8000
ν	0.2
k	-
p	0.20

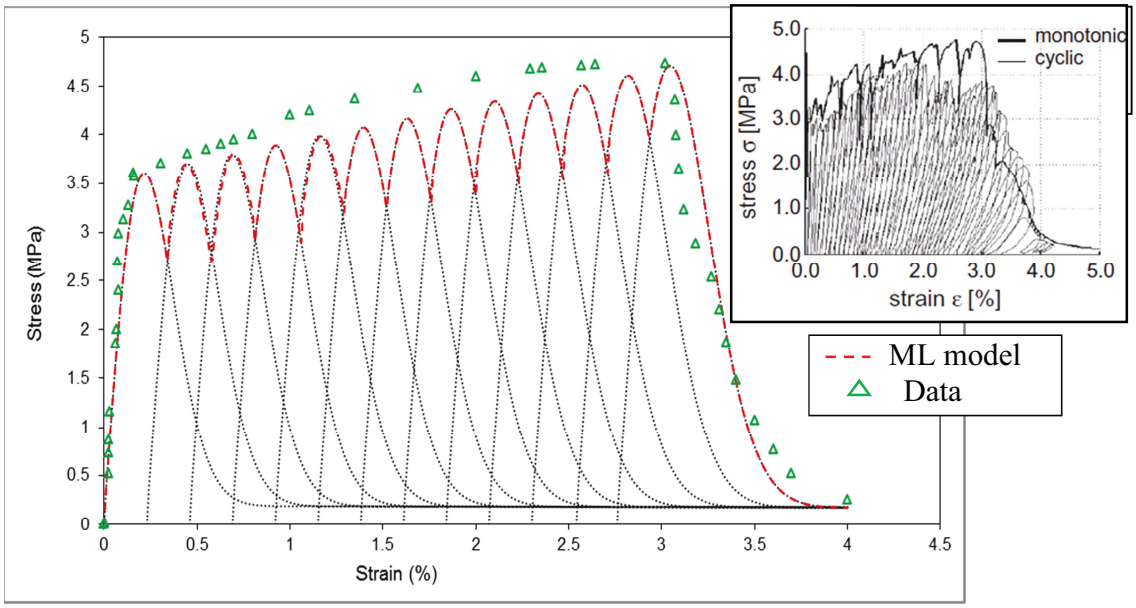

Fig. 4.9 Comparison of analytical results with test data for uniaxial tension of SHCC with PVA fibers.

One of their experimental works is selected to simulate the stress-strain constitutive relationship by using multi-layered microplane model. The properties of the composite and fibers are given in Table 4.3. The number of cracks is estimated by using equations of crack spacing by Lee et al.[100]. The interfacial bond strength is assumed to be 0.63 MPa for the calculation of crack spacing. This value is taken form the work by Katz et al[102] in which the bond properties of carbon fibers has been investigated by experiments. This value of bond strength is average value that has been selected for the present simulation. This value can vary for different mix proportions and type of carbon fibers as wide range of properties is expected for carbon fibers.

The material parameters are adjusted to fit the data values. The behavior for ML(multi-layered) represents the uniform distribution of tensile strength. The material parameters are listed in Table 4.4. The crack spacing is calculated as 7.6 mm which gives total 40 numbers of cracks. The value of k is variable for each ML model, i.e., 135000, 1320000, 1290000, 1260000, 1230000, 1200000, 117000, 1150000, 1130000, 1100000, 1075000, 1045000. 1025000, 1000000, 980000, 960000, 950000, 930000, 910000, 890000, 870000, 855000, 845000, 825000, 810000, 790000, 775000, 765000, 750000, 735000, 725000, 715000, 700000, 690000, 680000, 665000, 655000, 645000, 635000, 625000 from 1st ML model to 40th ML model. The verification results are shown in Fig. 4.10 which shows satisfactory agreement with test data. The k parameter can be expressed as function of tensile strength so that one can obtain parameter for known values of tensile strengths. For carbon fibers k parameter can be expressed as $9E10^{7} f_t^{-2.349}$. In the field of fiber-reinforced cementitious materials, aramid fibers have also been used and their properties are effectively used in the field applications as aramid fibers give more tensile strengths and higher initial modulus. In the present study, the stress-strain relationship under uniaxial tensile loading for aramid fibers has also been simulated using multi-layered microplane model. The experiment has been done by Walton and Majumdar[33]. The material properties are given in Table 4.5. The material parameters are adjusted to fit the data values. The number of cracks is estimated by using equations of crack spacing by Lee et al.[100]. The interfacial bond strength is assumed to be 3.0 MPa for the calculation of crack spacing. The behavior for each ML (multi-layered)

Table 4.3 Material properties for SHCC under uniaxial tension with carbon fibers

Properties	**Uniaxial tensile loading**[29)]
Fiber type	Carbon fiber
Specimen size (mm)	304.8x76.2x12.7
Fiber volume (%)	4%
Fiber length (mm)	10
Fiber diameter (μm)	20
Stress at first cracking (MPa)	6.0
Tensile strength (MPa)	8.2

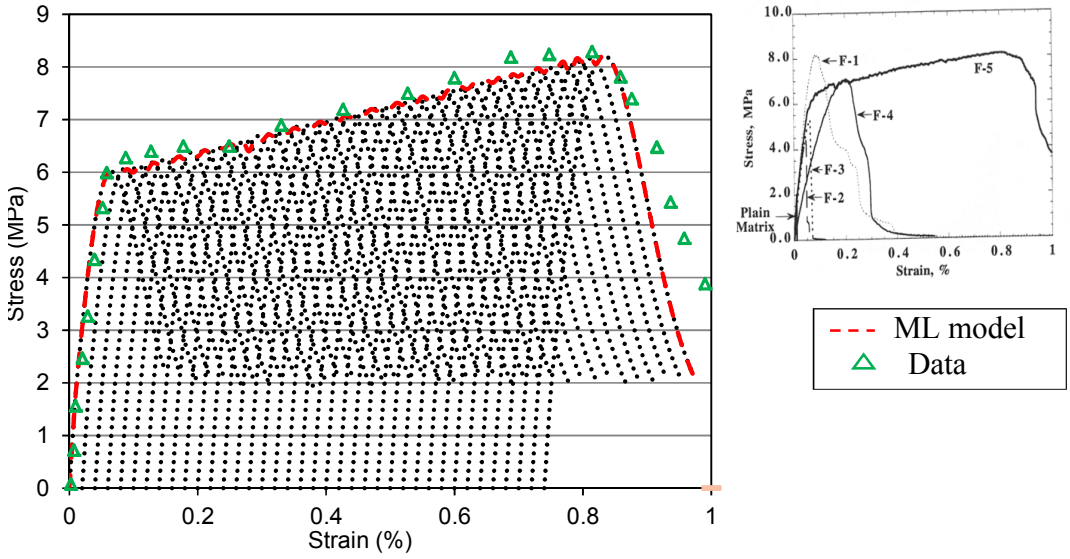

Fig. 4.10 Comparison of analytical results with test data for uniaxial tension of SHCC with carbon fibers.

Table 4.4 Model parameters for analytical verification of uniaxial tesnion with carbon fibers

Model Parameters	**Uniaxial tension ML[29)]**
E_N (MPa)	40000
ν	0.2
k	-
p	0.20

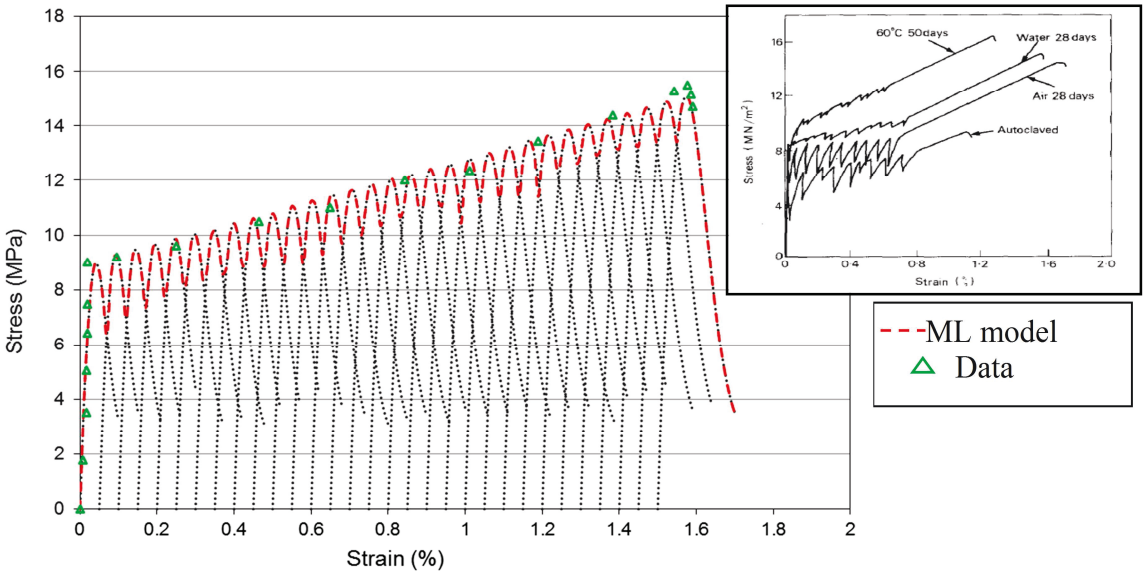

Fig. 4.11 Comparison of analytical results with test data for uniaxial tension of SHCC with aramid (Kevlar) fibers.

Table 4.5 Material properties for SHCC under uniaxial tension with aramid (Kevlar) fibers

Properties	**Uniaxial tensile loading**[29)]
Fiber type	Aramid fiber
Specimen size (mm)	150x50x10
Fiber volume (%)	2%
Fiber length (mm)	51
Fiber diameter (μm)	11.9
Stress at first cracking (MPa)	9.0
Tensile strength (MPa)	15.0

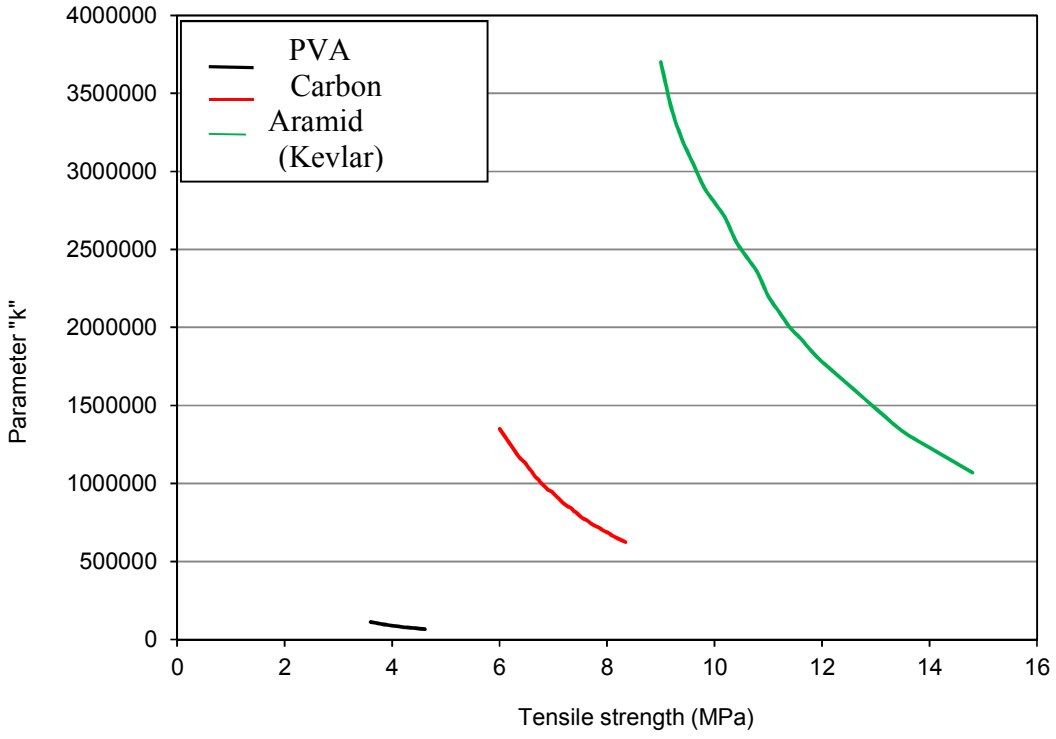

Fig. 4.12 Comparison of softening parameter k as function of fiber type used for SHCC.

Table 4.6 Model parameters for analytical verification of uniaxial tesnion with aramid fibers

Model Parameters	**Uniaxial tension ML[29)]**
E_N (MPa)	90000
ν	0.2
k	-
p	0.20

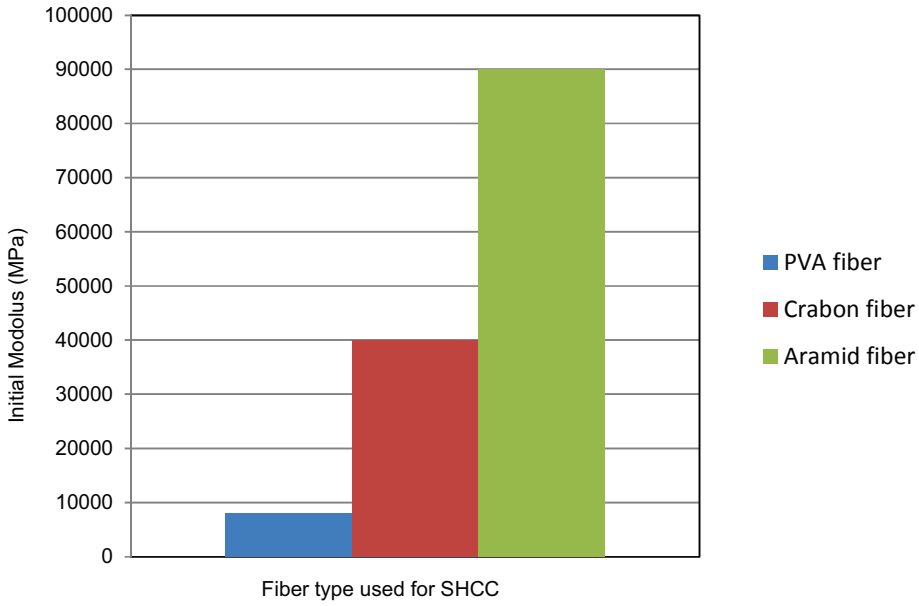

Fig. 4.13 Comparison of initial modulus as function of fiber type used for SHCC.

represents the uniform distribution of tensile strength. The material parameters are listed in Table 4.6. The crack spacing is calculated as 5mm which gives 30 total numbers of cracks. The value of k is variable for each ML model, i.e., 3700000, 3400000, 3200000, 3050000, 2900000, 2800000, 2700000,2550000, 2450000, 2350000, 2200000, 2100000, 2000000, 1930000, 1850000, 1780000, 1720000, 1660000, 1600000, 1540000, 1480000, 1420000,

1360000, 1310000, 1270000, 1230000, 1190000, 1150000, 1110000, 1070000 from 1st ML model to 30th ML model. The verification results are shown in Fig. 4.11 which shows satisfactory agreement with test data. The *k* parameter can be expressed as function of tensile strength so that one can obtain parameter for known values of tensile strengths. For aramid fibers *k* parameter can be expressed as $8E10^{8} f_t^{-2.441}$. Finally, the material parameters adjusted for the uniaxial tensile behavior of SHCC with various fiber types are compared and presented as function of fiber type. These parameters are softening parameter and initial modulus which are basically variable parameters for different materials. This comparison is shown graphically in Fig. 4.12 for softening parameter and in Fig. 4.13 for initial modulus.

4.6.2 Comparison of analytical results with experimental data for total crack width

This model can efficiently be used to simulate total crack width at increasing load steps. The simulation results are verified by comparing with experimental data[52]. In this work, the average crack widths are measured at 0.5%, 1% and 2% strain values with 4, 8 and 12 number of cracks respectively at corresponding strain values. The total crack width can be evaluated by multiplying the crack width with number of cracks and considering standard deviation value for crack width given in the experimental data.

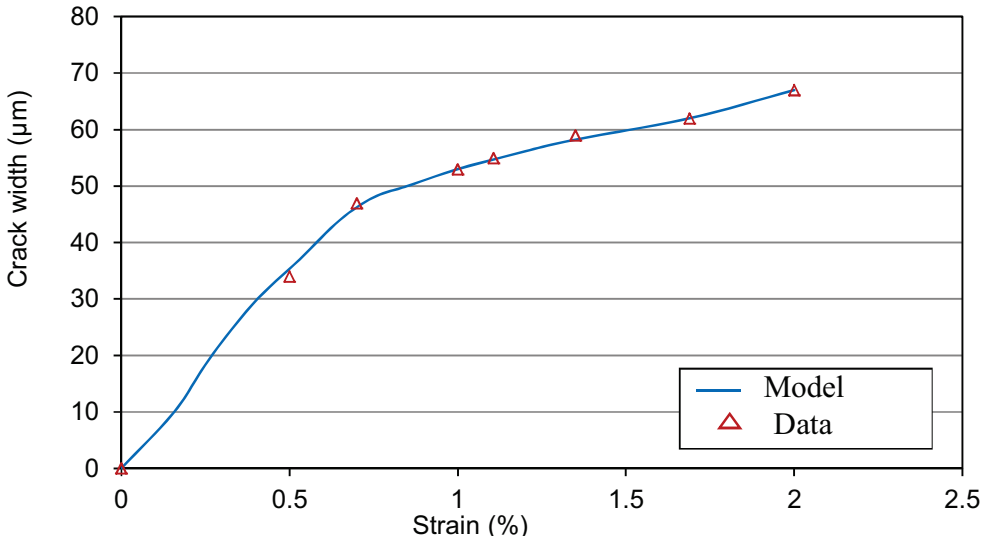

Fig 4.14 Comparison of analytical results with test data for total crack width of SHCC.

The fiber and matrix properties are given in Table 4.7. For simulation of total crack width, Eq. 4.15 is used. For this purpose, tensile strength/loads are taken from the experimental data of uniaxial tensile stress-strain relationship at each crack[52]. The mean volume fraction is considered as 2.25%. The uniform distribution of fiber volume fraction is considered from 1st crack (minimum) to 12th crack (maximum). The standard deviation value is considered as 5%. Hence considering equally spaced cracks, the values of volume fraction from 1st crack to 12th crack are calculated as 1.68%, 1.8%, 1.9%, 2.02%, 2.13%, 2.25%, 2.36%, 2.47%, 2.58% 2.7% 2.81% and 2.92%.

Table 4.7 Material properties for total crack width

Properties	**Total crack width**[52]
Specimen size (mm)	100x40x24
Fiber volume (%)	2.25
Fiber length (mm)	12
Fiber diameter (µm)	40
Stress at first cracking (MPa)	3.6
Tensile strength (MPa)	4.7

Table 4.8 Material properties for uniaxial compression

Properties	**Uniaxial compression**[83]	**Uniaxial compression**[84]
Fiber volume (%)	2.0	2.0
Fiber length(mm)	38	12
Fiber diameter(µm)	38	39
Peak stress(MPa)	49.9	51
Peak strain (%)	0.27	0.32

The total cross sectional areas of bridging fibers are calculated corresponding to above fiber volume fractions at each crack. The stiffness of bridging fibers is calculated as

$$k_f = E_f A_{fi} / L \tag{4.21}$$

where L is the debonding length of bridging fiber that is considered as $L_f/2$ in this case where L_f is the length of fiber. The E_f is the elastic modulus of fibers that is considered constant and adjusted by the first crack width of measured data, i.e. , E_f = 4740 MPa. The simulation results are shown in Fig. 4.14 which shows satisfactory agreement with experimental data.

Table 4.9 Model parameters for analytical verification of material behavior

Model Parameters	**Uniaxial compression**[83]	**Uniaxial compression**[84]
E_N (MPa)	35000	30000
ν	0.20	0.2
d	39	38

4.6.3 Comparison of analytical results with experimental data for crack spacing/distribution

To model crack distribution and number of cracks, the data[37] is referred. In this case total of 12 cracks are observed during strain-hardening zone. The crack distribution by experimental results may be attributed to non-uniform distribution of mechanical properties. This whole range is divided uniformly into 12 uniform statistical intervals. The first crack will appear at the middle of the first statistical interval and this sequence will continue from left to right. The verification results are shown in Fig.4.15 which depicts a satisfactory agreement with experimental data of crack distribution at 0.5%, 1.0% and 2.0% strain values. It is clear from figure that at 0.5% strain, number of cracks is four, at 1.0% strain number of

cracks is eight and at 2.0% strain number of cracks is twelve which verify the experimental results for number of cracks based on uniform statistical increase of fiber volume.

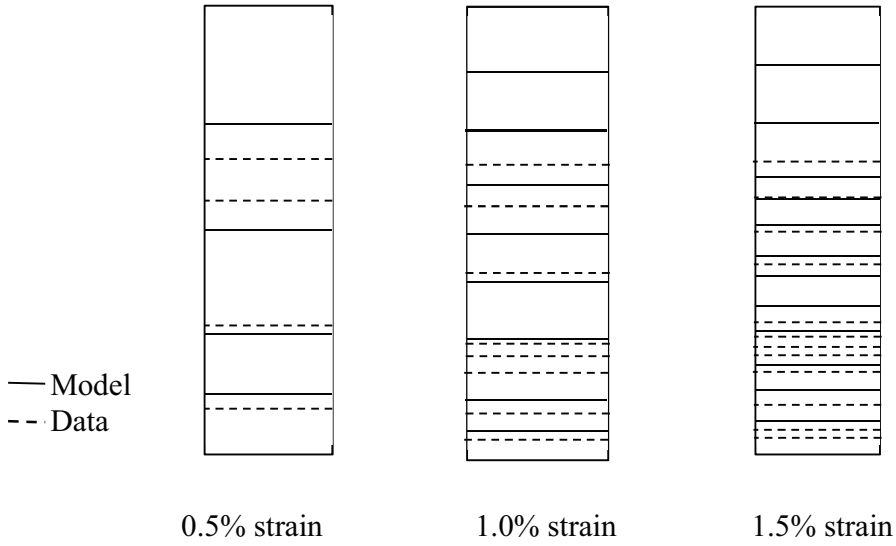

Fig. 4.15 Comparison of model results with test data for crack distribution/spacing of SHCC.

4.6.4 Comparison of analytical results with experimental data for uniaxial compression

The presented microplane model can also be implemented for simulating uniaxial compression behavior. The analytical results are compared for two different experimental data by Sirijaroonchai[83] and Zhou[84]. The related fiber and material properties are given in Table. 4.8. For uniaxial compression, the assumptions are considered, i.e.,

$$C_V = C_N, \qquad \varepsilon_V = \varepsilon_N, \qquad C_D = 0 \tag{4.22}$$

The tangent modulus is calculated as arctan function as

$$C_N^{\ T} = E_N / (1 + (\omega \varepsilon_N)^2) \tag{4.23}$$

where

$$\omega = \pi E_N / 2d \tag{4.24}$$

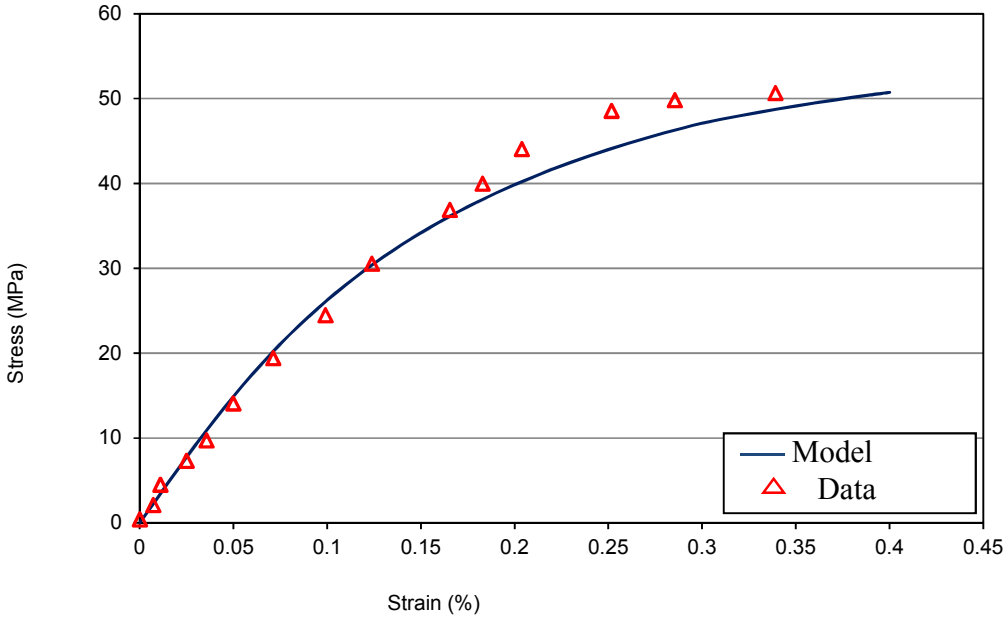

Fig. 4.16 Comparison of analytical results with test data for uniaxial compression of SHCC.

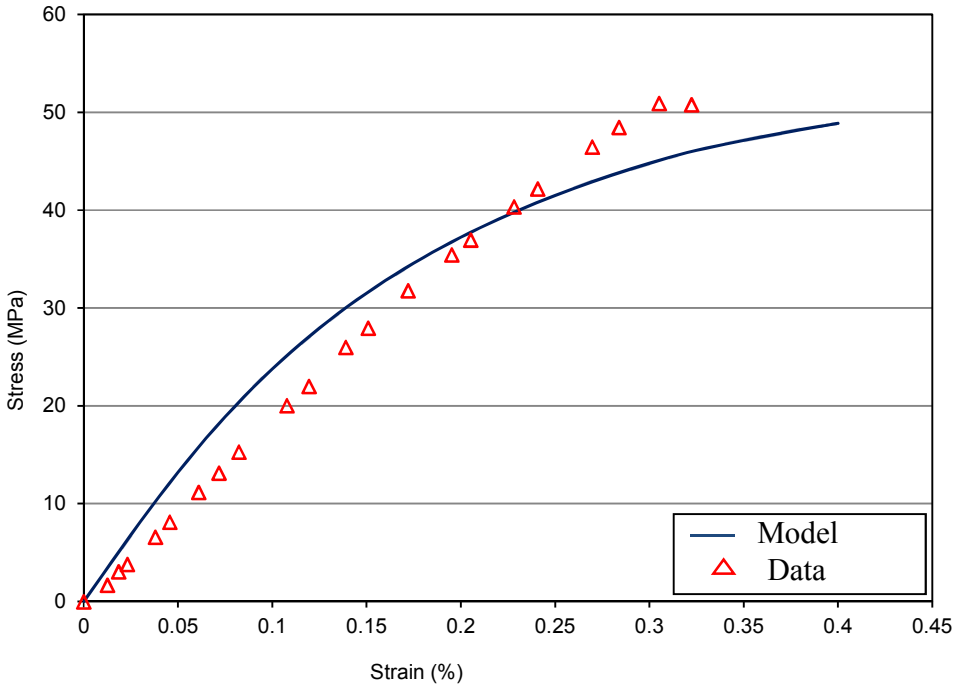

Fig. 4.17 Comparison of analytical results with test data for uniaxial compression of SHCC.

in which d is compressive strength parameter. The elastic material constants E_N (initial modulus) and Poisson's ratio ν are fixed and then d is identified by computation. The adjusted value of material parameters are shown in Table 4.3. The analytical results show satisfactory agreement with experimental data as shown in Figs. 4.16- 4.17.

4.7 Discussions on Results

The results of multi-layered microplane model opened the way to more realistic approach to simulate multiple cracking associated with strain-hardening. This approach is the use of multi-layered microplane model in which each layer of microplane represents the stress-strain relationship for each statistically increased tensile strength in strain hardening region. The presented model satisfies the mechanism of strain hardening in appropriate manner. The verification results are shown in Fig. 4.8 which depicts the complete mechanism of stress-strain behavior of SHCC under uniaxial tensile loading. The exponential function has been used as one single continuous function. The rising part of the ML model represents the linear elastic behavior of SHCC that is approximated by a curve. The first crack appears at the first cracking strength. Due to pull out of fibers the stiffness is reduced which is represented by drop in first curve. During sliding of fibers at interfacial surface, the interlocking of material at interfacial surface occurs which requires more strength to recover. To balance this interfacial resistance, the stress starts increasing again till the tensile strength more than the first crack which resulted in opening of second crack. This mechanism continued till strain softening/ localization of one of the cracks starts due to rupture/debonding of fibers.

The simulation is done for three different types of fibers under uniaxial tensile loading. The experimental data for SHCC with PVA fibers is used for comparison resulted in total twelve number of cracks. The assembly of these twelve micro-cracks depicts the overall strain hardening behavior. This multi-layered model resulted in suitable value of initial modulus. The data for uniaxial tensile loading for stress-strain relationship is also simulated for SHCC with carbon and aramid fibers. The softening parameters and initial modulus are expressed as function of fiber type. The softening parameter is found to be inversely

proportional to the tensile strength. SHCC with carbon fibers and aramid fibers resulted in high values of softening parameters and initial modulus than SHCC with PVA fibers.

The advantage of multi-layered microplane model is that it can simulate not only the maximum tensile strength but also first cracking strength, strain-hardening, multiple cracking, number of cracks and softening of SHCC. All these behavior are much significant for design of SHCC structures to be used under service load conditions. From the present research, the multi-layered microplane model proved to be the suitable model to predict all of the above mentioned mechanical behavior of strain hardening cement-based composites. The model to simulate total crack width is also based on practical approach, i.e., the increase in crack width with increasing tensile strength. The formulation is attributed to bridging fiber stiffness, area of bridging fibers (distributed based on statistical variation of fiber volume) and elastic modulus of fibers. Hence fiber pull out displacements are considered the main source of increase in crack width at increasing tensile strength of material. The results show agreement with experimental data that reflects the applicability of the present model. In the same way, the crack distribution based on statistical variation of fiber volume/tensile strength gives more justified results with experimental data which is in agreement of the applicability of the model for crack distribution and spacing for strain hardening cementitious composites. The implementation of statistical distribution of fiber volume is the proved close to the practical scenario.

4.7 Summary

The results show the applicability of multi-layered microplane model with good agreement with experimental data. This model has an advantage of predicting total crack width, crack distribution/spacing and number of cracks. In this way the phenomenon of multiple cracking and stress-strain relationship for uniaxial tensile loading can be predicted. This model is comparatively more realistic to state crack distribution behavior of SHCC. The multi-layered microplane model has wide range of applicability. This can be implemented for various strengths of the SHCC material and fiber volume. The material behavior can be simulated for a wide range of tensile or compressive strengths and fiber volume as fiber

volume is observed the main parameter that identifies the SHCC material behavior. Being three dimensional analytical characteristics, this model can be extended to multi-axial loading of strain-hardening cementitious composites along with uniaxial behavior. Various experimental data is available for biaxial and triaxial compressive behavior[48]. This can contribute an efficient advantage of this model.

The main advantage of the present model is that the phenomenon of multiple cracking can be well explained by using the multi-layered microplane model for small sized specimen equal to about the size of one element used in FEM for simulation of larger structures. For this purpose the computational time for each simulation is very less, i.e., within minutes while for the same simulation of with fiber and matrix interaction at cracking, the computational time is within hours. The program code is written in Fortran 90 including assembling of stiffness matrix and spherical integration. The strain increments are set prior to the start of program and strain and stress increments are updated after each assembling of stiffness matrix. It involves very less time to run and generate the results.

Chapter 5

Modelling of Time-dependent Behavior of SHCC

5.1 Model Background

Strain-hardening cementitious composites (SHCC) are the material which exhibit strain hardening, quasi-ductile behavior with a tensile strain capacity of up to 5%. Due to the favorable mechanical properties, it has become a promising alternative building material. This pseudo-ductility is achieved by the formation of fine closely spaced cracks which do not widen significantly during the strain hardening phase resulting in its capability to use for durable structures[56)].

The long-term behavior of SHCC has recently received the attention as the mechanical behavior of cement-based material is highly time-dependent. The creep is a well-known phenomenon in terms of continued deformations under sustained load. It has been determined that three main causes of macroscopic tensile creep of SHCC are the matrix creep, time-dependent fiber pull-out and the formation of additional multiple cracks over time. It has also been found that time-dependent fiber pull-out causes cracks widening under sustained loading[57)].

The time-dependent single fiber pull out experiments were carried out to investigate the sources and mechanism of tensile creep. The results of these experiments may be helpful to understand the phenomenon of cracking creep strain. The cracking creep strain is considered the additional and significant source of time-dependent deformation that is associated with formation of new cracks over time[31]).

This phenomenon of formation of new cracks and widening of cracks under tensile sustained loads need to be analytically quantified and simulated for durability design models of structures. The phenomenon of creep and creep fracture has been investigated in a computational framework for SHCC. This has been done at a macro-level using a

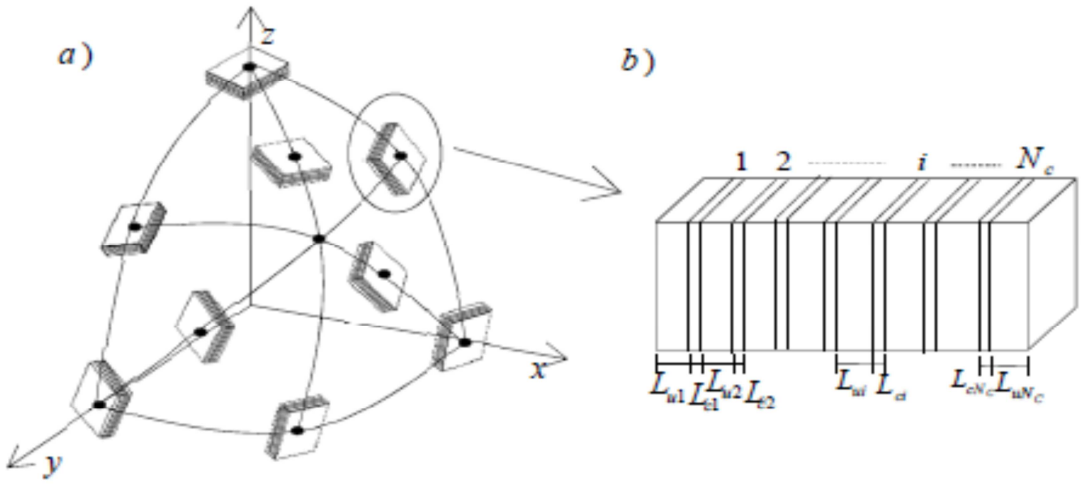

Fig. 5.1 a) Position of multilayered-microplanes on sphere b) Single multi-layered microplane

homogeneous material model incorporating non-proportional creep for the behavior of SHCC[57].

To study the mechanical time-dependent behavior of SHCC, the experimental work has been done in the recent past. The first step in this regards was the tensile creep, shrinkage and rate dependence characterization on uncracked SHCC specimens. The results of these experiments revealed the identification of new sources of time-dependent tensile strain that encourages the researchers to do more experiments on cracked SHCC to precisely model the phenomenon of time-dependent crack initiation and fiber pull-out creep[30].

In the present study the time-dependent behavior of SHCC is modelled by using multi-layered microplane model. The multi-layered model is an efficient tool to simulate the multiple cracking behavior of SHCC along with phenomenon of widening of cracks over time at micro-level. The simulation of tensile creep and shrinkage behavior is the main target of the present study which has been characterized on each layer of microplane and the constitutive relationship of SHCC can be developed. The creep and shrinkage are simulated by using power law as function of load duration. The age effect is usually inversely proportional to the material parameters used in power law curve to fit the data. For fiber-reinforced cementitious composites usually age effect and loading rate are not much

significant factors under sustained loading as compared to concrete and especially soil and clays. The present study reflects the time-dependent behavior as function of load duration only. In the present study, the normal component of strains and stresses will be considered because the tangential stiffness in assumed negligible due to flexible nature of synthetic fibers. The constitutive relationship of SHCC is modelled by considering multi-layered microplanes. The position of these multi-layered microplanes on the sphere is shown in Fig. 5.1 (a).

5.2 Mechanism of Time-dependent Behavior

The inherent crack control of SHCC is demonstrated by applying direct tensile stress on specimen. Once the matrix strength is exceeded, more cracks arise instead of significant widening of first crack upon further deformation. The crack control is a dominant feature of SHCC and holds the key to understanding and predicting its short and long term behavior. The main mechanism of creep are identified as follows

i) The initiation of new cracks under sustained load.
ii) The widening of new cracks due to fiber pull-out.
iii) The matrix creep.

It is shown for the particular fiber that a potential fourth mechanism, namely fiber creep, does not contribute to the creep in the SHCC[33).] The uncracked specimen creep is smaller relative to the time-dependent deformation of cracked specimen. This fact implies that the mechanism of crack initiation and widening due to fiber pullout dominate. To interpret these creep mechanisms, it is useful to study the trends in macroscopic tensile behavior in connection with the micro behavior of individual fiber pull-out. The cracks are controlled to small widths (in micro-range up to 50-150μm) over a large tensile deformation range. The bond slip-hardening can contribute to the rate-enhanced composite strength at small deformation. In the later stages, i.e., at larger deformation, as cracks grow wider, the cracks become too wider for this fine grained SHCC to allow further significant cracking viscosity, or delayed resistance to crack widening.

5.3 Modelling of Time-dependent Behavior of SHCC

Following the same formulation of multi-layered microplane model, explained in chapter 4, the incremental macroscopic time-dependent stress-strain relationship can be represented as

$$\Delta\sigma_{ij} = C_{ijrs}(\Delta\varepsilon_{rs} - \Delta\varepsilon_{rs}^{creep} - \Delta\varepsilon_{rs}^{sh}) \tag{5.1}$$

where $\Delta\sigma_{ij}$ and $\Delta\varepsilon_{rs}$ are the macroscopic stress and strain increments, $\Delta\varepsilon_{rs}^{creep}$ and $\Delta\varepsilon_{rs}^{sh}$ are the strain increments for tensile creep strain and shrinkage strains, C_{ijrs} is the stiffness tensor which can be evaluated as

$$C_{ijrs} = \frac{3\pi}{2}\int n_i n_j n_r n_s C_N F(n)\, dS \tag{5.2}$$

$$\Delta\varepsilon_{rs}^{sh} = n_r n_s \dot{\varepsilon}_{rs}^{sh} \Delta t \tag{5.3}$$

$$\Delta\varepsilon_{rs}^{creep} = n_r n_s (\dot{\varepsilon}_{rs}^{creep'} + \dot{\varepsilon}_{rs}^{creep''}) \Delta t \tag{5.4}$$

where C_N is the incremental normal secant moduli for current loading for a microplane. The formulation to calculate cracking strain for static loading is given in detail in chapter 4. (F(n) = 1 which is a weight function of the normal direction that can introduce anisotropy in its initial state). n with subscripts i, j, r, s are the direction cosines. $\dot{\varepsilon}_{rs}^{sh}$ is the rate of shrinkage strain. Δt is the increment at each loading stage . The rate of shrinkage strain can be calculated as, using the power law,

$$\dot{\varepsilon}^{sh} = b_1.b_2(t - t_0)^{b_1 - 1} \tag{5.5}$$

where t is time at current loading and t_0 is initial time of loading. b_1, b_2 are the constants that can be adjusted by identification with test data. In Eq. 5.4, $\dot{\varepsilon}_{rs}^{creep'}$ is the rate of tensile matrix creep strain and $\dot{\varepsilon}_{rs}^{creep''}$ is the creep cracking strain. The tensile matrix creep component can be evaluated as

$$\dot{\varepsilon}^{creep'} = a_1.a_2(t-t_o)^{a_1-1}\sigma_N \tag{5.6}$$

where a_1, a_2 are the constants that can be adjusted by identification with test data for creep and σ_N is the normal sustained loading stress.

5.4 Time-dependent Crack Width Model

The creep cracking strain is dependent on time-dependent fiber pull out displacements. These time-dependent fiber pull out displacements can be attributed to the time-dependent crack widths. If sufficient data of fiber pull out creep is available then the cracking creep strain can be calculated as

$$\dot{\varepsilon}^{creep''} = \frac{1}{L_o}\sum_{i=1}^{N_{C(t)}}(\dot{w}_{ci(t)}) \tag{5.7}$$

where $N_{c(t)}$ is the time-dependent number of cracks, L_o is the original length of specimen and $w_{c(t)}$ is the time-dependent crack widths. The time-dependent fiber pull out displacement can be calculated as function of difference of time at initial loading and current loading as follows

$$u_{f(t)} = c_1(t-t_0)^{c_2} = w_{c(t)} \tag{5.8}$$

where $u_{f(t)}$ is the time-dependent fiber pull out displacement, $w_{c(t)}$ is the time-dependent crack width,c_1, c_2 are the parameters that can be adjusted by identification with experimental data. The rate of time dependent crack width can be formulated as

$$\dot{w}_{c(t)} = c_1.c_2(t-t_0)^{c_2-1} \tag{5.9}$$

where $\dot{w}_{c(t)}$ is the rate of time-dependent crack width. Hence cracking creep strain can be formulated by using Eq. 5.7.

5.5 Algorithm for Calculations

The Eq. 5.1 represents the macroscopic constitutive incremental relationship for short time and time-dependent behavior. The relationship is sufficient to simulate time-dependent behavior of SHCC for drying shrinkage and tensile creep. The step by step algorithm for calculation of simulations is given below:

- The macroscopic strain increments are imposed at the first step for normal strains for uniaxial tensile loading. These increments are updated at each stage of loading.

- These macroscopic normal strains are transformed in to strain at each microplane by multiplying direction cosines, i.e., the global normal strain is transformed into local normal strain.

- Based on the local normal strain, the normal secant moduli are calculated for single multi-layered microplane as shown in Fig. 5.1 (b). This function is then integrated over 21 integration points on the spherical surface. This numerical integration formula is based on work by Bazant and Oh[58] in which the comparison of microplane models for different integration point formula is reported. For the present research, the 21-point formula is used.

- After calculating global stiffness tensor, the incremental macroscopic stress is calculated by using Eq. 5.1 without time-dependent strains.

- This algorithm is repeated for each imposed increment of strain up to the level when sustained load for tensile creep starts to apply.

- The sustained load for tensile creep is applied in the absence of drying shrinkage as practically drying shrinkage is measured separately by using different set up. Therefore drying shrinkage and tensile creep are calculated separately and then added to get total time-dependent behavior if required.

- After this stage, the stress increments become zero as now stress becomes constant. The applied stress is usually a certain percentage of static first cracking strength of the material to practically reduce the chances of static cracking strain to be appeared. In this case, the left hand side of Eq. 5.1 becomes zero.

- For the right hand side of Eq. 5.1, the stiffness tensor cannot be zero. Therefore, the term within brackets becomes zero which gives the strain equal to strain due to tensile creep or drying shrinkage or total time-dependent strain.

- Then the creep matrix strain and creep cracking strain are calculated in the absence of drying shrinkage as drying shrinkage is separately simulated for sealed creep specimens.

- The both components of tensile strain are calculated by imposing time increments as rate functions. The material parameters for matrix creep are adjusted by identification with experimental data. The time function is a scalar parameter so that it is universal in all directions. The strain field is also assumed uniform. Therefore coordinate transformation is enough and summation over the microplanes is not required for time-dependent strains.

- For the creep cracking strain, the time-dependent number of cracks are taken from the experimental data and time-dependent crack widths are calculated from Eq. 5.8. If sufficient data for time-dependent fiber pull-out displacements is not available then the data for time-dependent crack width can be simulated directly as time-dependent displacements are attributed to time-dependent crack widths.

- For simulation of drying shrinkage, the Eq. 5.5 is used. The parameters are adjusted by identification with experimental data.

- The results are plotted for tensile creep, drying shrinkage and time-dependent crack widths and compared with experimental data.

5.6 Comparison of Analytical Results with Experimental Data

The tensile creep is simulated in the present study by using two different test data. The tensile sustained load is applied on the pre-cracked specimens. The material properties are given in Table 5.1. This kind of test data is fully representative of the model presented as the mechanism of time-dependent fiber pull-out and widening of cracks over time is significantly observed in the pre-cracked specimens. The results are shown in Fig. 5.2 and Fig. 5.3 for tensile creep data. The simulation is done by following the algorithm explained in the previous section. The model parameters are adjusted by identification with test data. The model parameters for tensile creep are shown in Table 5.2. For the explicit time integration used for the present simulation, the time step is selected as small as possible to improve the integration efficiency. The time step is used equal to 0.1 day for numerical time integration. The age of SHCC at loading or drying is 14 days while the loading rate up to maximum stress for creep is 0.1mm/sec. The relative humidity during the test is 65% and temperature is 23 ^{0}C .

Table 5.1 Material properties for test data

	Fiber volume	Length of Fiber	Diameter of fiber	Specimen size	Gauge length	Loading as % of tensile strength for creep specimen	
Properties	2%	12mm	40µm	80X30X15 mm	80mm	1[32]	2[31]
						60%	70%

Table 5.2 Model parameters for verification

Test data	Drying shrinkage[5]		Tensile creep[2]		Tensile creep[5]		Time-dependent crack width[2]	
Model parameters	b_1	b_2	a_1	a_2	a_1	a_2	c_1	c_2
	0.7	0.15	0.015	0.15	0.0033	0.2826	0.035	0.25

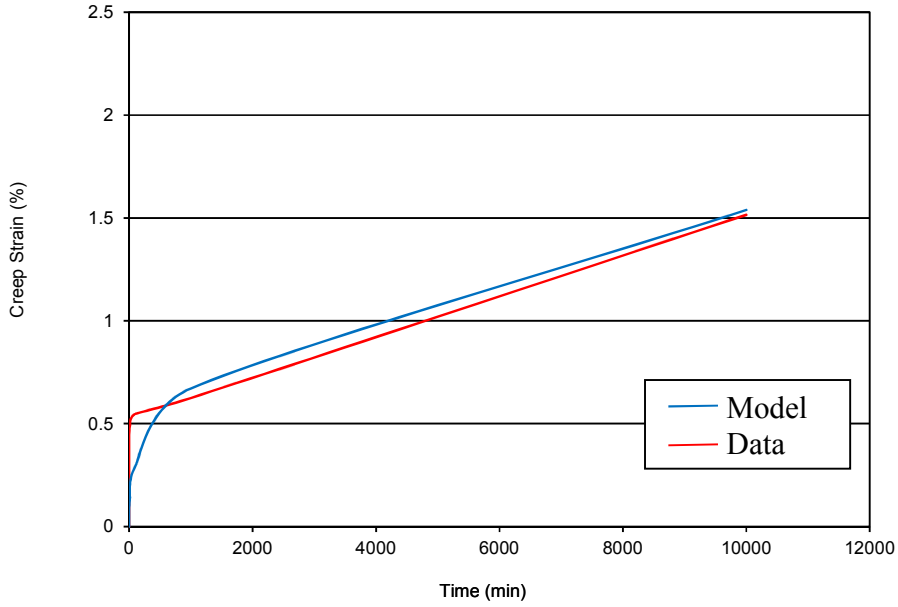

Fig. 5.2 Comparison analytical results of tensile creep strain with experimental data[57)]

The time-dependent crack width data is available that is a result of work by Boshoff et al[32)]. The number of cracks has been observed over time. Because of this kind of data, it become possible to fully depict the mechanism of creep cracking strain and to model them successfully. A very few such kind of test data is available. It is the recent focus of researchers these days. The analytical results are shown in Fig. 5.4. The model parameters are given in Table 5.2 while material properties are shown in Table 5.1.

The drying shrinkage is also simulated as shown in Fig. 5.4. The drying shrinkage is measured separately for the same properties of specimens shown in Table 5.1. The value of shrinkage strain is significant for SHCC and it cannot be ignored to model the time-dependent behavior. For that purpose two specimens were tested and average shrinkage is reported and then simulated. The model parameters adjusted by the identification with test data are given in Table 5.2. The time-dependent constitutive relationship resulted in the tensile creep-stress curve that is shown in Fig. 5.5. The simulation results are compared with experimental data. The model parameters values are given in Table 5.2.

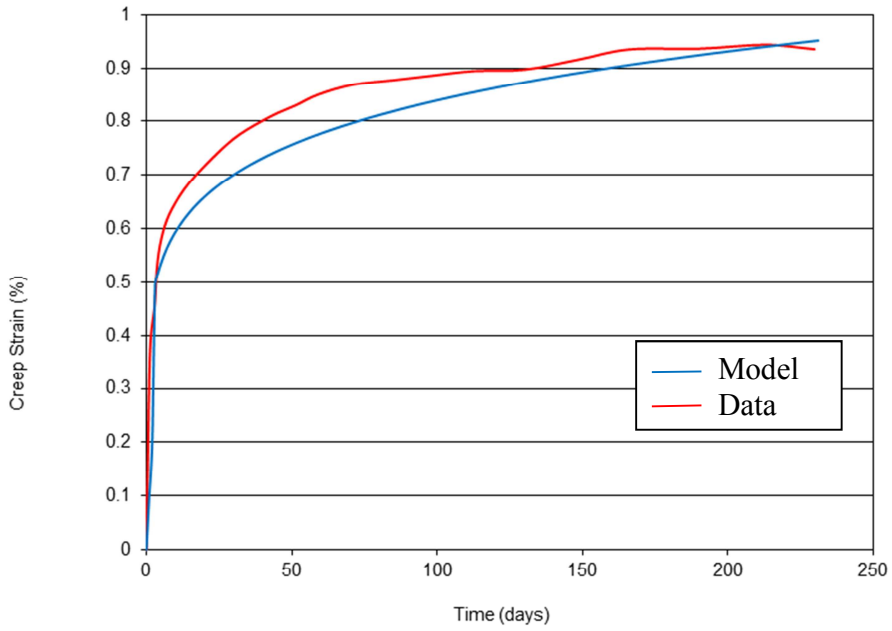

Fig. 5.3 Comparison analytical results of tensile creep strain with experimental data[31)]

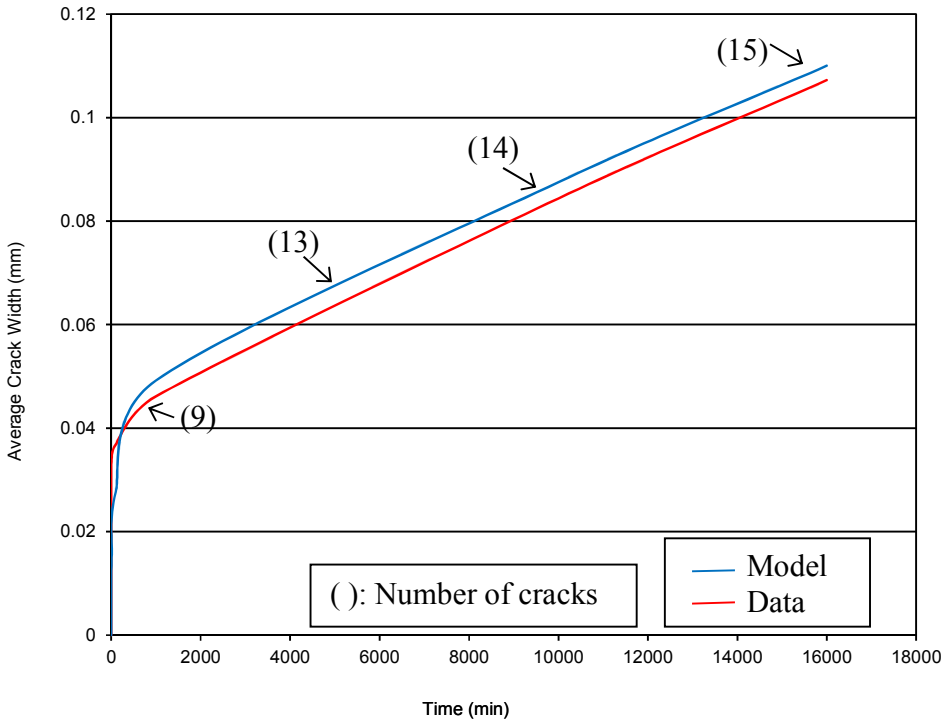

Fig. 5.4 Comparison analytical results of time-dependent crack width with experimental data[32)]

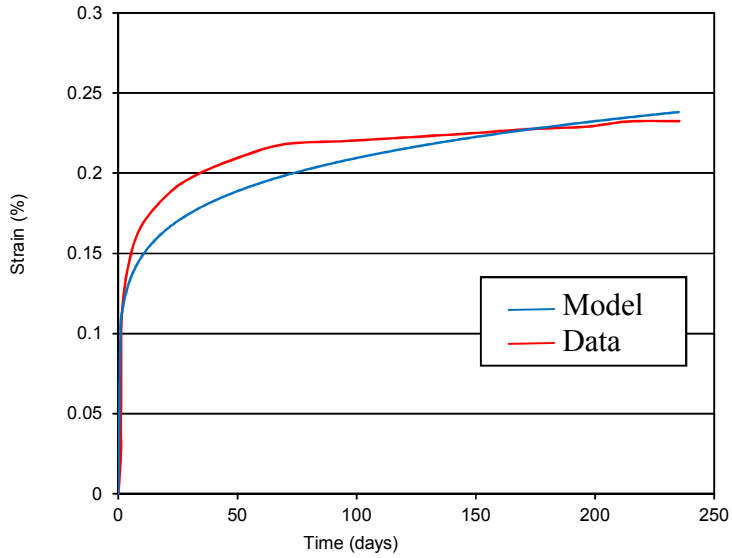

Fig. 5.5 Comparison analytical results of drying shrinkage with experimental data[31)]

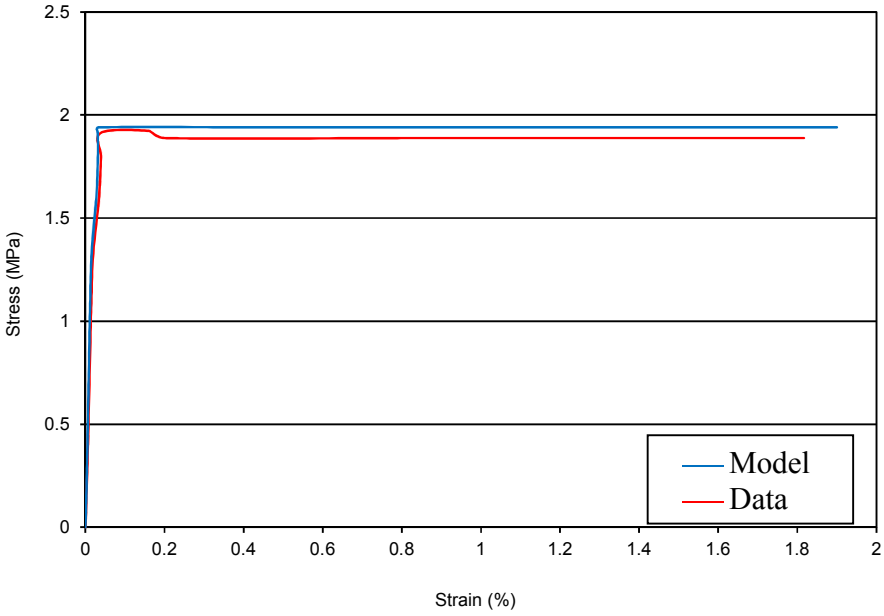

Fig. 5.6 Comparison analytical results of tensile creep with experimental data[32)]

5.7 Discussions on the Results

The simulation results of tensile creep strain are shown in Fig. 5.2 . This experimental data is resulted by measuring tensile creep for pre-cracked specimen. The purpose of pre-cracking of the specimen is to investigate the widening of purely time-dependent cracks, i.e., time-dependent fiber pull-out displacements. For the proposed model such kind of data has been considered the most appropriate. The applied sustained stress in this case is 60% of the static tensile stress which gives value equal to 1.94 MPa. The drying shrinkage in this case is measured separately for the same mix proportion of specimen that gives value of strain equal to 0.04mm. As compared to the total tensile creep strain value about 2% , the drying shrinkage is considered almost negligible.

The analytical results show a good agreement to experimental data except the creep strain larger times. This is because of average adjustments of the parameters by the identification of test data. If the focus has been given to creep at larger time during adjustment then the creep at later stage of times can also give more closer results. The Fig. 5.3 also shows the tensile creep model verification for another test data. For this case, the creep is measured with completely sealed specimen by applying Sikagard 63N sealant supplied by Sika SA. The drying shrinkage is measured separately for the specimen with same mix proportions. The drying shrinkage test is applied for two specimens and average of both values is reported that is also simulated as shown in Fig. 5.5.

For tensile creep data of Fig. 5.3, the sustained load is applied 70% of the static tensile load on pre-cracked specimen. The value of applied sustained load is 1.84 MPa. The comparison results show good agreement at early age and at later stage of times as well. The Fig. 5.4 represents the analytical results compared with test data for crack widths. For this case, the number of cracks over time was also reported in the reference. Based on these available test data values, it became easier to implement the presented model to simulate time-dependent crack width. The results show good agreement with test data.

5.8 Summary

In the present study the time-dependent behavior of SHCC is modelled by using multi-layered microplane model. The multi-layered model is an efficient tool to simulate the multiple cracking behavior of SHCC along with phenomenon of widening of cracks over time at micro-level. The simulation of tensile creep and shrinkage behavior is the main target of the present study which has been characterized on each layer of microplane and the constitutive relationship of SHCC can be developed.

In the present study, the normal component of strains and stresses will be considered because the tangential stiffness in assumed negligible due to flexible nature of synthetic fibers. The constitutive relationship of SHCC is modelled by considering multi-layered microplanes. The presented model is applicable to tensile creep that is the main advantage and focus of the present research as phenomenon of micro-cracks are associated with tensile creep behavior of SHCC. Given sufficient test data, the present model will be extended to be used for developing new SHCC materials for multiple cracking for given mix proportions and fiber information. The fiber characteristics and mix proportion information is used as input to estimate number of cracks. The prediction of stress-strain relationship or strain-time relationship with multiple cracking information is output of the present model.

Chapter 6
CONCLUSIONS AND RECOMMENDATIONS

6.1 General

The dissertation presented consists of three ways to implement microplane to model the mechanical behavior of SHCC under different types of loading. The first half comprises of the general introduction, background of the problem being investigated, research significance and practical applications of the research findings. Some of the information and knowledge which play an important role in this research and might be unfamiliar to some engineers are briefed as literature review.

The analytical model methodology for uniaxial tensile loading has been presented. This portion of the research is partitioned into three parts. The first part consists of analytical model to simulate the uniaxial stress-strain relationship by using tri-linear function. The microplane model has been considered as base of the presented analytical model. The original microplane model has been implemented for concrete and brittle plastics with exponential function for uniaxial tensile loading. The behavior of SHCC as pseudo-ductile material is tri-linear under uniaxial tensile loading conditions. To simulate this behavior, the use of tri-linear function is the most appropriate methodology that resulted in satisfactory agreement with the experimental data. In the second part of this chapter, the crack widths under uniaxial tensile loading have been simulated by using equivalent tangential fiber bridging stiffness approach. In the third part of the chapter, the crack spacing and distribution has been simulated for multiple cracking phenomenon of SHCC. All of these models have been compared with experimental data and resulted in good agreement.

The analytical model is presented to simulate the uniaxial tensile behavior by using multi-layered microplane model has been proposed. This model methodology has been presented based on statistical variation of fiber volume due to spatial distribution of short random synthetic fibers. The focus of this analytical approach is to model the strain-hardening region that is accompanied by multiple cracking. This methodology is implemented for multi-layered microplane model. The concept of multilayers attributes the multiple cracking phenomenon of SHCC. The crack width is simulated based on cracking strain approach is also proposed. The mechanism under uniaxial tensile loading reveals that the crack widths are attributed to fiber pull-out displacements for SHCC. Based on this mechanism, the analytical model is proposed to simulate total crack widths. The crack spacing and distribution is modelled based on varying strength along the length of specimen. The uniaxial compression behavior is simulated based on microplane model using arctan function is also explained. All of the proposed models are compared with experimental data for SHCC that show a satisfactory agreement.

The time-dependent modelling of SHCC by using multi-layered microplane model is proposed that is main focus of the present research. The proposed model is basically an extension of the model proposed in chapter 4. This proposed model in chapter 5 includes drying shrinkage and tensile creep parameters. The tensile creep is further based on matrix creep and time-dependent fiber pull-out displacements. The fiber creep itself is proved to be almost negligible as by the experiments done on single fiber creep by the researchers in the recent past. Thus the above mentioned mechanisms are incorporated in the proposed model for to simulate time-dependent behavior of SHCC. The time-dependent crack widths are also simulated. The results of simulation of the model presented are compared with the experimental data to ensure the applicability and validity of the model for time-dependent behavior of SHCC.

6.2 Main Conclusions

The main conclusions of the present research corresponding to the objectives defined in Chapter 1 are summarized as follows.

Table 6.1 Main conclusions of the present research

<table>
<tr><td colspan="2">OBJECTIVE 1:
Develop an analytical model able to predict the uniaxial tensile stress-strain relationship of SHCC based on microplane model using tri-linear tension property and multi-layered microplane model.</td></tr>
<tr><td>Chapter 3</td><td>1. The tri-linear function is used to model the uniaxial tensile behavior of SHCC.
2. The tri-linear function is dependent on first cracking strength of SHCC and maximum tensile strength. These strength are the most significant parameters considered for the durability design of SHCC.
3. The same approach is also effective to model three dimensional behavior of SHCC as microplane model has three dimensional characteristics.</td></tr>
<tr><td>Chapter 4</td><td>1. The spatial distribution of fiber volume is attributed to the statistical variation of matrix strength.
2. The fiber pull-out displacements are attributed to the crack widths which represents the cracking strain of SHCC.
3. The multi-layers of microplane (cracks) attributed to the multiple cracks of SHCC.
4. The bridging fiber stiffness is a variable parameter from crack to crack.
5. The multi-layered model is presented which represents the macroscopic behavior along with the number of multiple cracks.</td></tr>
<tr><td colspan="2">OBJECTIVE 2:
Develop an analytical model able to predict time-dependent behavior of SHCC based on</td></tr>
</table>

multi-layered microplane model.	
Chapter 5	1. The time-dependent fiber pull-out is the main source of time-dependent tensile creep. 2. The time-dependent behavior of SHCC is associated with time-dependent increase in number of cracks. 3. The extension of multi-layered microplane model to model time-dependent behavior is sufficient to predict the mechanical behavior of SHCC in both loading condition, i.e., short term and time-dependent.
OBJECTIVE 3: Develop an analytical model able to predict the crack widths of SHCC material.	
Chapter 3	1. Fiber bridging stiffness is the main parameter for the source of crack width increase and crack width control. 2. The linear variation of the equivalent tangential fiber stiffness is used form first cracking strength to the maximum tensile strength. 3. The number of cracks is also incorporated as important parameter to simulate multiple cracking behavior.
Chapter 4	1. Fiber bridging stiffness is the main parameter for the source of crack width increase and crack width control. 2. The uniform statistical variation is implemented for the fiber bridging stiffness from 1st crack to N_C number of cracks.
OBJECTIVE 4: Develop a model to simulate the multiple cracking of SHCC along with crack distribution and spacing	

Chapter 3	The formation of potential cracks is modelled when stress is equal to first cracking strength
Chapter 4	The crack distribution of SHCC is be modelled by assuming uniform discrete distribution of fibers along the length of specimen.
OBJECTIVE 5: Verify the present model by using identified material parameters by comparing the results with experimental data.	
The effectiveness and validity of the presented model for short term and time-dependent behavior of SHCC is verified by comparing with experimental data. The material parameters are carefully identified.	

6.3 Discussions on Results

The results of simulation for uniaxial tensile loading compared with experimental data represents that the tri-linear function may prove an efficient tool to model tension property of SHCC. This property is simulated in terms of secant modulus in normal direction. The normal component of stresses and strains on each microplane is considered for simplicity. Also, the tangential component of the strain is considered almost negligible as synthetic fibers are much flexible producing almost insignificant shear resistance in tangential direction. In this way the proposed model can be more simplified with less parameter to be identified. This is the main advantage of the use of microplane model that microplane model involves less parameters.

There is potential in the present model to modify considering the volumetric and deviatoric components of stresses and strains along with tangential component to get well described macroscopic behavior of SHCC. The crack width data is modelled by considering equivalent tangential stiffness of bridging fibers. This simulation approach gives almost closer data fit results. Here the model parameter needed to adjust at each increment of strain.

This makes the calculation process a little tedious. Inspite of this fact, the present model seems sufficient to simulate crack width. The crack distribution is simulated along with crack spacing. This behavior of multiple cracking is very important to model for durability point of view. The Fig. 3.6 shows comparison of crack distribution with experimental data.

This specimen is tested under uniaxial tensile loading giving first cracking strength as 3.9 MPa and maximum tensile strength as 4.5 MPa resulting in ductile behavior. From multiple cracking simulation results, it is clear that the assumptions those are considered for the present model are much closer to the practical scenario and give more factual results.

The advantage of multi-layered microplane model is that it can simulate not only the maximum tensile strength but also first cracking strength, strain-hardening, multiple cracking, number of cracks and softening of SHCC. All these behavior are much significant for design of SHCC structures to be used under service load conditions. From the present research, the multi-layered microplane model proved the suitable model to predict all of the above mentioned mechanical behavior of strain hardening cement-based composites. The model to simulate total crack width is also based on practical approach, i.e., the increase in crack width with increasing tensile strength. The formulation is attributed to bridging fiber stiffness, area of bridging fibers (distributed based on statistical variation of fiber volume) and elastic modulus of fibers. Hence fiber pull out displacements are considered the main source of increase in crack width at increasing tensile strength of material. The results show agreement with experimental data that reflects the applicability of the present model.

In the same way, the crack distribution based on statistical variation of fiber volume/tensile strength gives more justified results with experimental data which is in agreement of the applicability of the model for crack distribution and spacing for strain hardening cementitious composites. The implementation of statistical distribution of fiber volume is the proved close to the practical scenario. The simulation results of tensile creep strain where the experimental data is resulted by measuring tensile creep for pre-cracked specimen. The purpose of pre-cracking of the specimen is to investigate the widening of purely time-dependent cracks, i.e., time-dependent fiber pull-out displacements.

For the proposed model such kind of data has been considered the most appropriate. The applied sustained stress in the first case is 60% of the static tensile stress which gives value equal to 1.94 MPa. The drying shrinkage in this case is measured separately for the same mix proportion of specimen that gives value of strain equal to 0.04mm. As compared to the total tensile creep strain value about 2% , the drying shrinkage is considered almost negligible.

The analytical results show a good agreement to experimental data except the creep strain larger times. This is because of average adjustments of the parameters by regression analysis. If the focus has been given to creep at larger time during adjustment then the creep at later stage of times can also give closer results. The tensile creep model verification for second case is presented. For this case, the creep is measured with completely sealed specimen by apply Sikagard 63N sealant supplied by Sika SA. The drying shrinkage is measured separately for the specimen with same mix proportions. The drying shrinkage test is applied for two specimens and average of both values is reported. The analytical results compared with test data for crack widths. For this case, the number of cracks over time was also reported in the reference. Based on these available test data values, it became easier to implement the presented model to simulate time-dependent crack width. The results shows good agreement with test data**.**

6.4. Recommendations for Future Research

The model for time-dependent behavior of SHCC presented in this dissertation captures only a part of the real phenomenon. Further research is required in order to develop an analytical model which can simulate the whole range of time-dependent sources. For that purpose, it is also recommended to have more research work to understand the mechanism of the tensile creep and other time-dependent sources of SHCC. In this regard, it is needed to implement the rigorous experimental testing program for tensile creep of SHCC material especially for time-dependent fiber pull-out creep.

Many sources of the mechanical behavior under sustained loading are still under investigation. The most important among which is the fiber creep mechanism. Up till now a very few experimental work has been done to investigate this phenomenon. In the future, it is recommended to give focus to investigate fiber creep with more elaborated experimental set up. It is also recommended to future research to develop an analytical model which can simulate complete three deformational behavior of SHCC in all loading regimes.

REFERENCES

1) www.eng.gifu-u.ac.jp., 2013.
2) www.pipelineandgasjournal.com., 2012.
3) Han et al.: Simulation of highly ductile fiber-reinforced cement-based composite components Under Cyclic Loading, *ACI Structural Journal*, pp. 749-757, 2003.
4) Simone et al.: Combined continuous/discontinuous failure of cementitious composites, *Computational Modelling of Concrete Structures, Proceedings for EURO-C*, pp 133-137, 2003.
5) Kabele, P.: Linking scales in modelling of fracture in high performance fiber reinforced cementitious composites, *Fracture Mechanics of Concrete Structures*, 2003.
6) Kanda et al.: Application of pseudo strain-hardening cementitious composites to shear resistant structural elements, *Proceedings of Fracture Mechanics of Concrete Structures* , 1998.
7) Mishra, D.: Design of pseudo strain-hardening cementitious composites for a ductile plastic hinge, PhD Thesis, University of Michigan, 1995.
8) Kabele et al.: Use of BMC for ductile structural members, *Proceedings of 5th International Symposium on Brittle Matrix Composites (BMC-5*), pp. 579-588, 1997.
9) Maalej, M., and Li, V.C.: Introduction of strain hardening engineered cementitious composites in the design of reinforced concrete flexural members for improved durability, *American Concrete Institute Structural Journal*, Vol. 92, pp. 167-176, 1995.
10) Kim et al.: Shear performance of precast SHCC infill walls for seismic retrofitting of non-ductile frames, *Magazine of Concrete Research,* Vol. 12, pp. 925-924, 2010.
11) Zijl, G. P. A. G. and Wittmann, F.: Durability of strain-hardening cement-based composites (SHCC*), RILEM State-of-the-art Reports*, 2010.
12) Wang et al.: Durability and service life of elements made with SHCC under imposed strain, *3rd International RILEM Conference on Strain Hardening Cementitious Composites*, pp. 33-41, 2014.

13) Lim, Y.M. and Li, V.C.: Durable repair of aged infrastructures using trapping mechanism of engineered cementitious composites, *Journal of Cement and Concrete Composites*, Vol. 19, No. 4, pp. 373-385, 1997.

14) Zijl, G. P. A. G. and Stander, H.: SHCC repair overlays for RC: Interfacial bond characterization and modelling, *Concrete Repair, Rehabilitation and Retrofitting II*, pp. 995-1003, 2009.

15) Wu et al.: Control of Cs leachability in cementitious binders, Journal of Material Sciences, pp. 1736-1739, 1996.

16) Li, V. C. : From mechanics to structural engineering - The design of cementitious composites for civil engineering applications Structural Engineering/Earthquake Engineering, Vol 10, pp. 37-48, 1993.

17) Paul, S. H. and Zijl. G. P. A. G.: Mechanical behavior of strain hardening cement based composites (SHCC) based on micromechanical design, *Civil Engineering Department, Stellenbosch University, South Africa,* 2015.

18) Li et al.: Matrix design for pseudo strain-hardening FRCC, *Master Structural*, Vol 28, pp. 586-595, 1995.

19) Kanda, T. and Li, V. C.: A new micromechanics design theory for pseudo strain-hardening cementitious composites, *ASCE Journal of Engineering Mechanics*, Vol 124, pp. 373-381, 1999.

20) Peled, A. and Shah, S. P.: Processing effect in cementitious composites: extrusion and casting*, J. Mater Civil Engineering*, Vol 34, pp. 107-118, 2003.

21) Song, G. and Zijl, G. P. A. G.: Tailoring ECC for commercial application, In: *Proceedings 6th RILEM Symposium on Fiber reinforced concrete (FRC),* pp. 1391-1400, 2004.

22) Li et al.: Tensile strain-hardening behavior of polyvinyl alcohol engineered cementitious composites (PVA-ECC), *ACI Mater. Journal*, pp. 483-492,2001.

23) Arnon, B. and Sidney, M.: Fiber reinforced cementitious composites, second edition, 2007.

24) Hikasa, J. and Genba, T.: Replacement for asbestos in reinforced cement products "Kuralon" PVA fiber, properties, structure, *International Man Made Fiber Congress*, 1986.

25) Zhijiang, Z. and Tian, C. Y.: High tenacity PVA fibers : a suitable alternative for asbestos, *International Man-Made Fiber Congress*, 1986.
26) www.nycon.com/pva-fibers, 2013.
27) Alexander, H. and Christian, C.: Carbon fiber sensor: Theory and applications, 2012.
28) Nishioka et al.: Properties and applications of carbon fiber reinforced cement composites, *Developments in Fiber Reinforced Cement and Concrete*, 1986.
29) Li, V. C. and Obla, K.: Effect of fiber length variation on tensile properties of carbon-fiber cement composites, Composites Engineering, Vol. 4, pp. 947-964, 1994.
30) Li, V. C. and Mishra, D. K.: Micromechanics of fiber effect on the uniaxial compressive strength of cementitious composites, Fiber Reinforced Cement and Concrete, pp. 400-414, 1992.
31) Akihama et al.: Mechanical properties of carbon fiber reinforced cement composites, *International Journal of Cement Composites and Light Weight Concrete*, Vol. 8, pp. 21-34, 1986.
32) Dobb et al.: Structural aspects of high modulus aromatic polyamide fibers, *Philosophical Transactions of Royal Society of Biological Sciences*, pp. 483-485, 1980.
33) Walton, P. L. and Mjumdar, A. J.: Properties of cement composites reinforced with Kevlar fibers, *Journal of Material Sciences*, pp.-1075-1083, 1978.
34) Ohgishi et al.: Mechanical properties of cement mortar pastes reinforced with polyamide fibers, *Transportation of Japan Concrete Institute,* pp. 309-315, 1984.
35) Konczalski, P. and Piekarski, K.: Tensile properties of Portland cement reinforced with Kevlar fibers, *Journal of Reinforced Plastic Composites*, pp. 378-384, 1982.
36) Walton, P. L. and Majumdar, A. J.: Creep of Kevlar 49-cement composites, Journal of Material Sciences, pp. 2939-2946, 1983.
37) Mechtcherine, V. and Schulze, J.: Testing the behaviour of strain hardening cementitious composites in tension, *Int RILEM Workshop on HPFRCC in Structural Applications, RILEM Publications S.A.R.L.*, PRO 49, pp. 37–46, 2005.
38) Vorel, J. and Boshoff, W. P.: Numerical modelling of strain hardening fibre-reinforced composites, *International Conference on Advanced Concrete Materials ACM*, pp. 271–278, 2009.

39) Kabele, P.: Multiscale framework for modeling of fracture in high performance fiber reinforced cementitious composites, *Engineering Fracture Mechanics*, Vol 74, pp. 194–209, 2007.

40) Lin et al.: On interface characterization and performance of fibre reinforced cementitious composites, *Concrete Science Engineering*, Vol 1, pp. 173–184, 1999.

41) Petr, J. and Viktor, M.: Behaviour of Strain-hardening Cement-based Composites (SHCC) under monotonic and cyclic tensile loading Part 2 – Modelling, *Cement & Concrete Composites,* Vol 32, pp. 810–818, 2010.

42) Vorel, J. and Boshoff, W. P.: Numerical simulation of ductile fiber-reinforced cement-based composite, *Journal of Computational and Applied Mathematics*, Vol 270, pp. 433–442, 2014.

43) Kabele, P.: Stochastic finite element modelling of multiple cracking in fiber reinforced cementitious composites, *Czech Technical University in Prague,* 2010.

44) Griffith, A. A.: The phenomena of rupture and flow in solids, *Philosophical Transactions of the Royal Society of London,* 1920.

45) Cornelissen, H. A. W. and Siemes, A. J. M.: Plain concrete under sustained tensile or tensile and compressive fatigue loadings, *Stevin Laboratory, Delft University of Technology,* pp. 68–79, 1984.

46) Boshoff, W. P. and Zijl, G. P. A. G.: Time-dependent response of ECC: Characterisation of creep and rate dependence, *Cement and Concrete Research*, Vol 37, pp. 725–734, 2007.

47) Boshoff et al: Characterizing the time-dependent behavior on the single fiber level of SHCC: Part 1: Mechanism of fiber pull-out creep, Vol. 39, pp. 779-786, 2009.

48) Boshoff et al.: Creep of cracked strain hardening cement-based composites, *Creep, Shrinkage and Durability Mechanics of Concrete Structures*, pp. 723-728, 2009.

49) Li, V. C. and Leung, C. K. Y.: Steady-state and multiple cracking of short random fiber composites, *Journal of Engineering Mechanics, ASCE*, Vol 118, pp. 2246–2263, 1992.

50) Fischer, G. and Li, V. C.: Effect of fiber reinforcement on the response of structural members, *Engineering Fracture Mechanics*, Vol 74, pp. 258-272, 2007.

51) Kabele et al.: Effects of chemical exposure on bond between synthetic fiber and cementitious matrix, *Textile Reinforced Concrete – Proceedings of the 1st International RILEM Conference,* pp. 91-99, 2006.

52) Jun, P. and Mechtcherine, V.: Behavior of strain-hardening cement-based composites (SHCC) under monotonic and cyclic tensile loading. Part 1-Experimental investigations, Cement and Concrete Composites, Vol 32, pp. 801-809, 2010.

53) Kabele, P.: Equivalent model of multiple cracking, Engineering Mechanics, Vol 9, pp. 75-90, 2002.

54) Cervenka et al.: ATENA program documentation, Part-1, theory, pp. 61-64, 2012.

55) Bazant et al.: Microplane model for brittle-plastic material: I Theory, *Journal of Engineering Mechanics, ASCE*, Vol 114, pp.1672-1687, 1988.

56) Bazant, Z. P. and Oh, B. H.: Crack band theory for fracture of concrete, Vol 16, pp. 155-177, 1983.

57) Bazant et al.: Microplane model M4 for concrete. I: Formulation with work-conjugate deviatoric stress, *Journal of Engineering Mechanics,* Vol 126, pp. 944-953, 2000.

58) Bazant, Z. P. and Zi, G.: Continuous relaxation spectrum for concrete creep and its incorporation inti microplane model M4, *Journal of Engineering Mechanics*, Vol 128, pp. 1331-1336, 2002.

59) Bazant et al.: Microplane Model M5f for Multiaxial Behavior and Fracture of Fiber-Reinforced Concrete, *Journal of Engineering Mechanics ASCE*, pp.66-75, 2007.

60) Bazant, Z. P. and Caner, F. C.: Microplane model M6f for fiber reinforced concrete, *XI Internationsl conference on computational plasticity, Fundamentals and Applications COMPLAS XI,* pp.796-806, 2011.

61) Bazant et al.: Microplane model M7f for fiber reinforced concrete, *Engineering Fracture Mechanics*, Vol 105, pp. 41-57, 2013.

62) Sumitro, S. and Tsubaki, T.: Micromechanical constitutive relationship of fiber reinforced concrete, Vol 18, pp. 419-424, 1996.

63) Pande, G. N. and Xiong, W.: An improved multi-laminate model of jointed rock masses, *International Symposium on Numerical Models in Geomechanics*, pp. 218-226, 1982.

64) Zienkiewicz, O. C. and Pande, G. N.: Time-dependent multi-laminate model of rocks, *International Journal of Numerical Methods in Geomechanics*, Vol 1, pp. 219-247, 1977.

65) Kojima et al.: Application of direct sprayed ECC for retrofitting dam structure surface: application for mitaka dam, *Concrete Journal*, pp. 35-39, 2004.

66) Li et al.: Shotcreting with ECC, 2009.

67) Benable concrete minimizes cracking and fracture problems, *MRS bulletin*, 2006.

68) Mitamura et al.: Repair construction of steel deck with highly ductile fiber reinforced cement composites-construction of mihara bridge, *Bridge Found,* Vol.39, pp. 88-91, 2005.

69) Li et al.: Field demonstration of durable link slabs for jointless bridge decks based on strain-hardening cementitious composites, *Michigan Department of Transportation Research Report RC-1471*, 2005.

70) Lepech, M. D. and Li, V. C.: Application of ECC for bridge deck slabs, *Material and Structures*, Vol. 42, pp. 1185-1195, 2009.

71) Li et al.: High performance material for rapid durable repair of bridges and structures, *Michigan Department of Transportation Research Report RC-1484*, 2006.

72) Li, M.: Multi-scale design for durable repair of concrete structure, PhD Dissertation, University of Michigan, 2009.

73) https://www.pavementpreservation.org, 2013.

74) https://en.wikipedia.org, 2012.

75) Jun, P. and Mechtcherine, V.: Behavior of strain-hardening cement-based composites (SHCC) under monotonic and cyclic tensile loading: Part 2-Modelling, *Cement and Concrete Composites*, pp. 810-818, 2010.

76) Vorel, J. and Boshoff, B. P.: Numerical simulation of ductile fiber-reinforced cement-based composite, Journal of Computational and Applied Mathematics, pp. 433-442, 2014.

77) Bazant, Z. P. and Gambarova, G. P.: Shear crack in concrete: Crack band microplane model, *Journal of Structural Engineering*, Vol 110, pp. 2015-2035, 1984.

78) Zijl, G. P. A. G.: Durability under mechanical load-Micro-crack formation ductility, *RILEM*, pp. 9-39, 2011.

79) Rokugo et al.: Direct tensile behavior and size effect of strain-hardening fiber-reinforced cement-based composites (SHCC), *FRAMCOS VI*, 2007.
80) Vorel, J. and Boshoff, W. P.: Numerical modelling of strain hardening fiber-reinforced composites, *International Conference on Advanced Concrete Materials, ACM,* Vol 100, pp. 271-278, 2009.
81) Ozbolt, J. and Bazant, Z. P.: Microplane model for cyclic triaxial behavior of concrete, *Journal of Engineering Mechanics,* Vol 118, pp.1365-1386 1992.
82) Kabele, P. and Horii, H.: Analytical model for fracture behaviors of pseudo strain-hardening cementitious composites, *Journal of Materials Concrete Structural Pavements*, Vol 3, pp.209-219, 1996.
83) Sirijaroonchai et al.: Behavior of high performance fiber reinforced cement composites under multi-axial compressive loading, *Cement and Concrete Composites,* Vol 32, pp.62-72, 2010.
84) Zhou et al.: Experimental study on mechanical behaviors of pseudo-ductile cementitious composites and normal concrete under biaxial compression, *VIII International Conference on FraMCos-8,* pp. 963-969, 2013.
85) Lepech, M. D. and Li, V. C.: Long term durability performance of engineered cementitious composites, *International Journal for Restoration of Buildings and Monuments*, pp. 119-132, 2006.
86) Boshoff, W. P. and Zijl, G. P. A. G.: Creep modelling of ductile fiber reinforced composites, *University of Stellenbosch*, South Africa, 2004.
87) Bazant, Z. P. and Oh, B. H.: Efficient numerical integration on the surface of a sphere, pp. 37-49, 1986.
88) Mura, T.: Micromechanics of defects in solids, Kluwer Academic Publisher, 1987.
89) Li, V. C. and Hashida, T.: Ductile fracture in cementitious materials, Fracture Mechanics of Concrete, pp. 526-535, 1992.
90) Lin et al.: On interface property characterization and performance of fiber reinforced cementitious composites, Concrete Science and Engineering, pp. 173-184, 1999.
91) http://www.kuraray.com, 2010.
92) http://www.cqjrwa.en.alibaba.com, 2014.
93) Kamal et al.: Evaluation of crack elongation performance of UHP-SHCC as a surface

repair material, *Creep, Shrinkage and Durability Mechanics of Concrete Structures*, pp. 519-525, 2009.

94) Lyanaga, S. and Kawada, Y., Encyclopedic Dictionary of Mathematics, *Massachusetts Institute of Technology Press*, 1980.

95) Albrecht, L. and Collatz, L.: Zur nllmerischen Allswertllng mehrdimensionaler Integrate, *Zeitsdtrrft fr"ir Allgewandte Mat/telllatlk wId MI'c/ulllik,* pp. 1-15, 1958.

96) Bazant, Z. P. and Oh, B. H. : Microplane model for progressive fracture of concrete and rock, *Journal of Engineering Mechanics*, Vol 111, pp. 559-582, 1985.

97) Stroud, A.: Approximate Calclliation of Mllltil'le Itltcgrals, 1971

98) Bazant, Z. P., and Oh, B. H.: Efficient Numerical Integration on the Surface of a Sphere, *Center for Concrete and Geomaterials*, 1985.

99) Zijl, G. P. A. G and Boshoff, W. P.: Mechanism of creep in fiber-reinforced strain-hardening cement composites (SHCC*), Creep, Shrinkage and Durability Mechanics of Concrete Structures*, pp 753-759, 2009.

100) Lee et al.: Prediction of ECC tensile stress-strain curves based on modified fiber bridging relations considering fiber distribution characteristics, *Computers and Concrete*, Vol. 7, pp. 455-468, 2010.

101) Xing, Y.: Constitutive equation of concrete using strain-space plasticity model, PhD Dissertation, New Jersey Institute of Technology, 1993.

102) Katz et al.: Bond properties of carbon fibers in cementitious matrix, *Journal of Materials in Civil Engineering*, pp. 125-128, 1995.

APPENDIX A

CRACK STRAIN MODEL FOR MULTIPLE CRACKING OF SHCC WITHOUT USING MICROPLANE MODEL

A.1 Introduction

The crack strain model for strain hardening cementitious composites under the state of multiple cracking is proposed by Kebele[53]. This constitutive model is established utilizing the methods of micromechanics of solids with defects[88]. A structural member is considered which is undergoing multiple cracking then it is possible to identify a volume element. This volume element contains numerous cracks. Such element is called representative volume element (RVE). It is acceptable and computationally convenient to idealize the structural member as one consisting of a homogeneous and continuous material (so-called equivalent continuum). When a sample of a fiber-reinforced composite material undergoes multiple cracking under uniform stress, a fine matrix crack, approximately perpendicular to the loading direction, propagates almost instantaneously through the specimen as soon as the load attains the composite first crack strength. As load increases, existing cracks open and new cracks are generated.

The matrix cracking initiates at preexisting microcracks or inhomogeneities. However, the process of matrix crack propagation from the initial defect has a far less significant effect on the overall stress-strain relationship than the fiber bridging (traction transfer) that takes place on these cracks and the evolution of multiple cracks width and quantity.

A.2 Normal Cracking Strain

Assuming instantaneous occurrence of a crack intersecting the RVE, it can be considered that each crack has a uniform opening displacement and that the local microscopic stress remains uniform. The cracking strain ε_{ij}^{mc} represents the contribution to

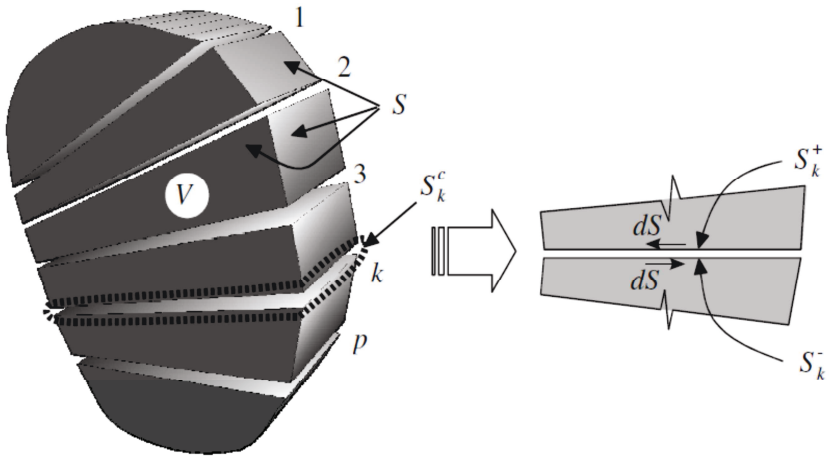

Fig. A1 Representative volume element in multiple cracking state[53].

the total macroscopic strain due to cracks. The expression for the cracking strain can be described considering that surface S_k^c for each crack is a union of the crack surface S_k^+ and S_k^- as shown in Fig. A1. The shape of surfaces S_k^+ and S_k^- is identical, but orientation of the increment dS_k^c and that of unit normal vector are opposite. Denoting by u_i^+ and n_i^+ the quantities associated with surface S_k^+ and u_i^- and n_i^- the quantities associated with surface S_k^-, cracking strain can be expresses in Eq. a1.

$$\varepsilon_{ij}^{mc} = \frac{1}{V}\sum_{k=1}^{p}\frac{1}{2}\int_{S_k^+}[(u_i^+ - u_i^-)n_j^+ + (u_j^+ - u_j^-)n_i^+]dS_k^+$$

$$\varepsilon_{ij}^{mc} = \frac{1}{V}\sum_{k=1}^{p}\frac{1}{2}\int_{S_k^+}(\delta_i n_j + n_i^+\delta_j n_i)dS_k^+ \qquad (a1)$$

where notation δ_i was introduced for relative displacement vector of crack surfaces:

$$\delta_i = u_i^+ - u_i^- \qquad (a2)$$

Component of this vector, which is normal to the crack surface, is called crack opening displacement (COD); tangential components are called crack sliding displacement (CSD) or crack slip. Considering the primary set of p^ξ cracks perpendicular to the ξ-axis, the normal components of cracking strain are expressed from Eq. a1 as:

$$\varepsilon_{\xi\xi}^{mc,\xi} = \frac{1}{V}\sum_{k=1}^{p^\xi}\frac{1}{2}\int_{S_k^{\xi+}}\delta_\xi^{\xi,k}\,dS_k^+$$

$$\varepsilon_{\eta\eta}^{mc,\xi} = 0$$

$$\varepsilon_{\zeta\zeta}^{mc,\xi} = 0 \qquad (a3)$$

Symbol $\delta_\xi^{\xi,k}$ stands for the crack opening displacement of the k-th crack of the primary multiple crack set. Considering a prismatic RVE of dimension l^ξ, l^η and l^ζ, the first of the Eq. a3 can be rewritten as:

$$\varepsilon_{\xi\xi}^{mc,\xi} = \frac{1}{l^\xi}\sum_{k=1}^{p^\xi}\frac{1}{l^\eta l^\zeta}\int_0^{l^\eta}\int_0^{l_\zeta}\delta_\xi^{\xi,k}\,d\eta\,d\zeta = \frac{1}{l^\xi}\sum_{k=1}^{p^\xi}\delta_\xi^{\xi,k} \qquad (a4)$$

Thus, the normal cracking strain corresponds to the sum of crack opening displacements $\delta_\xi^{\xi,k}$ divided by the size l^ξ (perpendicular to cracks) of the RVE. Since the cracks are considered cutting throughout the RVE, the normal bridging stress σ^b must be in equilibrium with the applied uniform stress $\sigma_{\xi\xi}$. The relationship between normal bridging stress and COD has been derived on the basis of micromechanics of fiber debonding and pullout by Li and Hashida[89] as:

$$\sigma^b(\tilde{\delta}) = \left(\frac{V_f\tau l_f}{2d_f}\right)g\left[2\left(\frac{\tilde{\delta}}{\frac{2\tau l_f(1+\eta)}{E_f d_f}}\right)^{\frac{1}{2}} - \left(\frac{\tilde{\delta}}{\frac{2\tau l_f(1+\eta)}{E_f d_f}}\right)\right] \qquad (a5)$$

Here $\tilde{\delta}$ is COD normalize by $l_f/2$; l_f ,d_f , E_f and V_f are the fiber length, diameter, Young's modulus and volume fraction, respectively; τ is the strength of frictional bond between fiber and matrix; g is a snubbing factor and $\eta = V_f E_f /[(1-V_f)E_m]$, where E_m is the matrix Young's modulus. Note that Eq. a5 assumes that fiber-matrix chemical bond is negligible and that fibers do not rupture. A more general $\sigma-\delta$ relationship, which includes these phenomena, can be found in work by Lin et al.[90]. By substituting p^{ξ} and Eq. a5 into Eq. a4, the desired RVE compliance equation can be expressed in the following form:

$$\varepsilon_{\xi\xi}^{mc,\xi} = \varepsilon_{\xi\xi}^{mc,\xi}(\sigma_{\xi\xi}) \qquad (a6)$$

If the RVE undergoes multiple cracking in more than one direction, the normal cracking strains associated with the secondary and tertiary crack sets are obtained in a likewise manner as for the primary set. Thus Eq. a3 and Eq.a6 can be generalized as follows:

$$\varepsilon_{ii}^{mc,i} = \varepsilon_{ii}^{mc,i}(\sigma_{ii})$$

$$\varepsilon_{ii}^{mc,j} = 0 \qquad (a7)$$

in which index i stands for the crack-normal direction ($i = \xi,\eta,\zeta$) and j is a crack-parallel direction ($j = \xi,\eta,\zeta$, except $j = i$). Summation rule over indices is not applied in the above equations.

A.3 Summary

The numerical model to simulate the cracking strain without using microplane model is explained in this Appendix. This model can simulate the macroscope constitutive relationship for multiple cracking state for SHCC. This model is also implemented into an FEM program, which is used to reproduce satisfactory verification results with test data. The CC3DNONLINCEMENTITIOUS2SHCC is suitable model for fiber reinforced concrete, such as SHCC (Strain Hardening Cementitious Composites) and HPFRCC or UHPFRC (high and ultrahigh performance fiber reinforced concrete) materials implemented in ATENA 2D V 4.0 by using present constitutive relationship. The tensile softening regime and the shear retention factor are modified based on the model, proposed in KABELE[53]. This model is based on a notion of a representative volume element (RVE), which contains distributed multiple cracks (hardening) as well as localized cracks (softening)[54] as explained in Chapter 2. For crack opening model, the crack-normal stress components are related to cracking strains corresponding to opening of multiple and localized cracks by piecewise linear relations (although linear hardening and softening are shown, a user should be allowed to input piecewise linear curves). For multiple cracks, it is assumed that they do not close unless exposed to crack-normal compression (plasticity-like unloading) while a localized crack is assumed to close so that normal stress decreases linearly to reach zero at zero COD (these assumptions may need to be revised in the future to some combination of plasticity and damage-like closure).

APPENDIX B

CALCULATION PROCEDURE FOR SHORT-TIME AND TIME-DEPENDENT BEHAVIOR OF SHCC

B.1 Introduction

The multi-layered microplane model for short-time behavior is based on microplane model originally proposed by Bazant and Gambarova[48]. In that study, the constitutive law for concrete within the crack band has been discussed by the microplane model. The micro-strains on weak planes of various orientations (the microplanes) are assumed to conform to the same macroscopic strain tensor, and the micro-stresses from all the microplanes are superimposed. Due to the neglect of shear stiffness on individual microplanes, the material behavior is completely characterized by the relation between the normal stress and strain for each microplane.

Strain-softening violates the basic hypothesis of the theory of plasticity, usually expressed as Drucker's stability postulate. The presence of friction on microcracking and the degradation of elastic stiffness due to progressive microcracking also invalidate Drucker's postulate. Thus, the theories that use loading surfaces and inelastic potentials can hardly provide a good model for progressive microcracking. Their use would be further complicated by the fact that the microcracks cause the elastic stiffness to become anisotropic. For these reasons, it appears preferable to describe the inelastic properties not globally but individually for planes of various orientations within the material. The microscopic deformations on these planes called the "microplanes". These must be suitably constrained to the macroscopic deformations.

The same concept can be implemented to predict the short-time micromechanical deformational behavior at each microplane and then by using kinematic constraints, the

microplanes are associated with global deformational behavior of SHCC. Due to pseudo ductile behavior, SHCC shows multiple cracking phenomenon. That is why it is necessary to implement multiple cracking in microplane model. This purpose has been achieved by introducing multi-layered microplane model. Before explanation of calculation procedure for the short-time deformational behavior of SHCC, it is needed to explain about the basic hypothesis of microplane model required to develop the constitutive relationship of stresses and strains.

B.2 Microplane Model

To model the tensile strain-softening due to microcracking, it is necessary to modify the above mentioned approaches in that the microstructure is constrained kinematically rather than statically, i.e., the strains on planes of various orientations are the resolved components of the same macroscopic strain, instead of stresses on planes of various orientations being the resolved component of the same macroscopic stress. The basic assumptions of this model may be summed up in the following 2 hypotheses.

Hypothesis I: The normal microstrain that governs the progressive development of cracking on microplane of any orientation is equal to the resolved macroscopic strain tensor for the same plane.

There are certain reasons for using hypothesis I as using resolved stresses rather than strains on the microplanes would cause computational problems for strain-softening. As two strains corresponding to a given stress, but only one stress corresponds to a given strain. The second reason may be that the microstrains must be stable when the microstrains are fixed. It has been experienced numerically that, in the case of strain-softening, the model becomes unstable if resolved stresses rather than strains are used in hypothesis I.

Hypothesis II: The stress relaxation due to all microcracks normal to $\vec{n}$ is characterized by assuming that the microstress on the microplane of any orientation is a function of the normal microstrain on the same plane.

$$s_n = F(e_n) \tag{b1}$$

where e_n and s_n are the normal microstrain and microstress respectively. In hypothesis II, shear stiffness on an individual microplane is neglected. The overall shear system of the microplane system is obtained entirely from the normal stiffness on the microplane. This hypothesis has an advantage of simplicity.

Hypothesis III: It is found that, considering the elastic deformation of isotropic material, the stiffness matrix always yields Poisson ratio $\nu^c = 1/4$ and also $E^c = E_n / 2$, in which E^c is the young's modulus of the material and E_n is the initial normal stiffness for the microplane. Since $\nu^c = 1/4$ is not suitable for SHCC material, a correction is needed. This adjustment can be made according to the hypothesis III. According to this hypothesis, the total macroscopic strain is a sum of strain due to microplane system and additional elastic strain ε_{ij}^a , i.e.,

$$\varepsilon_{ij} = e_{ij} + \varepsilon_{ij}^a \tag{b2}$$

B.3 Calculation Procedure for Short-term Behavior

B.3.1 Constitutive relationship

The detailed step by step procedure to calculate numerically micromechanical short-time behavior of SHCC under uniaxial tensile loading is given as follows.

1. The increments for the macroscopic normal strains are imposed as $\Delta\varepsilon_{rs}$.
2. In the first step, for first increment of macroscopic imposed strain, the microstrain is calculated by using hypothesis I.

$$e_{rs} = n_r n_s \varepsilon_{rs} \tag{b3}$$

where latin lower case subscripts refer to Cartesian coordinates $x_r (r = 1,2,3)$; n_r are the direction cosines of the unit normal $\vec{n}$ of the microplane; and repeated latin lower case subscripts indicate a summation over 1,2,3.

3. The constitutive relationship at each microplane is derived as

$$ds_{ij} = D^{c}_{ijrs}\, de_{rs} \qquad (b4)$$

4. The stiffness matrix can be derived by applying equilibrium conditions expressed by means of principle of virtual work. The stiffness tensor can be calculated as follows.

$$D^{c}_{ijrs} = \frac{3}{2\pi}\int_{0}^{2\pi}\int_{0}^{\pi/2} a_{ijrs}\,\frac{ds_n}{de_n}\, f(\vec{n})\sin\phi\, d\phi\, d\theta \qquad (b5)$$

with

$$a_{ijrs} = n_i n_j n_r n_s$$

where D^{c}_{ijrs} is the tangent stiffnesses of the microplane system. $dS = \sin\phi\, d\theta\, d\phi$ as integraton need to be made over the entire surface of the sphere, since the value of e_n and s_n are equal at any two diametrically opposite points on the sphere. Function $f(\vec{n})$, introducing the relative frequency of the microplanes of various orientations $\vec{n}$ that characterizes the initial anisotropy of the material. In this case, the initial isotropy is assumed and then $f(\vec{n}) = 1$.

Uniaxial Tension: For uniaxial tension the tangent secant modulus is calculated by using exponential function as follows

$$C_N^T = E_N e^{-k\varepsilon_N{}^p}(1 - kp\varepsilon_N{}^p) \qquad (b6)$$

in which E_n, k and p are the material parameters. The values of those are identified during simulations.

Uniaxial compression: For uniaxial compression, arctan function is used to calculate tangent modulus, i.e.,

$$s_n = \frac{2}{\pi}|\sigma_0|\arctan(\omega e_n) \qquad (b7)$$

where σ_0 is the asymptotic plastic stress value that is adjusted during simulation and

$$\omega = \frac{\pi E_n}{2|\sigma_0|}, \qquad E_n = 2E\frac{(1+\nu^m)}{(1+\nu)} \tag{b8}$$

5. The integral of stiffness tensor is evaluated by approximated as finite sum

$$D_{ijrs} = \sum_{\alpha=1}^{N} w_\alpha [a_{ijrs} C_N]_\alpha \tag{b9}$$

where w_α is the weights associated with integration points. In the present model, 21-point integration formula is used.

6. The compliance to the additional elastic strain ε_{ij}^a is as follows after satisfying isotropic condition.

$$C^a_{ijrs} = \frac{1}{9K^a}\delta_{ij}\delta_{rs} + \frac{1}{2G^a}(\delta_{ir}\delta_{js} - \frac{1}{3}\delta_{ij}\delta_{rs}) \tag{b10}$$

where K^a is the additional bulk modulus and G^a is the additional shear modulus. The value of each additional modulus can be calculated as follows.

$$K^a = \frac{1+\nu}{9(\nu^m - \nu)}E^m \ (for \quad \nu \le \nu^m, G^a \to \infty) \tag{b11}$$

where ν^m is equal to 1/4 and E^m is equal to $0.4\pi E_n$.

7. The total stiffness is calculated by adding stiffness of microplane system and additional elastic stiffness.

$$[D_{ijrs}] = [(D^{c^{-1}})_{ijrs} + C^a_{ijrs}]^{-1} \tag{b12}$$

8. The macroscopic incremental stress-strain relationship is evaluated by the following relation.

$$\Delta \sigma_{ij} = D_{ijrs} \Delta \varepsilon_{rs} \tag{b13}$$

9. For next iteration, stresses are updated and stored in array.

$$\sigma_{r+1} = \sigma_r + \Delta \sigma_{ij} \tag{b14}$$

10. The same calculation procedure is repeated for next imposed strain increments.

$$\varepsilon_{r+1} = \varepsilon_r + \Delta \varepsilon_{rs} \tag{b15}$$

This calculation procedure is followed to calculate the ML (Multi-layerd) model representing the macroscopic uniaxial tensile behavior of strain hardening cementitious composite. The results are shown in Chapter 4 in detail. The multi-layered model is simulated which depict the behavior of material at each crack. The number of cracks and corresponding tensile strength in strain hardening zone are taken from experimental data.

B.3.2 Calculation procedure for crack widths

The equation to calculate the total displacement at i-th crack stage for maximum N_c number of cracks can be expressed as follows

$$(w_i)_T = \sum_{j=1}^{i} (w_j) + g_i \tag{b16}$$

where $(w_i)_T$ is the total crack width at i-th crack stage and w_j is the crack width of j-th crack that can be evaluated as

$$w_j = \frac{Af_{t(j)}}{A_{f(j)}k_{f(j)}} \qquad (b17)$$

where k_{fj} is the stiffness of bridging fibers at j-th crack and f_{tj} is the tensile strength at j-th crack. In Eq. b16, g_i is the sum of all crack openings due to increase of load beyond the initial cracking load at each crack stage, i.e.,

$$g = \sum_{i=2}^{N_C}\left(\frac{P_{fi} - P_{f(i-1)}}{k_{f(i-1)}.A_{f(i-1)}}\right) + \sum_{i=3}^{N_C}\left(\frac{P_{fi} - P_{f(i-1)}}{k_{f(i-2)}.A_{f(i-2)}}\right) + \ldots$$
$$+ \sum_{i=N_C-1}^{N_C}\left(\frac{P_{fi} - P_{f(i-1)}}{k_{f(i-1)}.A_{f(i-1)}}\right) + \left(\frac{P_{fN_C} - P_{f(N_C-1)}}{k_{f(N_C-1)}.A_{f(N_C-1)}}\right) \qquad (b18)$$

where p_{fj} is the load at j-th crack stage and $p_{f(j-1)}$ is the load at $j-1$ crack stage. In Eq. b18, the summation is taken place while the upper limit is larger than the lower limit and last term is for $j = i$.

B.4 Calculation Procedure for Time-dependent Behavior

The time-dependent behavior is a significant factor in the micromechanical deformational aspects of strain hardening cementitious composites. Due to phenomenon of time-dependent cracking in the material, it becomes a need of hour to predict the time-dependent behavior of SHCC. The tensile creep and drying shrinkage is the most happening phenomenon has been observed for SHCC. The tensile creep is associated with time-dependent fiber pull-out creep and formation of new cracks over time. These behaviors can be characterized on each microplane and then transformed to represent the global behavior.

These aspects are described in the form of numerical model in Chapter 5. The step by step calculation procedure for simulation of time-dependent behavior of SHCC is explained in this Appendix. The sustained load is applied for tensile creep on SHCC specimen equal to certain fraction of static tensile loading.

1. The increments for the macroscopic normal strains are imposed as $\Delta\varepsilon_{rs}$.
2. In the first step, for first increment of macroscopic imposed strain, the microstrain is calculated by using hypothesis I explained in Section B.2.

$$e_{rs} = n_r n_s \varepsilon_{rs} \tag{b19}$$

where latin lower case subscripts refer to Cartesian coordinates $x_r (r = 1,2,3)$; n_r are the direction cosines of the unit normal $\vec{n}$ of the microplane; and repeated latin lower case subscripts indicate a summation over 1,2,3.

3. The constitutive relationship at each microplane is derived as

$$ds_{ij} = D^{c}_{ijrs} (de_{rs} - de^{sh}_{rs} - de^{cr}_{rs}) \tag{b20}$$

where de^{sh}_{rs} is the strain increment for drying shrinkage and de^{cr}_{rs} is the strain increment of tensile creep strain at each microplane.

4. The stiffness matrix can be derived by applying equilibrium conditions expressed by means of principle of virtual work. The stiffness tensor can be calculated as follows.

$$D^{c}_{ijrs} = \frac{3}{2\pi} \int_0^{2\pi} \int_0^{\pi/2} a_{ijrs} \frac{ds_n}{de_n} f(\vec{n}) \sin\phi \, d\phi \, d\theta \tag{b21}$$

with

$$a_{ijrs} = n_i n_j n_r n_s$$

where D^{c}_{ijrs} is the tangent stiffnesses of the microplane system. $dS = \sin\phi \, d\theta \, d\phi$ as integraton need to be made over the entire surface of the sphere, since the value of e_n and s_n are equal at any two diametrically opposite points on the sphere. Function $f(\vec{n})$, introducing the relative frequency of the microplanes of various orientations $\vec{n}$ that

characterizes the initial anisotropy of the material. In this case, the initial isotropy is assumed and then $f(\vec{n}) = 1$.

Uniaxial Tension: For uniaxial tension the tangent secant modulus is calculated by using exponential function as follows

$$s_n = E_n e_n e^{-(e_n/k)^p} \qquad (b22)$$

in which E_n , k and p are the material parameters. The values of those are identified during simulations.

5. The integral of stiffness tensor is evaluated by approximated as finite sum

$$D_{ijrs} = \sum_{\alpha=1}^{N} w_\alpha [a_{ijrs} C_N]_\alpha \qquad (b23)$$

where w_α is the weights associated with integration points. In the present model, 21-point integration formula is used.

6. The compliance to the additional elastic strain ε_{ij}^a is as follows after satisfying isotropic condition.

$$C^{\,a}_{ijrs} = \frac{1}{9K^{\,a}}\delta_{ij}\delta_{rs} + \frac{1}{2G^{\,a}}(\delta_{ir}\delta_{js} - \frac{1}{3}\delta_{ij}\delta_{rs}) \qquad (b24)$$

where K^a is the additional bulk modulus and G^a is the additional shear modulus. The value of each additional modulus can be calculated as follows.

$$K^a = \frac{1+\nu}{9(\nu^m - \nu)} E^m \ (for \quad \nu \le \nu^m, G^a \to \infty) \qquad (b25)$$

where ν^m is equal to ¼ and E^m is equal to $0.4\pi E_n$.

6. The total stiffness is calculated by adding stiffness of microplane system and additional elastic stiffness.

$$[D_{ijrs}] = [(D^{c^{-1}})_{ijrs} + C^{a}_{ijrs}]^{-1} \qquad (b26)$$

7. The macroscopic incremental stress-strain relationship is evaluated by the following relation.

$$\Delta\sigma_{ij} = D_{ijrs}(\Delta\varepsilon_{rs} - \Delta\varepsilon^{sh}_{rs} - \Delta\varepsilon^{cr}_{rs}) \qquad (b27)$$

where $\Delta\sigma^{cr}_{ij}$ is the stress increments associated with cracking strain $\Delta\varepsilon^{cr}_{rs}$ under short time loading, i.e.,

$$\Delta\sigma^{cr}_{ij} = C_{ijrs}\Delta\varepsilon^{cr}_{rs} \qquad (b28)$$

$$\Delta\varepsilon^{cr}_{rs} = n_r n_s \Delta\varepsilon_{cri} \qquad (b29)$$

8. For next iteration, stresses are updated and stored in array.

$$\sigma_{r+1} = \sigma_r + \Delta\sigma_{ij} \qquad (b30)$$

9. The same calculation procedure is repeated for next imposed strain increments.

$$\varepsilon_{r+1} = \varepsilon_r + \Delta\varepsilon_{rs} \qquad (b31)$$

10. This algorithm is repeated for each imposed increment of strain up to the level when sustained load for tensile creep starts to apply.

11. After this stage, the stress increments become zero as now stress become constant. The applied stress is usually a certain % age of static first cracking strength of the material to practically reduce the chances of static cracking strain to be appeared. In this case, the left hand side of Eq. b9 becomes zero.

$$0 = D_{ijrs}(\Delta\varepsilon_{rs} - \Delta\varepsilon^{sh}_{rs} - \Delta\varepsilon^{cr}_{rs}) \qquad (b32)$$

12. For right hand side of Eq. b28, the stiffness tensor cannot be zero. Therefore, the term within brackets become zero which gives the strain equal to strain due to tensile creep or drying shrinkage or total time-dependent strain.

$$\Delta\varepsilon_{rs} = \Delta\varepsilon_{rs}^{sh} - \Delta\varepsilon_{rs}^{cr} \tag{b33}$$

13. Then the creep matrix strain and creep cracking strain are calculated in the absence of drying shrinkage as drying shrinkage is separately simulated for sealed creep specimens.

14. The both components of tensile strain are calculated by imposing time increments as rate functions. The material parameters for matric creep are adjusted by regression analysis of experimental data. Time is a scalar parameter so that it is universal in all directions. The strain field is also assumed uniform. Therefore coordinate transformation is enough and summation over the microplanes is not required for time-dependent strains. The tensile creep is calculated by using following relationship.

$$\dot{\varepsilon}^{creep'} = a_1.a_2(t-t_o)^{a_1-1}\sigma_N \tag{c34}$$

15. For the creep cracking strain, the time-dependent number of cracks are taken from the experimental data and time-dependent crack widths are calculated from Eq. b18. If sufficient data for time-dependent fiber pull-out displacements is not available then the data for time-dependent crack width can be simulated directly as time-dependent displacements are attributed to time-dependent crack widths.

$$\dot{\varepsilon}^{creep^{cr}} = \frac{1}{L_o}\sum_{i=1}^{N_c}\dot{w}_{c(t)} \tag{c35}$$

$$\dot{w}_{c(t)} = c_1.c_2(t-t_0)^{c_2-1} \tag{c36}$$

16. For simulation of drying shrinkage, the Eq. b37 is used. The parameters are adjusted by identification of experimental data.

$$\dot{\varepsilon}^{sh} = b_1.b_2(t-t_0)^{b_1-1} \qquad (c37)$$

17. For calculation of creep, drying shrinkage and time dependent crack width, the step-by-step time integration scheme is followed in which time t is subdivided by discrete times (0,1,2,3,……) in time steps $\Delta t_r = t_r - t_{r-1}$. The time t_o coincides with the time the first stress is introduced in to the material. The time step or time increment is taken equal to 0.1 day.

18. The results are plotted for tensile creep, drying shrinkage and time-dependent crack widths and compared with experimental data.

B.5 Summary

The calculation procedure for simulation of short-time behavior is summarized here. This behavior is simulated for uniaxial tensile loading and uniaxial compression. The micromechanical deformational behavior is significantly illustrated in this study. This step by step algorithm is very useful to understand the flow of calculation procedure to simulate the model. The identification of parameters is an important factor during the simulation. The parameter values play a vital role in predicting the behavior of material. In this study the material parameters are identified carefully and presented in Chapter 4 in detail. The detailed model description is explained in Chapter 4 along with verification of numerical model with experimental data.

In the present study the time-dependent behavior of SHCC is modelled by using multi-layered microplane model. The multi-layered model is an efficient tool to simulate the multiple cracking behavior of SHCC along with phenomenon of widening of cracks over time at micro-level. The simulation of tensile creep and shrinkage behavior is the main target of the present study which has been characterized on each layer of microplane as power law and the constitutive relationship of SHCC can be developed. In the present study, the normal component of strains and stresses will be considered because the tangential stiffness in

assumed negligible due to flexible nature of synthetic fibers. The constitutive relationship of SHCC is modelled by considering multi-layered microplanes. The presented model is applicable to tensile creep that is the main advantage and focus of the present research as phenomenon of micro-cracks are associated with tensile creep behavior of SHCC. The step by step calculation algorithm is presented to make good understanding of the numerical model simulation for time-dependent behavior of SHCC.

APPENDIX C

VARIOUS SYNTHETIC FIBERS FOR SHCC

C.1 Introduction

High strength PVA fibers have been developed mainly for asbestos replacement. The fibers are produced by wet or dry spinning, and boron is added to achieve high strength and stiffness by forming intermolecular bonds. The fibers are surface treated to enhance their compatibility with the matrix and to enable efficient dispersion. The surface treatment, combined with the inherent affinity of this polymer for water, due to the presence of OH-groups, leads not only to the efficient dispersion, but also to a strong bond in the hardened compoites. The properties of PVA fibers demonstrate that their modulus of elasticity can be of the same order of magnitude as that of the cementitious matrix.

PVA fibers tend to rupture instead of pull-out of a cementitious matrix, due to the strong chemical bonding and the resulting slip-hardening response during pull-out were able to produce composites with an ultimate tensile strain exceeding 4% with a fiber volume of only The PVA fibers are thermally stable. It has been also found that the PVA –cement composites has a better freeze-thaw durability than any other type of fiber. In this appendix, the properties of some common used PVA fibers are highlighted. The commercial applications of PVA fibers has been significantly increased in the past decades. This fact has opened new ways of commercial production of various brands and types of PVA fibers.

C.2 PVA fiber (Type-A)

PVA fiber (Type-A) is a class of polyvinyl alcohol fibers manufactured by company-A. This class of PVA fibers has wide range of properties. The characteristics and properties of this kind of fibers also increase the application field of area for this category. The

properties and application of this category of PVA fibers is mentioned in detail in the following sectons.

C.2.1 Characteristics of PVA fiber (Type-A)

These fibers have the following distinguishing properties

1. High tenacity.
2. High modulus.
3. Low elongation.
4. Light weight.
5. Good resistance against chemicals (alkaline).
6. Good adhesion to cement matrix.

The general range of values of certain important properties of PVA fiber (Type-A) are also given in Table C.1. The alkaline resistance of these fibers is compared with the other materials which are supposed to have better alkali resistance. This comparison is shown in Fig. C.1 in which the strength reduction of fiber (index) is calculated for different materials.

Table C.1 Properties of PVA fibers (Type-A)

Properties	Values
Tensile strength (MPa)	880-1600
Elongation (%)	6
Tensile modulus (GPa)	25-41
Specific gravity (g/cm^3)	1.3

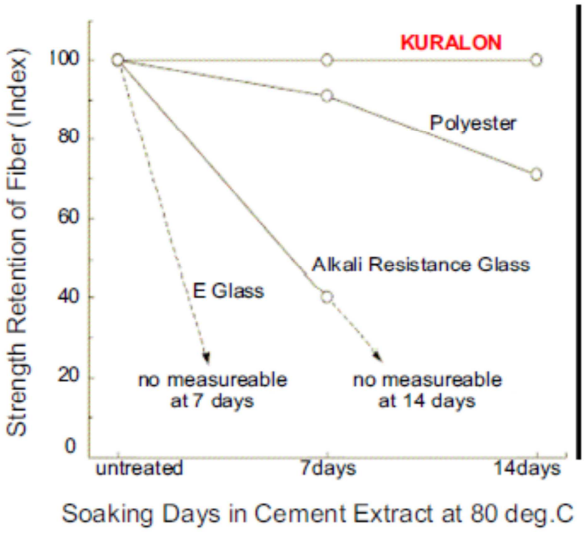

Fig C.1 Comparison of alkaline resistance of PVA fibers (Type-A) with other materials[91].

C.2.2 Performance of PVA Fibers (Type-A)

These fibers are difficult to be pulled out from matrix and can bridge between internal surfaces of cracks. In this way this fiber prevents cracks from growing wider and matrix can be bent more without breaking. PVA fibers cannot improve the stress at initial cracking of tensile and bending property. However, after initial cracking, they bear the stress instead of matrix. These fibers can improve the deformation capacity of matrix and especially improve the bending stress. PVA fiber (Type-A) (RCS 18X8) 0.6kg/m^3 (=1.0 lbs/yd^3) can reduce 50% of shrinkage cracking width shown in Fig. A.2. This fiber disperses one big crack to many small cracks, and then water-tightness and flexural strength of concrete/mortar can be kept. ECC (Engineered Cementitious Composites) can show the feature of multiple cracking.

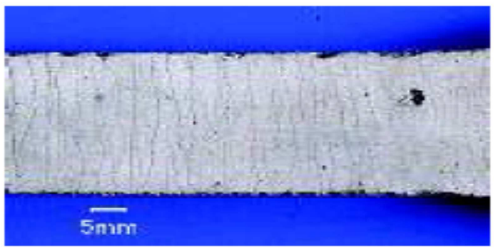

Fig. C.2 Multiple micro crack[91]

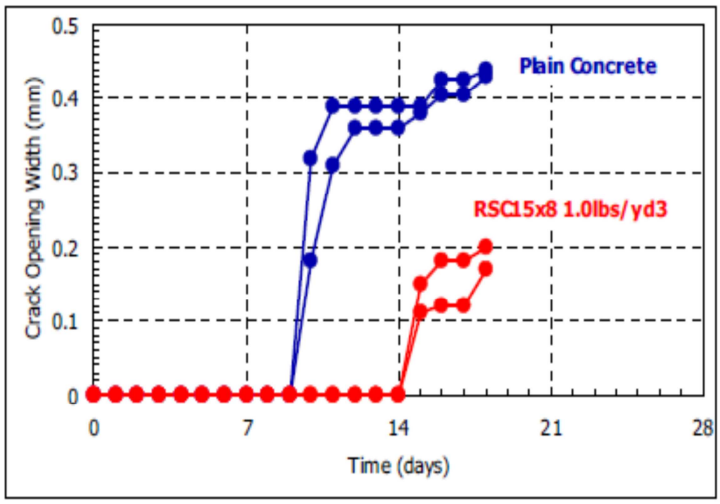

Fig. C.3 Crack opening in 20 ^{0}C , 60% R.H. condition[91].

Table C.2 Types and properties of various PVA fibers (Type-A)

Type	Diameter (micron)	Length (mm)	Tensile strength (GPa)	Modulus (GPa)	Note
RMS702	26	6	1.6	39	Resin-bundled type
RSC15	40	8	1.4	36	Cracking control
RECS15	40	8,12	1.6	41	Resin-bundled type
RECS100	100	12	1.2	28	Resin-bundled type
RF400	200	6,12	1.0	27	
RFS400	200	18	1.0	27	Resin-bundled type
RF1000	310	15	1.0	29	
RF4000	660	30	0.9	23	

C.2.3 Types of PVA fiber (Type-A)

There are various types of PVA fibers (Type-A) depending upon their properties and other dimensional characteristics. The fineness and length of various types varies from 26 micron/6 mm to 660 micron/40 mm. The fiber type can also be selected depending upon mix design. One type is called resin-bundled type that is used to control the dispersibility of fibers to avoid re-aggregating during the mixing process (fiber ball). The various types are shown in Table C.2.

C.2.4 Applications of PVA fibers (Type-A)

There is wide range of applicability for PVA fibers (Type-A) in the construction field. Now days the PVA fiber production and utility has increased to much extent. The brief applications of PVA fibers are given as follows.

1. Building wall (Cladding wall).
2. Permanent formworks (precast).
3. Bridge deck slab.
4. OA panel for floor
5. Wind proof panel for railways
6. Retrofit
7. Shotcrete for slope stabilization.
8. Shotcrete for tunnel lining.
9. Overlay for concrete road pavement.
10. Concrete slab on grade.
11. Heavy concrete floor surface.

The type of fibers used for different applications may be different. The choice of type of PVA fiber depends on desired characteristics of structure. Other than the type of fiber, the fiber volume or contents of fiber is also very important. PVA fibers (Type-A) represent the immense range of applicability around the world. Some applications along with type of fiber used and fiber contents are shown in Table C.3.

Table C.3 Applications of different types of PVA fibers (Type-A)

Application	**Fiber type**	**Fiber contents**	**Functions**
Building wall (cladding)	RMS702, RECS15	1-1.5vol%	Toughness, cracking control
Permanent formworks	RECS15, RF4000	2-2.5vol%	Toughness, cracking control
Bridge deck slab.	RECS100	0.075vol%	Cracking control, abrasion prevention
OA panel for floor	RECS100, RF400	2.5-3vol%	Impact strength, toughness
Wind proof panel for railways	RFS400	2.5vol%	Cracking control, toughness
Retrofit	RMS702, RECS15, RECS100	0.1-2vol%	Cracking control, toughness
Shortcrete for slope stabilization.	RFS400, RF4000	0.75-1vol%	Cracking control, toughness
Shortcrete for tunnel lining.	RF4000	0.75-1vol%	Toughness
Overlay for concrete road pavement.	RF4000	0.75vol%	Toughness, frost damage resistance
Concrete slab on grade.	RECS100, RF4000	0.15,0.46vol%	Cracking control, toughness
Heavy concrete floor surface.	RSC15	0.077vol%	Cracking control

Fig C.4 Application of PVA fiber (Type-A) as curtain wall[91].

Fig C.5 Application of PVA fiber (Type-A) as permanent framework[91].

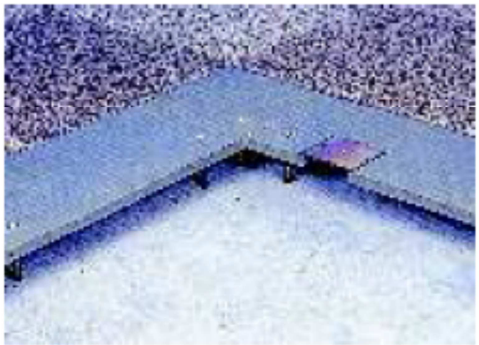

Fig C.6 Application of PVA fiber (Type-A) as floor panel[91].

Fig C.7 Application of PVA fiber (Type-A) as shortcreting for slope stabilization[91)].

Fig C.8 Application of PVA fiber (Type-A) as tunnel lining[91)].

C.3 PVA Fibers (Type-B)

PVA fiber (Type-B) products are of different diameters and lengths are available in the market for use in fiber reinforced concrete, stucco and precasr. PVA fibers (Type-B) are specially designed for use in concrete and mortar products for the purpose of controlling plastic shrinkage, thermal cracking and improving abrasion resistance. PVA fibers (Type-B) meet the requirements of ASTM C-116, section 4.1.3 and AC-32 at 1.0 lb (0.45kg) per CY.

The following advantages of these fibers can be summarized briefly.

1. Molecular bond with the concrete.
2. Reduces the formation of plastic shrinkage cracking in concrete.
3. Provides multi-dimensional reinforcement.
4. Improves impact, shatter and abrasion resistance of concrete.
5. Enhances durability and toughness of concrete.
6. Excellent, “no fuzz” finishability.

These fibers can be added directly to the mixing system during or after the batching of the ingredients and mixed at high speed for a minimum of five minutes. Additional mixing does not adversely affect the distribution or overall performance of PVA fibers (Type-B). The addition of these fibers at the normal or high dosage rate does not require any mix design or application changes. A water reducer or super-plasticizer is recommended in concrete products where improved workability and finishability are desired.

Fiber reinforced concrete can be finished by most finishing techniques. These fibers do not affect the finishing characteristics of concrete. These fibers can be used in power/hand troweled concrete, colored and broom finished concrete and can be pumped and placed using conventional equipment. Hand screeds can be used, but vibratory and laser screeds are recommended to provide added compaction and bury surface fibers.

The packaging of PVA fibers (Type-B) is done as follows

1. (30) 1 lb (0.45 kg) paper beater bags per box, 600 lbs per pallet.
2. (30) 1 lb (0.45 kg) water soluble bags per box, 600 lbs per pallet.
3. (21) 40 lb (18 kg) paper bulk bags, 840 lbs per pallet.
4. NYCON-PVA Fibers are packaged in pre-measured 1 lb (0.45kg) degradable “toss-in” paper beater bags, water soluble bags or bulk bags.

These fibers utilize the mixing activity to disperse the fibers into the mix. These fibers act with a molecular bond in the concrete with a multi-dimensional fiber network.

Table C.4 Properties of various types of PVA fibers (Type-B)

Type	RECS100	RF4000	RFS400	RMS702	RSC15	RECS15
Diameter (micron)	20	660	200	24	38	38
Length (mm)	13	30	19	6	8	8
Specific gravity	1.3	1.3	1.3	1.3	1.3	1.3
Tensile strength (MPa)	1200	800	1000	1600	1400	1600
Flexural strength (GPa)	25	23	29	39	30	40
Melting point	435^0F	435^0F	435^0F	435^0F	435^0F	435^0F
Color	White	Yellow	White	White	White	White
Water absorbtion	<1%by weight	<1%by weight	<1%by weight	<1%by weight	<1%by weight	<1%by weight
Alkali resistance	Excellent	Excellent	Excellent	Excellent	Excellent	Excellent
Corrosion resistance	Excellent	Excellent	Excellent	Excellent	Excellent	Excellent

These fibers do not affect curing process chemically. PVA fibers (Type-B) can be used in all types of concrete. Synthetic fibers help the concrete at early ages, which is especially beneficial where stripping time and handling is important. The material properties for various type of PVA fibers (Type-B) are given in Table C.4.

C.4 High Tenacity and High Modulus PVA fiber (Type-C)

The High Tenacity and High Modulus PVA fiber is the product name of this type of PVA fiber. This type is used as concrete board. This product is available as raw material as shown in Fig. C.9. The place of origin of this product is Anhui, China. This product is available in the market with brand name. The fineness of high tenacity and high modulus PVA fiber is 2.0+/-0.25dtex. The other properties are given in Table C.5. The main features of this type of PVA fiber are as follows.

- Flame Retardant
- Anti-Bacteria
- Anti-UV, Eco-Friendly
- Chemical-Resistant
- Radiation-Resistant

Fig C.9 High tenacity and high modulus PVA fiber (Type-C)[92)].

Table C.5 Properties of high tenacity and high modulus PVA fibers (Type-C)

PVA Fiber (Type-C)	
Material:	Polyvinyl Alcohol
Diameter:	2.0+/-0.25dtex
Tenacity:	11.5CN/dtex min.
Elongation:	7.5% max.
Modulus (0.1-0.4%):	280+/-20CN/dtex
Density:	1.29g/cm3
Hot Water Solubility (900 C,1hour)	≤2%
Length:	5mm / 6mm multiple
Formula	(CH2CHOH)n

C.5 Anti-crack concrete PVA fibers (Type-D)

The anti-crack concrete PVA fiber is especial type of fibers that are used for fiber reinforced roofing carport material. This type of material has origin of China. It has the following properties. The other significant properties and characteristics are given in Table C.6. This type of fibers are shown in Fig. C.10.

- High tensile strength and modulus.
- Good chemical compatibility with Portland cement.
- Anti-crack property.

Fig. C.10 Anti-crack PVA fibers (Type-D)[92].

Table C.6 Properties of anti-crack PVA fibers (Type-D)

Properties	
Length	6, 8, 10, 12mm
Finenss	2.0±0.25 dtex (To adjust from 1---15dtex) (10---50um)
Tensile Strength	≥11.5cn/dtex
E-Modulus	≥280cn/dtex
Elongation	6.5%+0.5
Decrement in 90°C hot water	1% max
Dispersion	1---3

C.6 Summary

PVA fibers have some structural strength and can also be used for shrinkage control. While they cannot replace reinforcing steel, they improve the mechanical properties of cured concrete, boosting its strength. High-performance fibers made of PVA, which is short for polyvinyl alcohol, were developed some 20 years ago by Company-A, a Japanese company. When added to concrete or mortar, the fibers develop a molecular and chemical bond with the cement during hydration and curing. This resulted in concrete with high tensile strength and amazing ductility whose makeup can significantly reduce a project's steel load.

Polyvinyl-alcohol engineered cementitious composite, PVA-ECC, was developed to be used in high-rises for earthquake remediation because it eliminates vertical sheer. While concrete is very strong side to side, any vertical movement will make it break or crack. Therefore, PVA-ECC allows movement like a blanket. This stuff would not crack, but it does multiple cracking to allow it to bend. It is literally bendable concrete. This sets PVA-ECC apart from glass-fiber reinforced concrete (GFRC) which is subject to vertical shear. According to materials by Company-A, PVA-ECC has strain-hardening capacity, while GFRC has none, meaning a PVA piece is less prone to failure when it cracks. The engineered cementitious product can be used for anything large or small, from vertical walls and horizontal countertops to precast slabs and patch-and-repair shotcrete.
These properties are ascertained by using an appropriate selection of PVA-fibers. Therefore, various kinds of PVA-fibers with different mechanical properties are briefly discussed in this Appendix.

APPENDIX D

FEM SIMULATION OF SHCC BY USING ATENA 2D V4.0

D.1 Introduction

The CC3DNONLINCEMENTITIOUS2SHCC is suitable for fiber reinforced concrete, such as SHCC (Strain Hardening Cementitious Composites) and HPFRCC or UHPFRC (high and ultrahigh performance fiber reinforced concrete) materials. The tensile softening regime and the shear retention factor are modified based on the model, proposed in KABELE[53]. This model is based on a notion of a representative volume element (RVE), which contains distributed multiple cracks (hardening) as well as localized cracks (softening)[54]. This model is a good representation of deformational behavior at global level. The short time behavior of SHCC can be simulated by using this model by ATENA 2D V.4.

The main advantage of this model is that it represents the multiple cracking phenomenon and strain hardening in three directions. That concept is similar to the idea of behavioral effect on the spherical surface in three dimensions. The only difference is that model by ATENA 2D V4 is representative of global deformational behavior while microplane model represents the constitutive relationship on the microplanes. Hence microplane model gives micromechanical deformations and then these micromechanical deformational behavior is constraint to get global or macroscopic behavior. Here the FEM simulation of SHCC by using a model by ATENA 2D V4 is done for uniaxial tensile loading. The results are shown in the later sections. The crack width with increasing tensile strengths in the strain hardening zone is also simulated by the model. The mesh sensitivity is also analyzed.

D.2 Model for Simulation of SHCC by ATENA 2D V 4

For FEM simulation of SHCC, the first step is the selection of appropriate dimensions of the model. The uniaxial tensile loading is applied on a specimen of SHCC with specific dimensions. One of the experimental works is done on these specific dog bone dumbbell shaped specimen by Mechterine[75]. Therefore, the dimension of ATENA model is selected equal to 80 mm X 30mm with thickness of 16 mm. To apply load on the top of the specimen and to fix the specimen from bottom, the steel palates are placed with dimension equal to 20 mm X 30 mm. The thickness of both steel plates is same as of SHCC specimen.

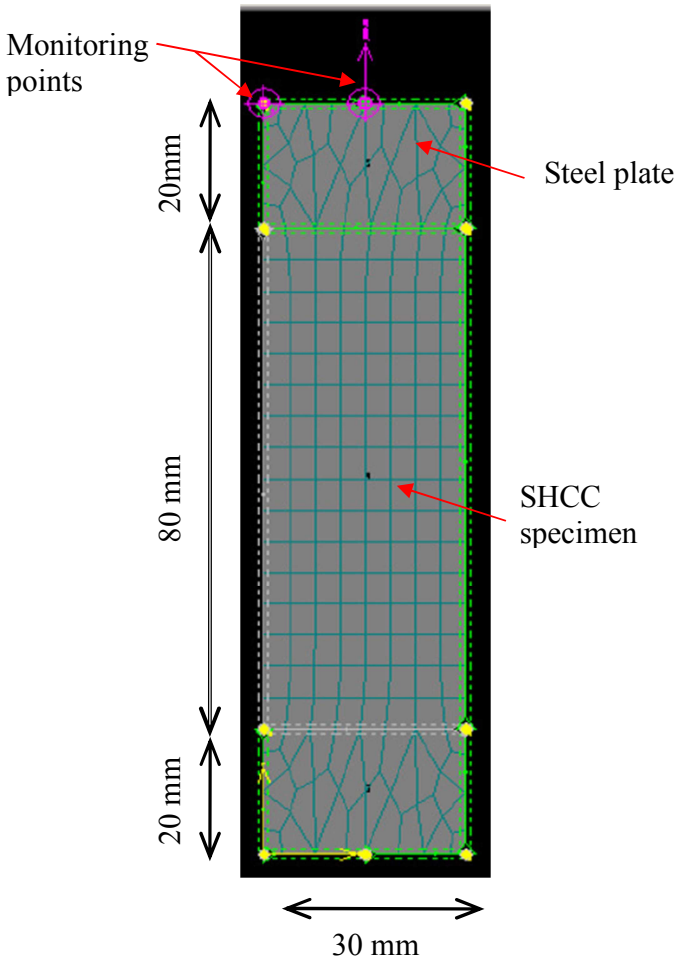

Fig. D.1 Model for simulation of SHCC.

The mesh size is selected based on the fiber length and crack spacing so that the multiple cracking can be simulated in FEM environment. The shape of mesh is shown in Fig D.1. Regular mesh has been selected for the specimen and irregular for the steel plates as specimen is of concern for the present analysis. The monitoring points are selected on the specimen to monitor load and displacement. The position of monitoring points is also shown in Fig. D.1. The uniaxial tensile load is applied on the specimen at the top steel plate in the middle.

D.3 Input material parameters

After making an appropriate model, the next step is to select suitable material parameters for simulation of SHCC material. For that purpose a complete set of input parameters are available in the ATENA. The material parameters are first taken from the experimental data or general values can be selected and then can be adjusted by trial and error as simulation will start. The basic parameters required for the simulation are shown in Fig. D.2. The elastic modulus value is input form the experimental data. The poison's ratio for SHCC is generally considered as 0.2. The tensile strength is also taken from the experimental data. For simulation of SHCC for uniaxial tensile loading, there is no need to input values for compressive strength. However, the general value can be input.

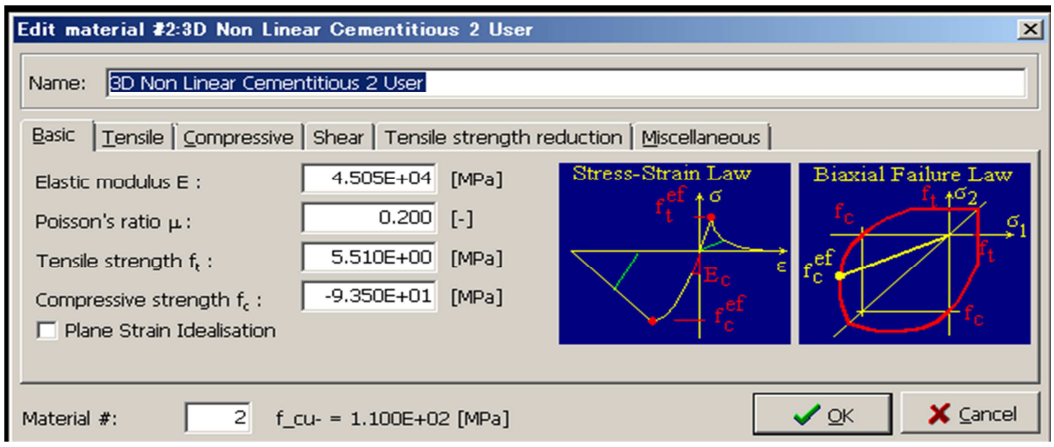

Fig. D.2 The basic input parameters for simulation of SHCC.

The most important parameters to be input are the parameters for the tensile loading. These parameters are shown in the Fig. D.3. Under the heading of tensile law function property, it is required to input three set of coordinates. These set of coordinates are taken from the experimental data. These coordinates are for strain and ratoi of tensile stress to tensile strength. These coordinate input is used to define the trilinear stress-strain relationship of SHCC. The input parameter window is shown in Fig. D.3.

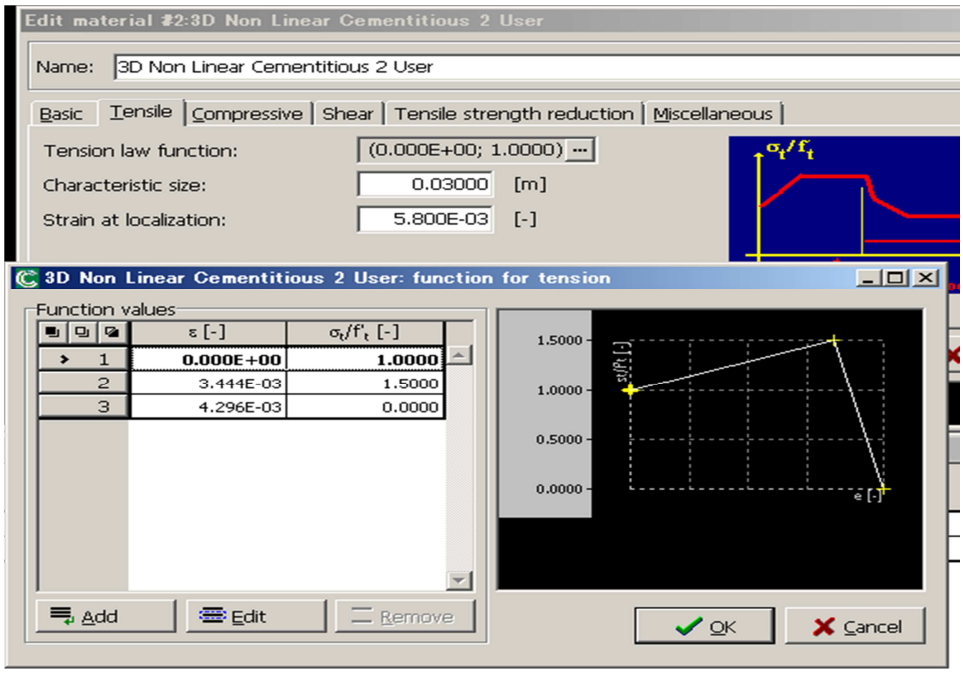

Fig. D.3 Tensile material parameters for simulation of SHCC.

D.3 Results

The simulation is done after inputting the material parameters. The material parameters are selected from the work by Kamal et al.[93]. The results of load and displacement relationship are shown in Fig. D.4. The crack distribution is also shown in Fig. D.5. At first the simulation results are compared for the first cracking load and displacement which are shown in Fig. D.4. The results are shown within the elements that is clear from the

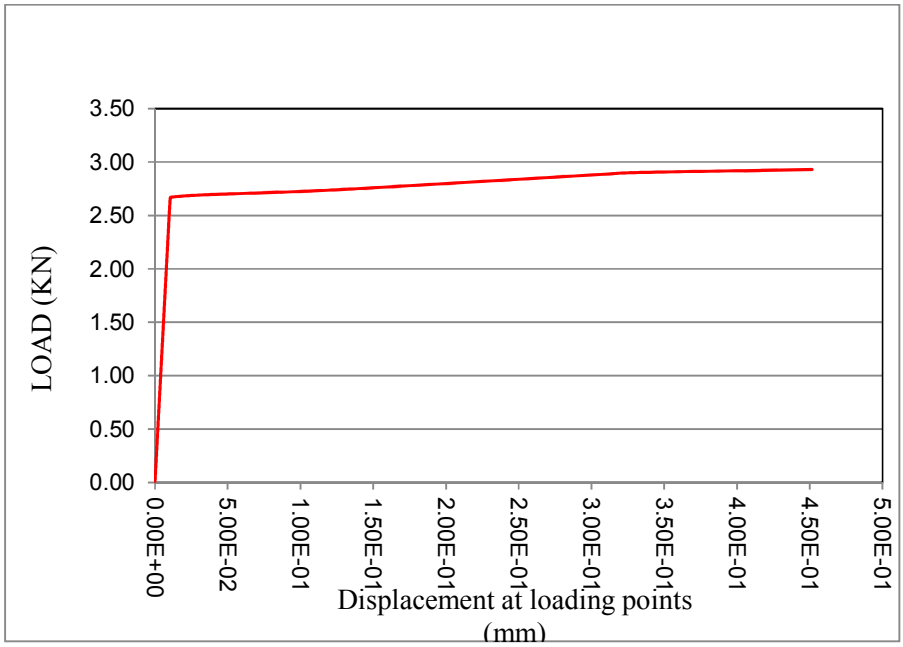

Fig. D.4 Load vs displacement relationship of SHCC under uniaxial tensile loading.

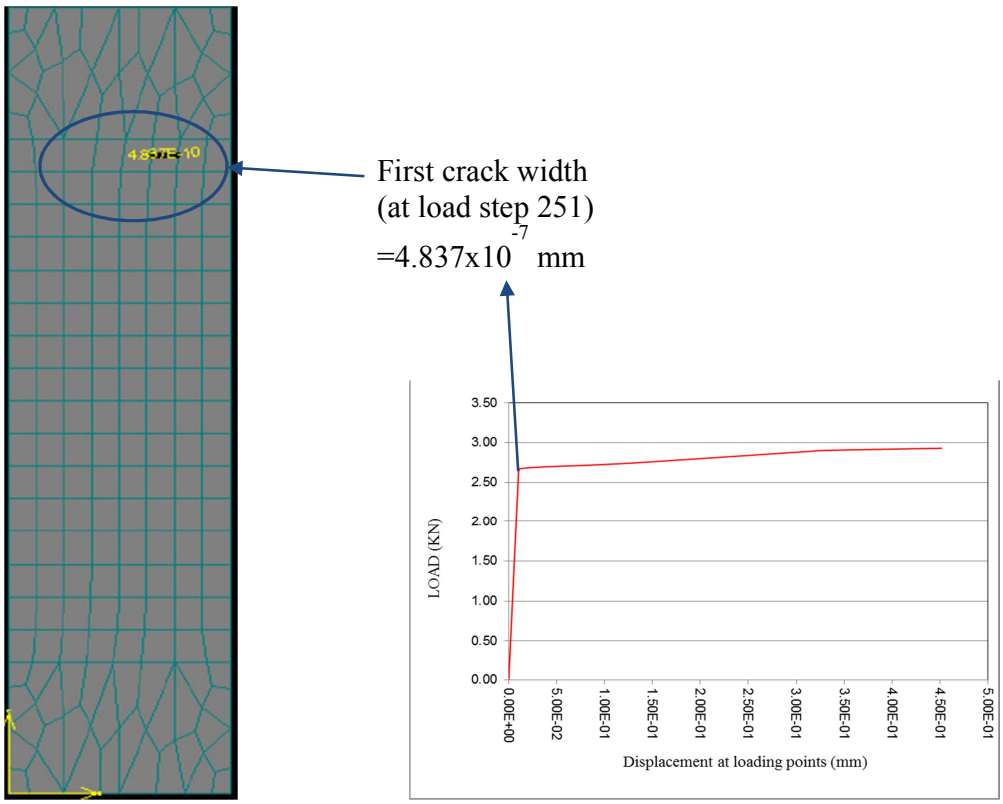

Fig. D.5 Crack width at first crack in SHCC

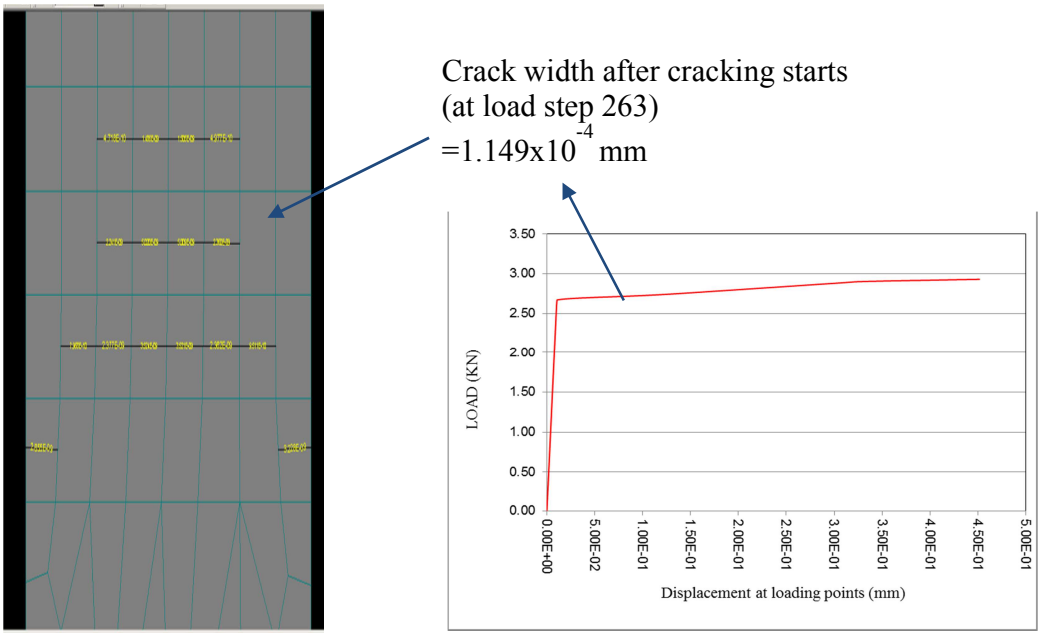

Fig. D.6 Simulation result of crack widths and their locations after cracking starts.

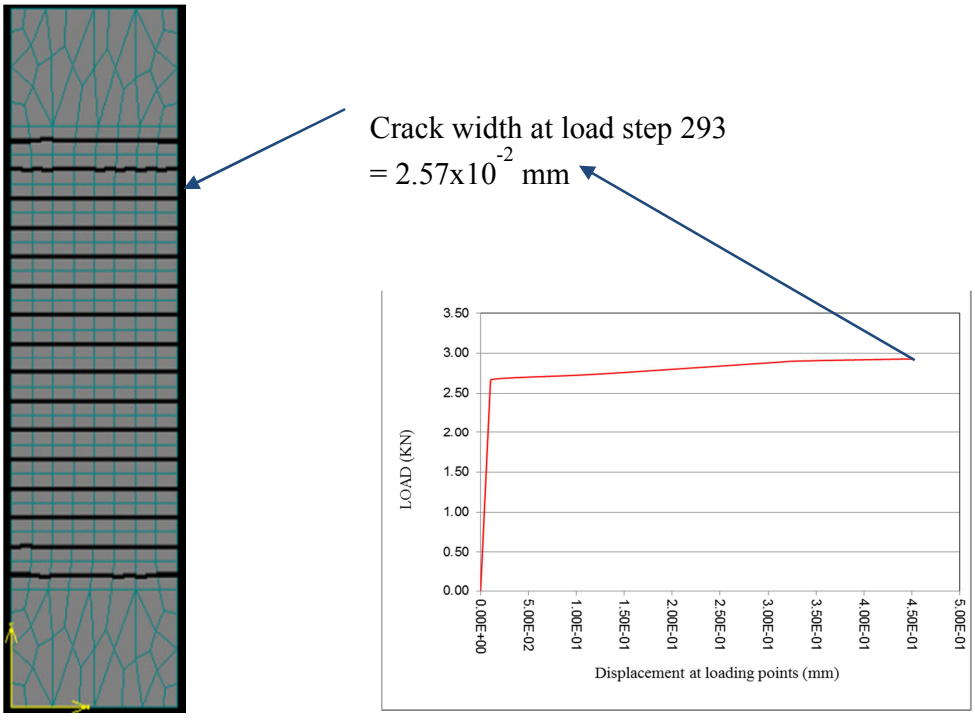

Fig. D.7 Simulation result of crack pattern and distribution within elements at load step 293.

crack distribution. The number of cracks is increased as well the crack width at load step 263 as shown in Fig. D.6. The crack width observed at first crack is $4.87x10^{-7}$mm that is much lesser than the crack width observed at load step 263 that is equal to $1.149x10^{-4}$mm. It is clear from Fig. D.6 that number of cracks is increased at increasing load level and also the crack width increased. The load is increased in the same manner and more increased crack width has been observed during simulation. The crack pattern and distribution is shown in Fig. D.7 at load level 293. These results prove that the number of cracks and crack width increases at increasing load levels.

E. 4 Summary

The simulation of strain hardening cementitious composites SHCC have been done to incorporate the uniaxial tensile behavior for short time loading. The model has the ability to simulate the crack width and the corresponding total displacements. The load is applied at fixed intervals with appropriate imposed increments. The model is kept closer to the practically examined specimen of SHCC. All of the material parameters are selected based on experimental testing of SHCC for uniaxial tensile loading. The results show the gradual increase in crack widths and number of cracks from load level 251 to 293. It shows that the same trend will continue and complete stress-strain relationship can be simulated for SHCC. The simulation by using ATENA 2D V4 takes much time as number of meshes are more. The mesh size is selected depending upon the crack spacing. So that the each element will show one crack and it can represent the multiple cracking behavior of the material. The crack spacing is estimated from the average fiber length. The given simulation is done considering the fiber length used in experimental testing and element sixe is kept less than the fiber length. These consideration are very important to simulate the uniaxial tensile behavior of SHCC.

APPENDIX E

INFLUENCE OF NUMBER OF MICROPLANES ON NUMERICAL RESULTS

F.1 Introduction

Some problems of physics and engineering require an accurate and efficient numerical integration over the surface of a sphere. One such problem is the determination of the relationship between the stress and strain tensors in a deformable material having nonlinear properties defined separately on planes of various orientations within the material. The numerical integration can be carried out over a rectangular domain in the (θ,ϕ) -plane where θ and ϕ are the spherical angular coordinates. However, for application in finite element programs involving hundreds of elements and hundreds of loading (or time) steps, numerical integration over the surface of a sphere may have to be carried out million-times or more, and then the use of a rectangular (θ,ϕ) domain is inefficient since too many integration points are wastefully crowded near the pole of the spherical coordinates. Moreover, functions that are smooth and well behaved on the surface of a sphere are not such in the (θ,ϕ) -plane[87].

The spherical integration is a fundamental part of calculation for constitutive relationship for microplane model. The microplanes are considered distributed over the surface of sphere. The constitutive relationships are established at each microplane and then integrated for the whole surface of sphere. The efficiency of the integration formula and the effect of number of microplanes on the integration efficiency should be analyzed prior to the selection of integration formula for unit sphere.

E.2 Influence of Number of Microplanes on Numerical Results

Normally, the integral for the calculation of stiffness tensor over the surface of a hemisphere has to be evaluated numerically. The numerical integration formula may be written in the form as follows.

$$D_{ijrs} = \sum_{\alpha=1}^{N} w_\alpha [a_{ijrs} C_N]_\alpha \qquad (e1)$$

Where w_α is the weights (or coefficients) and $\alpha = 1,2,....., N$ are the numbers of the numerical integration points on the hemisphere surface of radius 1, defined by unit vector $\vec{n}^\alpha$.
Since there are six independent incremental stiffnesses in Eq. e1, the numerical integration is carried out six times for each point of the material where the stiffness is needed. In a finite element program, the numerical integration over a hemisphere must be repeated for all the finite element and all the integration points within each element, and for all the loading steps. Obviously, it is important to use a very efficient numerical integration formula.

The numerical integration by means of a rectangular mesh is simple but rather inefficient. One reason is that the integration points are wastefully crowded near the pole. More importantly, functions that are smooth on the spherical surface near the pole may be unsmooth in the (θ, ϕ) plane. Therefore, optimal integration formulas should be constructed directly for the surface of the sphere. The greatest efficiency is achieved with a regular (uniform) distribution of the integration points over the spherical surface. Such a distribution is given either by the centroids of the faces of a regular polyhedron inscribed to the sphere. The regular polyhedron (Platonic solid) with the greatest possible number of faces is the icosahedron, having 20 faces[94].

So, we cannot have, for a hemisphere, a numerical integration formula with more than N=10 for regularly spaced points. In Fig. E.1, the integration points are pictured as the vertices of a dual dodecahedron. Such a numerical integration formula, which ha equal weights, was given by Albrecht and Collatz[95]. This formula is of 5th degree, which might seem to suffice for good accuracy, as it does for elastic behavior. However, this formula with

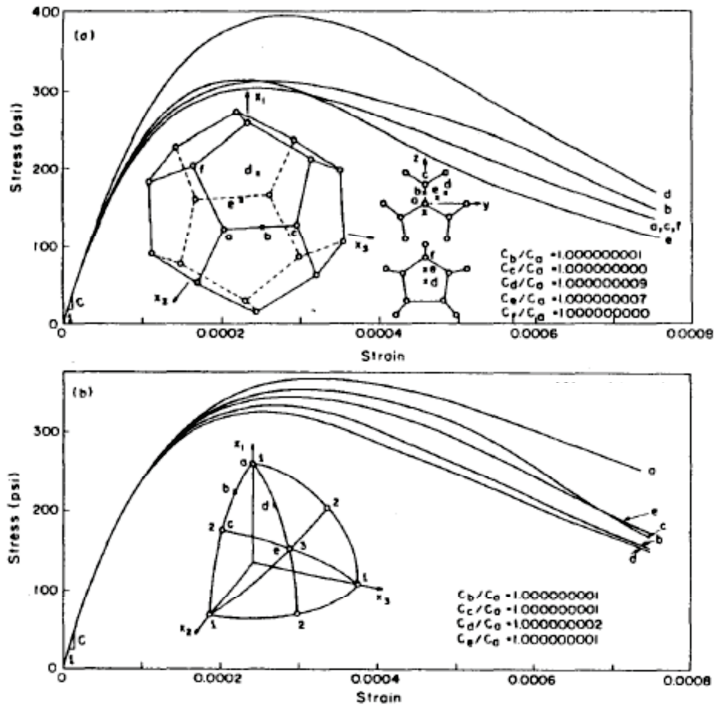

Fig. E.1 Response curves for uniaxial stress of various orientations with respect to integration points for Albrecht and Collatz's integration formulas[95] a) 2x10 points b) 2x13 points.

lesser number of integration point (microplanes) is not efficient for strain softening. To get a better idea of the accuracy of the integration formula, the following test has been proposed[96].The stress-strain curves calculated with the help of the numerical integration formula must remain nearly the same when the set of the integration points is arbitrarily rotated as a rigid body with respect to the material. While the applied stress or strain is not rotated. The maximum difference among the stress-strain curves for all such possible rotations is a measure of the error.

Consider the calculation of the tensile stress-strain curve for uniaxial stress. We specify the strain ε_{11} to increase in small steps $\Delta\varepsilon_{11}$. For each such loading step, the incremental stiffness matrix is evaluated with the help of Eq. e1. Then solve the increments $\Delta\sigma_{11}$ and all remaining $\Delta\varepsilon_{ij}$ components from the conditions that all $\Delta\sigma_{ij}$ components except $\Delta\sigma_{11}$ must be zero.

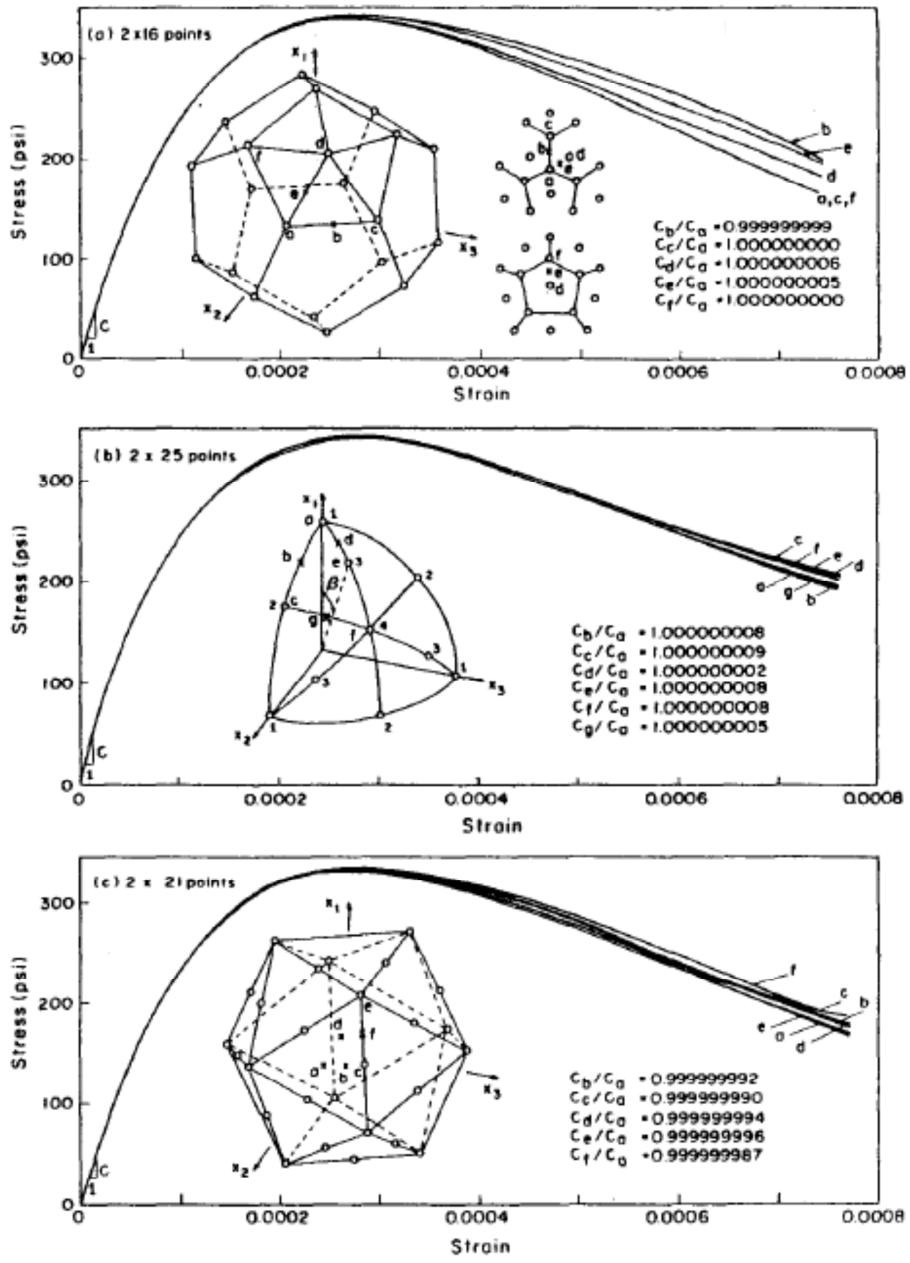

Fig. E.2 Response curves for uniaxial stress of various orientations for formulas: a) Finden[63] b) McLaren[98] c) Bazant and Oh[97].

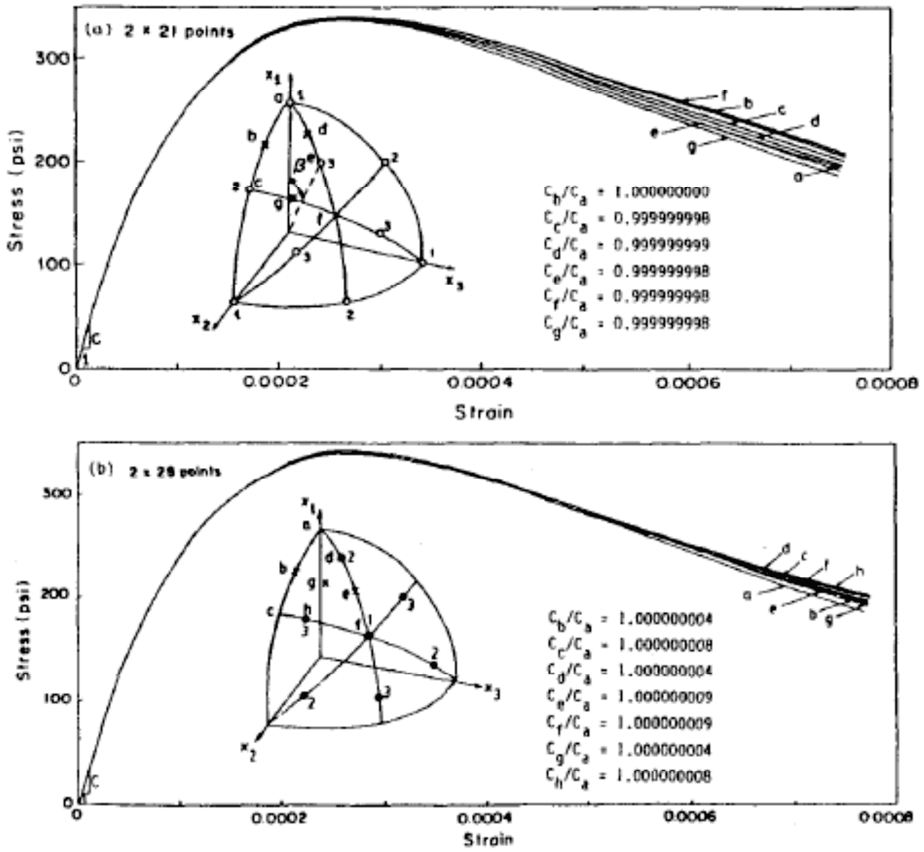

Fig. E.3 Response curves for uniaxial stress of various orientations formulas: a) Bazant and Oh[98] b) Stroud[97].

The calculations of the response curves for uniaxial tensile stress have been carried out by using Eq. e2.

$$s_n = E_n e_n e^{-(e_n k)^p} \qquad (e2)$$

In Eq. e2, E_n = 3485000psi, k = 6280 and p = 1 is considered. The calculations are repeated for various orientations of axis x_1 of the uniaxial stress σ_{11} relative to the set of integration points. In particular, the orientations coinciding with one integration point and other orientation considered are labelled in Fig. E.1 and Fig. E.2 as a,b,c,……., and the corresponding response curves are labelled the same.

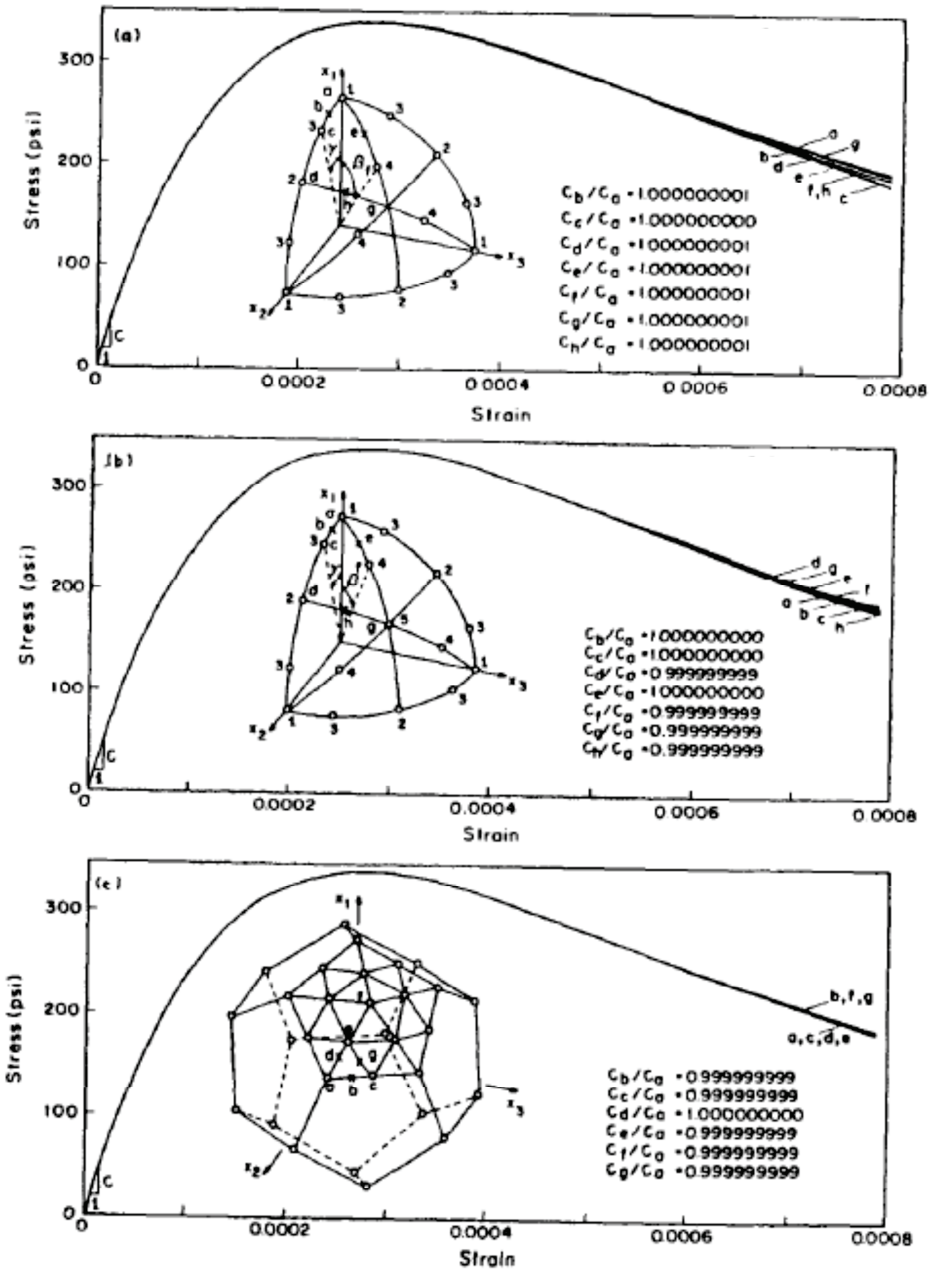

Fig. E.4 Response curves for uniaxial stress of various orientations for new Bazant and Oh[98] formulas : a) 2x33 points b) 2x37 points c) 2x61 points.

For Albrecht and Collatz's 10 point integration formula based on the faces of icosahedron, the response curves for various σ_{11} orientations are found to differ enormously from each other within the strain –softening range as shown in Fig. E.1, even though their initial (elastic) slopes $C_a, C_b, C_c, \ldots\ldots$ are nearly the same for all orientations. Therefore, the

formula of a higher degree, for which the spacing of integration points and the weights are nonuniform, must be used in the case of strain softening. The arrangement of the integration points for various applicable known formulas[97] are shown in Fig E.2 and formulas by Bazant and Oh[98] are shown in Fig. E.3 and Fig. E.4.

Based on testing the responses to the uniaxial stress of various orientations, as indicated by the curved in Fig E.3(a) and Fig. E.4, the new formulas with N= 33, 37 and 61 points appear to be the superior to the existing centrally symmetric formulas.

F.3 Summary

The efficiency of the integration formulas are explained here briefly that resulted in the conclusion that increasing the number of microplanes (integration points) reduces the error of spread. As the number of microplanes is increased, the distribution over the hemisphere surface becomes uniform. It has also been noted that the degree of the formula is not very indicative of the accuracy based on the test with various σ_{11} -directions. The formulas with N=33 and 37 appear to be approximately equally accurate, even though their degree are 11 and 13 respectively. Hence the new formula with N= 21 perform much better than Finden's formula[97] with N=16, as shown in Fig. E.2(c), Fig. E. 3(a) and Fig. E.2(a), even though they are all of the 9^{th} degree.

.